

EDDY HEAT FLUXES AND STABILITY OF PLANETARY WAVES

by

CHARLES AUGUSTIN LIN

B.S., University of British Columbia
(1974)

SUBMITTED IN PARTIAL FULFILLMENT
OF THE REQUIREMENTS FOR THE
DEGREE OF

DOCTOR OF PHILOSOPHY

at the

MASSACHUSETTS INSTITUTE OF TECHNOLOGY

May, 1979

Signature of Author.
Department of Meteorology, May 1979

Certified by.
Thesis Supervisor

Accepted by.
Chairman, Departmental Committee on Graduate Students

WITHDRAWN
FROM
MIT LIBRARIES
JUN 20 1979
LIBRARIES

EDDY HEAT FLUXES AND STABILITY OF PLANETARY WAVES

by

CHARLES AUGUSTIN LIN

Submitted to the Department of Meteorology on May 16, 1979, in partial fulfillment of the requirements for the degree of Doctor of Philosophy.

ABSTRACT

A two-level, quasi-geostrophic, mid-latitude β -plane model with surface friction is used to examine the heat transport and energetics of winter stationary waves, which are forced by realistic topographic and diabatic heating fields. It is found that the heat transport of stationary waves and its efficiency are underestimated. The energetics show that the surface conversion terms due to topography and friction are overestimated considerably, due to inadequate resolution of surface phenomena. The results suggest stationary forcing alone is not sufficient to account for the observed efficient heat transport of stationary waves.

As a first step towards determining the effects of a basic state wave on the baroclinic stability problem, the stability of the baroclinic Rossby wave in a zonal shear flow is examined. Linearized theory is used with an adiabatic and frictionless version of the earlier model. The perturbations consist of truncated zonal Fourier harmonics. There are two important zonal scales in the stability problem: the basic wave scale and the radius of deformation. The former occurs as an explicit scale while the latter is the natural response scale of perturbations of a baroclinic zonal flow. The ratio of these two scales, together with two non-dimensional parameters which describe the amplitudes of the barotropic and baroclinic components of the basic wave, constitute the three parameters in our parameter study of the stability problem. Parameter space is partitioned according to the dominant energy source for instability: the Lorenz and Kim regimes are characterized by significant horizontal and vertical shears of the basic wave respectively, while the Phillips regime is characterized by a strong zonal shear flow. A fourth regime, the mixed wave regime, where the horizontal and vertical shears of the basic wave are comparable and both large, is also identified. Growth rates, vertical structures, kinetic energy and heat transport spectra and energetics are examined for the most unstable mode in each regime. When the basic wave scale is larger than the radius of deformation, higher harmonics of the basic wavenumber are excited;

when the two scales are comparable, only the perturbation zonal flow and basic wave harmonic components have significant amplitude. Away from the Phillips regime, the most unstable mode has a non-zero meridional wavenumber. Approximate analytic expressions giving the parametric dependence of the meridional wavenumber for the most unstable mode are derived for each regime.

For the case of most interest for the atmosphere, the basic state consists of a planetary scale (wavenumbers 1 and 2) baroclinic Rossby wave in a zonal flow near the minimum critical shear of the two-level model. The most unstable mode grows at the baroclinic time scale and propagates with a phase velocity close to that of the basic wave. For basic wavenumber 1, the kinetic energy and heat transport spectra peak at wavenumber 3, much like the observed spectra in planetary scales. The results for basic wavenumber 2 is similar. The baroclinic eddy-eddy interaction is comparable to the baroclinic eddy-mean flow interaction.

Thesis Supervisor: Peter H. Stone
Title: Professor of Meteorology

DEDICATION

TO MY PARENTS.

ACKNOWLEDGEMENTS

I wish to express my gratitude to my thesis advisor, Professor Peter H. Stone. His guidance throughout this investigation has provided me with experience of incomparable value.

Financial support during my stay at M.I.T. came from a Research Assistantship supported by the National Aeronautics and Space Administration under Grant NGR 22-009-727. Computer time and facilities were provided by the Goddard Institute for Space Studies.

My stay at M.I.T. has been made enjoyable in part by the graduate students of the Department of Meteorology at M.I.T. I thank them for their friendship. I also wish to thank Ms. Isabelle Kole for drafting the figures and Ms. Virginia Mills for typing the manuscript. I am also grateful to my parents for their constant guidance and encouragement.

TABLE OF CONTENTS

	Page
Abstract.	2
Dedication.	4
Acknowledgements.	5
Table of contents	6
List of figures	8
List of tables.	11
I. Introduction.	12
II. Basic formulation.	29
II-1. Basic equations in a two layer atmosphere	29
II-2. Free solutions of the basic equations	34
III. Heat transport by stationary waves.	48
IV. Linear stability problem of Rossby waves in a baroclinic zonal flow	69
IV-1. Preliminary considerations.	69
IV-2. Linearized perturbation equations	70
IV-3. Some properties of unstable modes	78
V. Results of stability analysis	83
V-1. Stability of a planetary scale basic wave.	83
V-2. Stability of a very large scale basic wave	93
V-3. Stability of a synoptic scale basic wave	100
V-4. Meridional scale of most unstable mode	108
V-5. Parametric dependence of meridional scale.	123
VI. Application to the atmosphere.	127
VII. Conclusions	136

	Page
References.	143
Biographical note.	147

LIST OF FIGURES

<u>Figure</u>		<u>Page</u>
1.1	Distribution of kinetic energy of transient and stationary eddies for different months. (from Oort and Peixoto, 1974)	15
1.2	Conversion of zonal available potential energy to transient ($C_1(P_M, P_{TE})$) and stationary ($C_1(P_M, P_{SE})$) eddy available potential energy for different months. (from Oort and Peixoto, 1974)	16
1.3	Spectra of eddy kinetic energy (K) and conversion of zonal available potential energy to eddy available potential energy (C_1). (from Tenenbaum, 1976)	17
1.4	Spectra of standard pressure amplitude due to surface topography and diabatic heating. (from Derome and Wiin-Nielsen, 1971)	19
1.5	Normalized spectrum of transient eddy kinetic energy at 50°N, 500 mb, in winter. (from Julian et al, 1970)	20
1.6	Magnitude of conversion of kinetic energy from wavenumber m to n, summed from m=1 to 30 in winter, $ C[K(m/n)] $. (from Tenenbaum, 1976)	25
2.1a	Horizontal geometry of β -plane model.	30
2.1b	Vertical geometry of β -plane model.	
2.2	Critical shear of the 2-level model as a function of zonal wavenumber.	36
2.3	Barotropic zonal flow ($\mu^2(u-c)/\beta$) as a function of for Rossby waves of wavenumbers 2, 4, 6.	37
2.4	Zonal shear ($\mu^2 u_r/\beta$) as a function of β_r/β for Rossby waves of wavenumbers 2, 4, 6.	38
2.5	Barotropic zonal flow ($\mu^2(u-c)/\beta$) as a function of zonal wavenumber (K) of Rossby wave, for zonal shear $\mu^2 u_r/\beta = 0$ and $\mu^2 u_r/\beta = 1$. Both baroclinic and barotropic modes are shown.	41
2.6	Amplitude ratio (β_r/β) as a function of zonal wavenumber (K) of Rossby wave, for zonal shear $\mu^2 u_r/\beta = 1$.	42
2.7	Comparison of phase speeds of Green modes obtained with a high vertical resolution model and phase speeds of neutral baroclinic Rossby waves in a two-level model.	45

<u>Figure</u>	<u>Page</u>
2.8 Vertical structure of streamfunction phase for the fastest growing Green mode in a high vertical resolution model.	46
3.1 Effects of friction on stationary wavenumber two forced by topography.	54
3.2 Effects of friction on stationary wavenumber two forced by diabatic heating.	55
3.3 Calculated stationary eddy heat flux as a function of longitude and latitude for winter.	56
3.4 Observed stationary eddy heat flux as a function of longitude and latitude, averaged over January 1973, 1974 and 1975.	57
3.5 Calculated and observed zonally averaged stationary eddy heat transport for winter, as a function of latitude.	59
3.6 Calculated spectra of northward stationary eddy heat transport and correlation coefficient.	60
3.7 Calculated spectra of energy conversions of stationary waves in winter.	63
5.1 Contours of constant growth rate ($\left \frac{\sigma_i/k}{U-c} \right $) of most unstable mode for planetary scale basic wave with non-dimensional wavenumber $\mu/k = 3.9$, and lowest truncation.	84
5.2 Growth rate ($\left \frac{\sigma_i/k}{U-c} \right $) and zonal shear ($\frac{U_z}{U-c}$) for lowest truncation along baroclinic, barotropic and mixed baroclinic-barotropic paths, for most unstable mode. $\mu/k = 3.9$	86
5.3 Spectra of barotropic and baroclinic perturbation wave amplitude ($ X_n $, $ Y_n $) for the most unstable mode and its meridional wavenumber (L_0). $\mu/k = 3.9$	88
5.4 Kinetic energy and heat transport spectra ($K(n)$, $\overline{v'T'}(n)$) for the most unstable mode. $\mu/k = 3.9$	91
5.5 Energetics of the most unstable mode. $\mu/k = 3.9$	92
5.6 As in Fig. 5.1 but for very large scale basic wave. $\mu/b = 10$	94
5.7 As in Fig. 5.2 but for $\mu/k = 10$	96

<u>Figure</u>	<u>Page</u>
5.8 As in Fig. 5.3 but for $\mu/k = 10$.	97
5.9 As in Fig. 5.4 but for $\mu/k = 10$.	98
5.10 As in Fig. 5.5 but for $\mu/k = 10$.	99
5.11 As in Fig. 5.1 but for synoptic scale basic wave. $\mu/k = 1.2$	101
5.12 As in Fig 5.2 but for $\mu/k = 1.2$.	102
5.13 As in Fig.5.3 but for $\mu/k = 1.2$.	103
5.14 As in Fig.5.4 but for $\mu/k = 1.2$.	104
5.15 As in Fig.5.5 but for $\mu/k = 1.2$.	107
6.1 Growth rate of most unstable mode as function of wave amplitude and meridional wavenumber. Basic wave is wavenumber one and zonal shear flow is near minimum critical shear.	129
6.2 Spectra of $ X_n $, $ Y_n $, $K(n)$ and $\overline{v'T'}(n)$ of all unstable modes of meridional wavenumber $l/k = 5$. Also shown are the energetics and correlation coefficient for heat transport. Parameters of basic flow as in Fig. 6.1.	130
6.3 Observed wavenumber spectra of meridional sensible heat flux for stationary and transient eddies, at 850mb, 60° N in winter. (from Kao and Sagendorf, 1970)	133
6.4 Kinetic energy and heat transport spectra, energetics and correlation coefficient for heat transport for most unstable even and odd perturbations. Basic wave is wavenumber two and zonal shear flow is near minimum critical shear.	134

<u>Table</u>		<u>Page</u>
1.1	The four major kinds of atmospheric eddies and their likely sources, and the amounts of kinetic energy and conversion of zonal available potential energy to eddy available potential energy, on an annual basis. (from Stone, 1977)	21
3.1	Sensitivity of forced stationary waves to variations of the friction coefficient, meridional wavenumber and diabatic heating.	67
5.1	Non-dimensional growth rate and meridional wavenumber for most unstable mode calculated from a second order expansion valid for the Lorenz regime, together with the exact values.	118
5.2	As in Table 5.1 but the second order expansion is valid for the Kim regime.	120

I. INTRODUCTION

Examination of time mean weather maps reveals the existence of perturbations (deviations from axial symmetry) of considerable amplitude. The existence of disturbances after time averaging suggests excitation by geographically fixed sources. The primary sources of such disturbances are (i) deflecting effects of mountain ranges on zonal currents and (ii) heating by a steady distribution of heat sources and sinks. The forcing of stationary waves by either topography (e.g. Charney and Eliassen, 1949) or diabatic heating (e.g. Smagorinsky, 1953) has frequently been discussed in the literature. Investigations including both forcing mechanisms have also been done (e.g. Derome and Wiin-Nielsen, 1971). Daily weather maps also show the existence of perturbations of comparable amplitudes with much shorter time scales, typically of the order of several days. These transient waves have conventionally been attributed to baroclinic instability of the zonal current (Charney 1947, Eady, 1949).

In order to better understand the stationary and transient components of atmospheric wave motions, the wind and temperature fields are often decomposed into the mean, stationary and transient components as follows: consider any field, such as meridional velocity v . Then

$$v = [\bar{v}] + \bar{v}^* + v'$$

where $[\cdot] = \frac{1}{L} \int_0^L \cdot dx$ and $\bar{\cdot} = \frac{1}{\tau} \int_0^\tau \cdot dt$ are zonal and time means respectively; asterisks and primes denote deviations from the zonal and

time means respectively. The time and zonal mean of a quadratic quantity such as meridional heat transport can be written in the following form (\bar{T} denotes temperature).

$$[\overline{vT}] = [\bar{v}][\bar{T}] + [\bar{v}^* \bar{T}^*] + [\overline{v'T'}]$$

The terms on the right hand side are referred to as the zonal mean (Z) component; the stationary eddy (SE) component and the transient eddy (TE) component respectively.

Holopainen (1970) examined the energetics of stationary waves by evaluating the various terms in the equations of balance of kinetic energy (KE) and available potential energy (APE) using observational statistics. Only those processes which affect the energy of stationary waves were considered. He found the dominant conversions in winter are ZAPE \longrightarrow SEAPE \longrightarrow SEKE, characteristic of atmospheric eddies generated by baroclinic instability of the zonal flow. Dissipation was found to be much more important than topographic forcing, SEAPE was destroyed by diabatic heating and the primary energy source of the stationary waves was ZAPE. Holopainen concluded that stationary disturbances are essentially free standing or slowly moving baroclinic waves, which need external forcing in order to occur on time-mean maps. He suggested the simplest model which would approximately produce the observed energetics of stationary waves was a baroclinic model with diabatic forcing as the only forcing mechanism.

Stone (1977), from physical considerations and observational evidence, classified atmospheric eddies into four major types: baroclinic and non-baroclinic SE's; and planetary scale and synoptic scale TE's.

The classification of SE's is based on the observation that summer SE's do not transport heat poleward while winter SE's do, and that the winter SE energy cycle is dominated by baroclinic conversions while that in the summer is not. Figs. 1.1 and 1.2, taken from the results of Oort and Peixoto (1974), show the distribution of TEKE and SEKE, and the conversions of ZAPE to TEAPE and SEAPE by the dominant horizontal processes for different months, respectively. In both winter and summer, SE's account for about 20% of the total eddy KE, but the conversion $ZAPE \longrightarrow SEAPE$ is about 50% of the total conversion in winter and almost 0% in summer. Also in winter the conversion $SEAPE \longrightarrow SEKE$ is the main source of SEKE (Holopainen, 1970). Since these conversions in winter imply strong poleward and upward transports of sensible heat, we see there is a strong baroclinic component in the SE's giving rise to efficient heat transporting waves in winter. The summer SE's transport almost no heat and are termed non-baroclinic. The non-baroclinic SE's are likely due to topographic forcing, as topographically forced waves do not transport heat (Derome and Wiin-Nielsen, 1971).

Stone's classification of the TE's was based on spectral analysis. Fig. 1.3 shows the eddy KE and the conversion $ZAPE \longrightarrow EAPE$ as a function of the zonal wavenumber in January, taken from Tenenbaum (1976). There are two peaks in both spectra: a primary peak at planetary scales (wavenumber 1-3) and a secondary peak at synoptic scales (wavenumbers 5-8). The presence of two peaks indicates at least two different physical processes are at work generating eddies in January. The topographic and diabatic forcings have similar spectra as both are primarily determined by the distribution of oceans and continents. Their

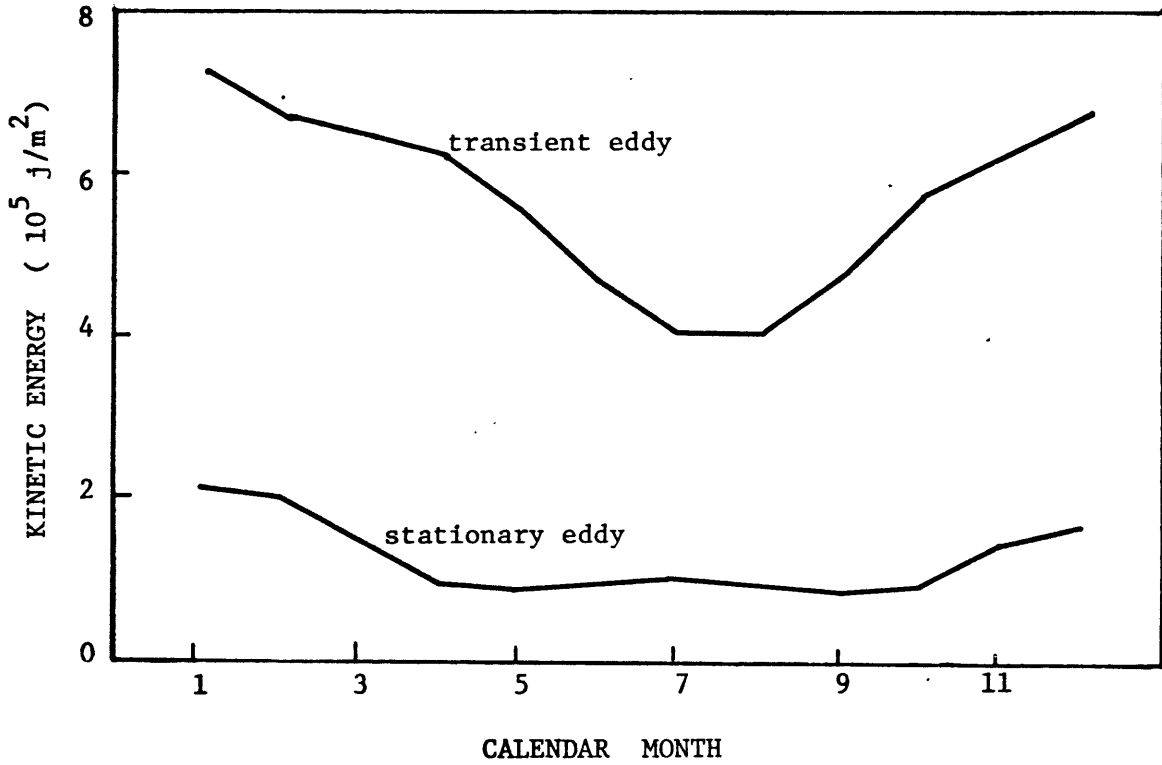


Fig. 1.1 Distribution of kinetic energy of transient and stationary eddies for different months. (from Oort and Peixoto, 1974)

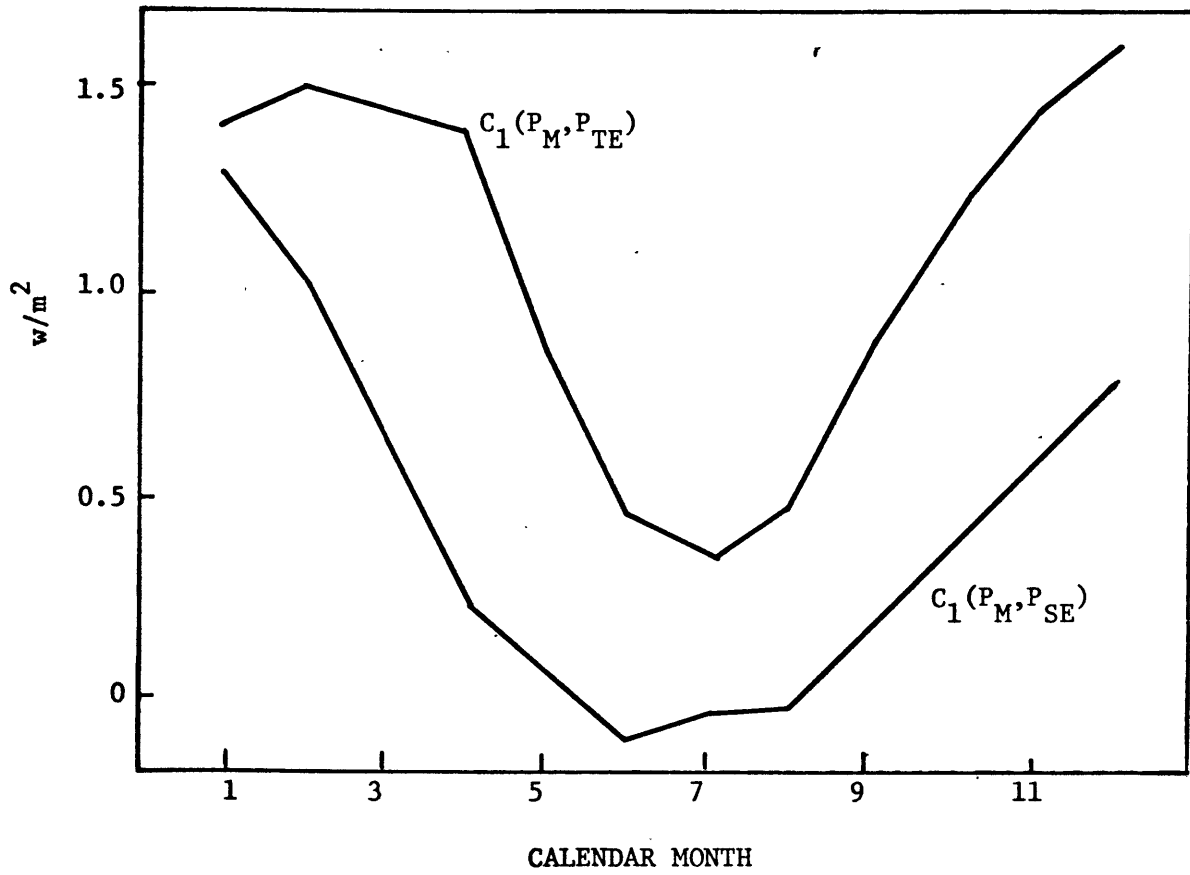


Fig. 1.2 Conversion of zonal available potential energy to transient ($C_1(P_M, P_{TE})$) and stationary ($C_1(P_M, P_{SE})$) eddy available potential energy for different months. (from Oort and Peixoto, 1974)

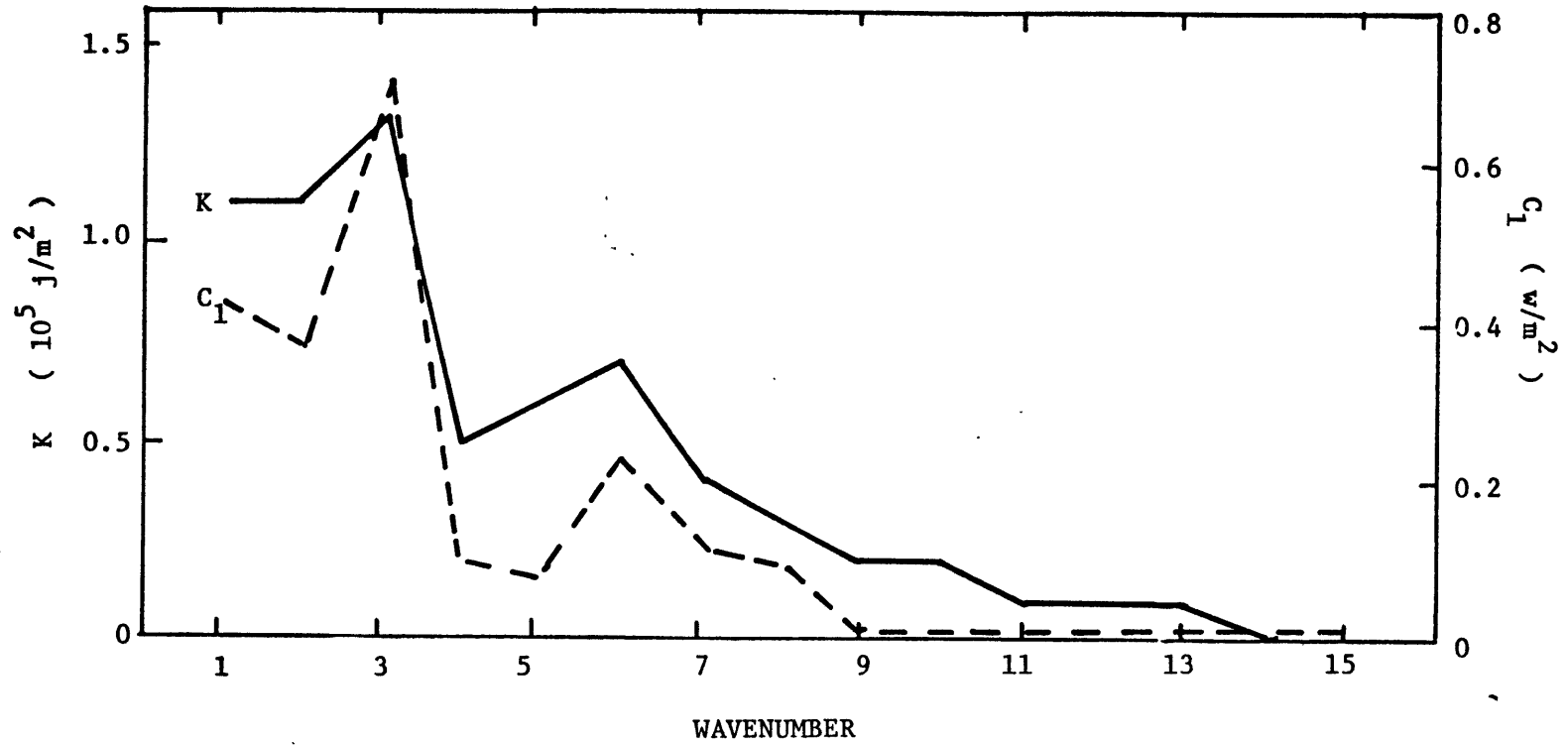


Fig. 1.3 Spectra of eddy kinetic energy (K) and conversion of zonal available potential energy to eddy available potential energy (C₁). (from Tenenbaum, 1976)

spectra, taken from Derome and Wiin-Nielsen(1971), are shown in Fig. 1.4. As planetary scales are dominant in these forcings, it is natural to associate the planetary scale peak in the observed spectra of Fig. 1.3 with these forcings. One would expect these forcings to give rise to SE's, but the planetary scale waves must also contain a substantial TE component: if we attribute all of the KE and conversion in wavenumbers four and higher to TE's, the partitioning of the total eddy KE and of the total baroclinic conversion $ZAPE \longrightarrow EAPE$ (see Figs. 1.1 and 1.2) still implies that at least half the KE and conversion in the planetary scales (wavenumbers 1 to 3) are due to TE's. That there is a lot of KE in planetary scale TE's is shown in Fig. 1.5, taken from Julian et al (1970). We see that a significant portion of TEKE in winter lies in the planetary scales. The synoptic scale TE's may be attributed to baroclinic instability, since their scale and structure are close to those of the dominant modes given by baroclinic instability theory.

Table 1.1 summarizes the four kinds of eddies classified by Stone (1977) with their likely sources, and estimates of the partitioning among them of the total KE and the total baroclinic conversion $ZAPE \longrightarrow EAPE$ on an annual basis. As we discussed earlier, the synoptic scale TE's and non-baroclinic SE's are likely due to baroclinic instability and topographic forcing respectively. The planetary scale TE's may also be associated with baroclinic instability, as their properties are similar to those of synoptic scale TE's, except for the different zonal scale. Their scale may be determined by external forcing such as diabatic heating.

The source of baroclinic SE's is unclear. Stone (1977) observed that planetary scale TE's and baroclinic SE's may be different mani-

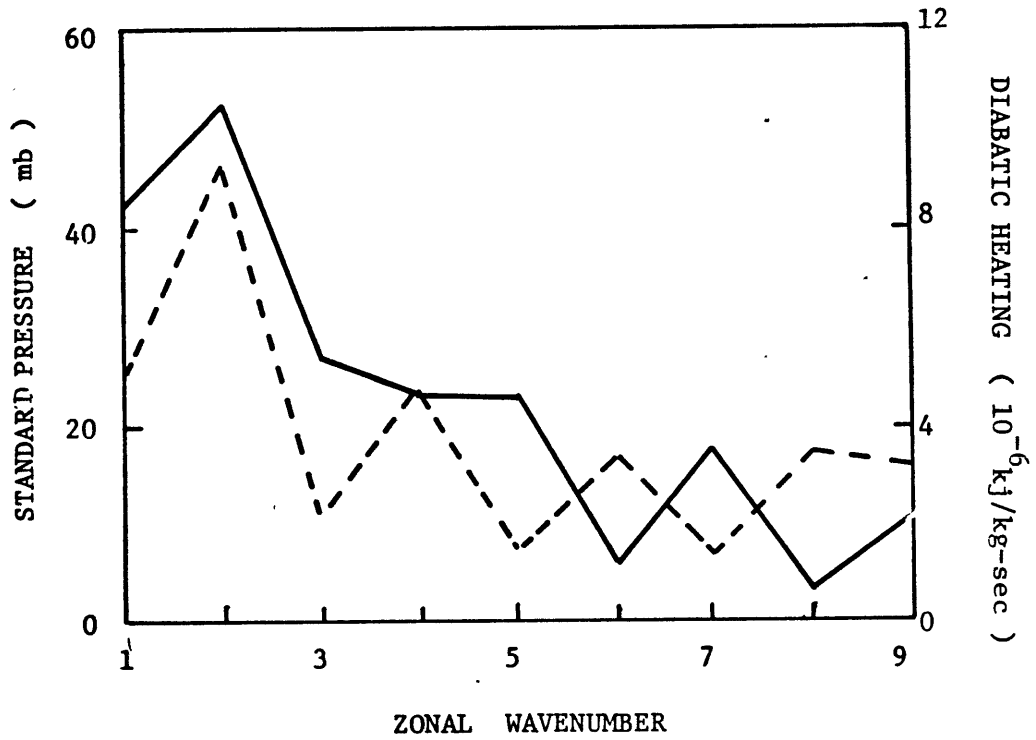


Fig. 1.4 Spectra of standard pressure amplitude due to surface topography (solid line) and diabatic heating (dashed line). (from Derome and Wiin-Nielsen, 1971)

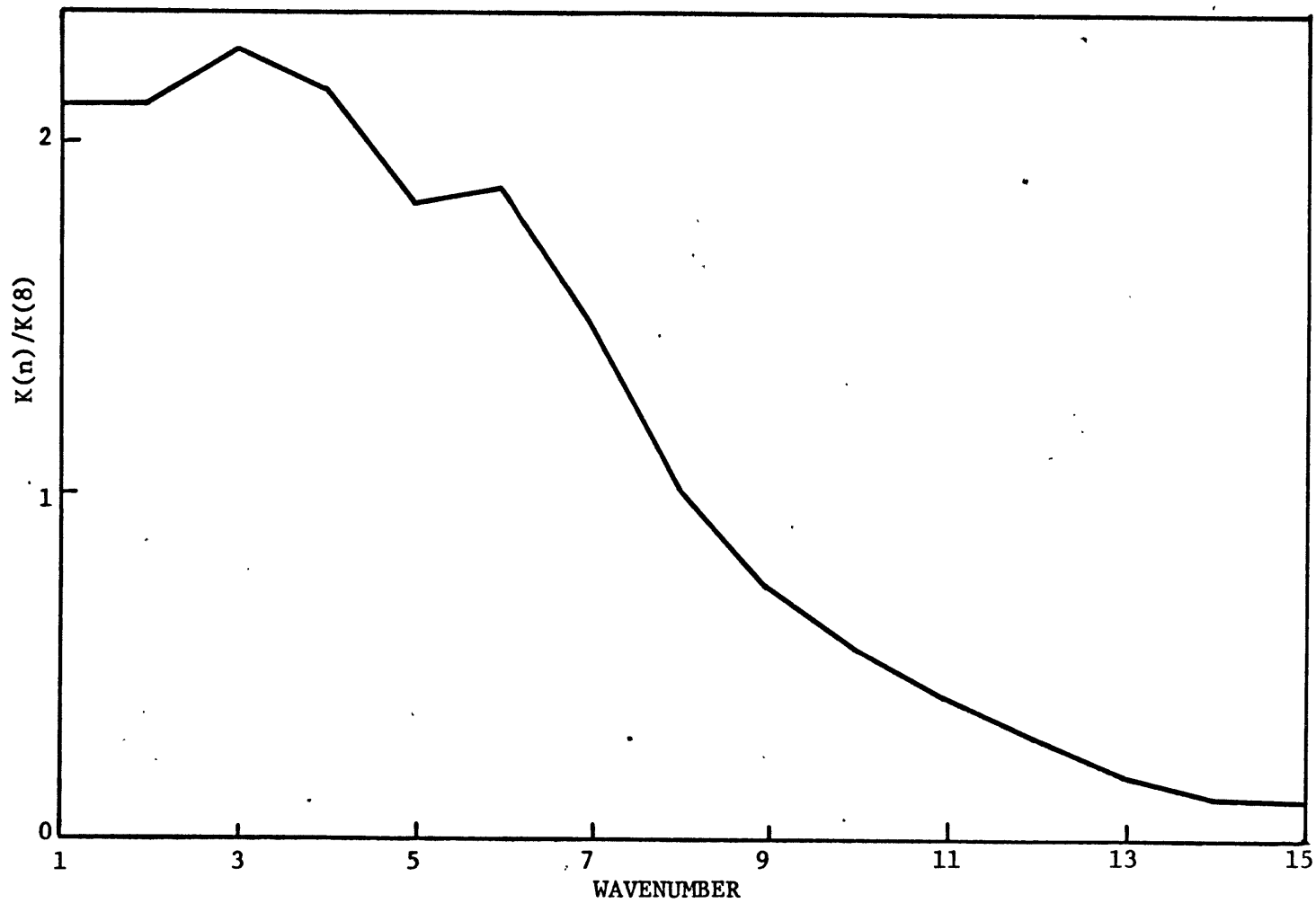


Fig. 1.5 Normalized spectrum of transient eddy kinetic energy at 50°N, 500 mb, in winter.
(from Julian et al, 1970)

EDDY TYPE	K_E	C_1	SOURCE
Synoptic-scale TE's	45%	40%	Baroclinic instability
Planetary-scale TE's	35%	30%	Baroclinic instability initiated by external forcing ?
Non-baroclinic SE's	10%	0%	Topographic forcing
Baroclinic SE's	10%	30%	Baroclinic instability in favored locations ?

-21-

Table 1.1 The four major kinds of atmospheric eddies and their likely sources, and the amounts of kinetic energy (K_E) and conversion of zonal available potential energy to eddy available potential energy (C_1), on an annual basis. (from Stone, 1977)

festations of a single phenomenon - eddies generated by a cooperation between diabatic heating and baroclinic instability. Such eddies would be of planetary scale and baroclinic in nature, and could contain both TE and SE components. A relation between baroclinicity and diabatic forcing is also suggested by the work of van Loon and Williams (1976). They examined records of temperature and sea level pressure from 1900 - 1972 and found that the period 1900 - 1941 was a warming period, during which the average temperature of the Northern Hemisphere increased, while the period 1942 - 1972 was a cooling period. They also found poleward transport of sensible heat by SE's took place in preferred longitude intervals on the front and rear sides of the Icelandic and Aleutian lows. A larger poleward flux in high latitudes during the warming period was found to be connected with a stronger meridional circulation, hence stronger baroclinicity, around the Icelandic low and on the east side of the Siberian high than during the cooling period. The lows and highs are in part diabatically forced, thus their results suggest that stronger baroclinicity coupled with diabatic heating gave rise to a larger SE heat transport.

Yao (1977) examined the maintenance of quasi-stationary waves by using a 2-level quasi-geostrophic spectral model on a β -plane. Diabatic heating was in the form of Newtonian cooling with an imposed thermal equilibrium temperature profile which varied only with latitude. Surface friction and topography were present at the bottom boundary. Topography of wavenumber n in the zonal direction and first mode in the meridional direction was used to force the quasi-stationary waves. The model's motion allowed for zonal wavenumbers 0, n , $2n$ and the first

three modes in the meridional direction. The cases $n = 2, 3$ were considered. The stationary solution was perturbed to find the quasi-equilibrium state. If the flow is not highly irregular, APE of the quasi-stationary waves was maintained by the conversion $ZAPE \longrightarrow SEAPE$. For $n = 3$ and moderate values of the imposed thermal equilibrium temperature gradient (ΔT_e) and the internal frictional dissipative time scale (k_1^{-1}), KE of these waves was maintained by the conversion $SEAPE \longrightarrow SEKE$. For smaller values of ΔT_e or k_1^{-1} , KE was supplied to the quasi-stationary waves by the conversion $ZKE \longrightarrow SEKE$ through the topographic forcing. The former case, characterized by the baroclinic conversions $ZAPE \longrightarrow SEAPE \longrightarrow SEKE$, is like the atmospheric winter regime when strong baroclinicity results due to the large pole-to-equator temperature gradient. Yao's results suggest that, in this case, the quasi-stationary waves are generated by baroclinic instability together with external forcing (topography); the latter is required to generate zonal thermal variations and hence SEAPE. Thus baroclinic instability and external forcing may work together to generate the baroclinic, efficient heating transporting SE's observed in winter.

Consideration of Holopainen's (1970), Stone's (1977) and Yao's (1979) works suggests the hypothesis that the efficient heat transport by SE's in winter is due to instability of a baroclinic flow with external forcing. The external forcing will force SE's and the resulting zonal flow and SE field will be unstable to small wavelike perturbations. As the basic flow is non-axisymmetric, interaction between the basic wave and the perturbation will generate further waves, i.e. a spectrum of waves. These waves will in general transport heat. For planetary

scale waves, such eddy-eddy interactions are in fact observed. Fig. 1.6, taken from the results of Tenenbaum (1976), shows the winter conversion of KE from wavenumber m to n , summed from $m = 1$ to 30, as a function of n . We see there are two peaks in the spectrum, in the planetary and synoptic scales. For the planetary scale peak at $n = 3$, the magnitude of this conversion is about 25% that of the conversion ZAPE \longrightarrow EAPE (Fig. 1.3). Thus eddy-eddy interaction is by no means negligible compared to eddy-mean flow interaction for these waves. For our hypothesis, the heat transport spectrum obtained as a result of eddy-eddy interaction will be of particular interest.

As a first step in examining our hypothesis, we will evaluate the heat transport and energetics of stationary waves forced by realistic topography and diabatic forcing in winter. The model used is similar to that of Derome and Wiin-Nielsen(1971). They examined forced stationary waves in mid-latitudes in winter but did not calculate their heat transports. We will find that the efficient heat transporting winter stationary eddies are not adequately modelled, and this will lead us to our next step, the study of the stability of a baroclinic Rossby wave in a zonal flow with shear. This problem will be the main subject of this thesis. The Rossby wave is a free wave and must satisfy a dispersion relation. For realistic profiles of the zonal flow, this constraint means that the waves are generally propagating relative to the earth. Thus the free Rossby wave cannot be identified with a forced stationary wave. However, the scale selection mechanism discussed above still operates. In particular, if realistic kinetic energy and heat transport spectra in the planetary scales are obtained with a planetary scale Rossby wave in the basic flow, studies of the stability of forced

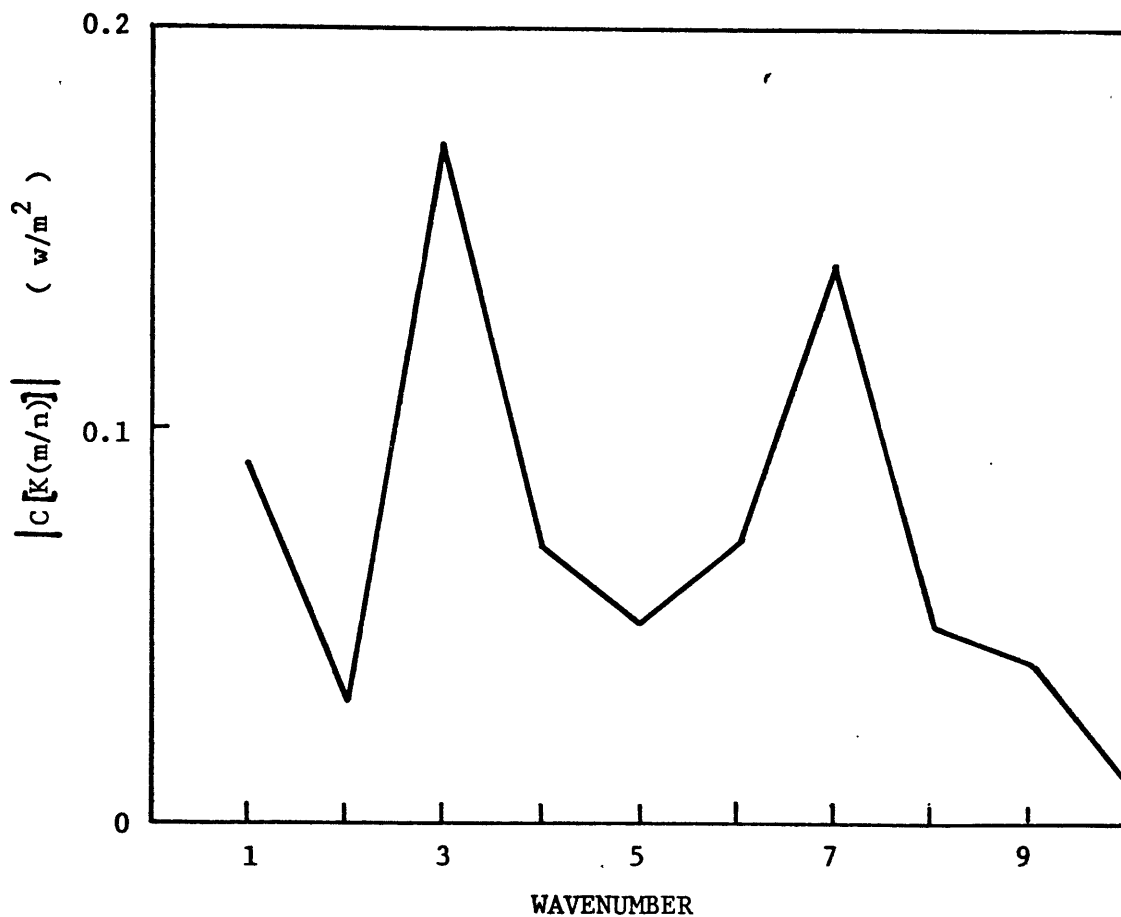


Fig. 1.6 Magnitude of conversion of kinetic energy from wavenumber m to n , summed from $m=1$ to 30 in winter, $|C [K(m/n)]|$.
(from Tenenbaum, 1976)

planetary scale waves will be justified.

The study of the stability of free planetary scale Rossby waves is of great interest aside from any insight it may give for the problem of the stability of stationary waves. In Chapter II, we will show that the neutral baroclinic Rossby wave in the 2-level model can be identified with slowly growing longwave modes, first discovered by Green (1960). Although these modes have small growth rates, they can attain large amplitudes. Gall (1976), in a numerical study using a general circulation model, examined the baroclinic instability of realistic zonal wind profiles. He found that long, deep baroclinic waves do attain much greater amplitudes than short, shallow waves. This is because the stabilizing effect of nonlinear wave-mean flow interaction occurs most rapidly in low levels and thus the short, shallow waves are affected more by non-linear effects. The "Green modes", being long, deep waves, can thus grow to finite amplitude. This is one possible source for the kinetic energy observed in planetary scale TE's. Whatever their source, these finite amplitude waves will affect the nature of the baroclinic stability problem. Thus from the point of view of having as realistic a basic state as possible, the stability of planetary scale Rossby wave is of interest in its own right.

The stability analysis of a non-axisymmetric basic state is also of importance because it provides a mechanism for selecting meridional scales. Simple models of baroclinic instability of a zonal flow (Charney 1947, Eady 1949, Phillips 1954) do not have any selection mechanism for the meridional scale of unstable baroclinic waves, as the most unstable mode has an infinite meridional scale. This difficulty is usually avoided

by placing walls at fixed latitudes so that the meridional scale is equal to this forced geometric scale. This artifice is unrealistic as there are no walls in the atmosphere. The meridional scale is also of crucial importance in finite amplitude dynamics of baroclinic waves. In Pedlosky's (1971) analysis of finite amplitude baroclinic instability is a 2-layer system with small dissipation, the meridional scale appears explicitly in the steady state wave amplitude. Studies by Kim (1975) and Pedlosky (1975a) have illustrated in two particular cases that the presence of a basic state wave leads to the selection of a finite meridional scale, in both cases of the order of the radius of deformation. Thus we will be particularly interested in examining the meridional scales selected in our stability analysis.

The stability of our basic flow to small perturbations will be examined using linear theory. The stability of non-axisymmetric flows has frequently been discussed in the literature. Lorenz (1972) examined the stability of the barotropic Rossby wave and applied the results to atmospheric predictability. Gill (1974) examined the same problem and identified Rayleigh instability and resonant triad regimes depending on the ratio of inertial to β -effects. Kim (1975) investigated the stability of the baroclinic Rossby wave as a means of generating energetic eddies in the ocean. These studies have no vertical shear in the zonal flow. For the investigation of our hypothesis, this is an unrealistic approximation as the zonal shear represents an important energy source for instabilities. Pedlosky (1975a) considered the stability of a baroclinic wave and a zonal flow at neutral stability as a mechanism for selection of meridional scale of motion. Merkin and Israeli (1978)

examined the stability of a stationary Rossby wave in a baroclinic zonal flow and applied the results to mountain induced cyclogenesis. Pedlosky's (1975a) basic wave is of synoptic scale and small amplitude. In Merkin and Israeli's (1977) study, the basic wave is of synoptic scale and the meridional wavenumber of the perturbation is fixed at one value. In our parameter study of the stability of Rossby waves in a baroclinic zonal flow, the basic wave will be of arbitrary scale with arbitrary amplitude; the meridional wavenumber will also be allowed to vary.

Chapter II presents the basic formulations of a 2-level quasi-geostrophic, mid-latitude β -plane model together with some exact, free solutions. The energetics and heat transport of SE's forced by realistic topography and diabatic heating are examined in Chapter III. Chapters IV and V present a parameter study of the stability of a Rossby wave in a baroclinic zonal flow. We present in Chapter VI some applications to the atmosphere, and the conclusions in Chapter VII.

II. BASIC FORMULATION

II-1. Basic equations in a two layer atmosphere

The synoptic and planetary scale waves of mid-latitudes can be described by the quasi-geostrophic system of equations. We assume the motion takes place in a cyclic zonal channel of width Y_0 in the y-direction and of length X_0 in the x-direction. The Coriolis parameter is assumed to have a constant meridional gradient, β , to take into account sphericity of the earth (Fig. 2.1.a). The governing equations in pressure co-ordinates are:

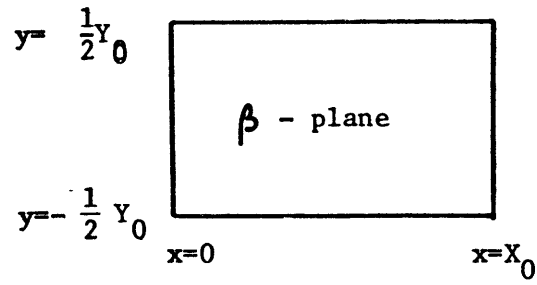
$$\frac{\partial}{\partial t} \nabla^2 \psi + J(\psi, \nabla^2 \psi + f) - f_0 \frac{\partial \omega}{\partial p} = 0 \quad (2.1)$$

$$\frac{\partial T}{\partial t} + J(\psi, T) - \sigma \omega = \frac{1}{c_p} H \quad (2.2)$$

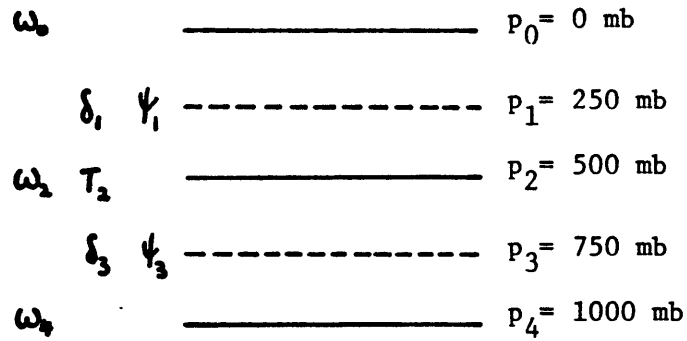
$$\frac{\partial \psi}{\partial p} = - \frac{RT}{f_0 p} \quad (2.3)$$

$$\delta = - \frac{\partial \omega}{\partial p} \quad (2.4)$$

In the above, t is time, p pressure, $J(A, B) = \frac{\partial A}{\partial x} \frac{\partial B}{\partial y} - \frac{\partial A}{\partial y} \frac{\partial B}{\partial x}$ the horizontal Jacobian, $f = f_0 + \beta y$ where f_0 is the Coriolis parameter at $45^\circ N$, ψ the geostrophic streamfunction for the horizontal flow, $\omega = \frac{dp}{dt}$ the vertical velocity, T the temperature, c_p the specific heat capacity at constant pressure, R the gas constant, $\sigma = - \left(\frac{\partial T}{\partial p} - \frac{RT}{c_p p} \right)$ the static stability, δ the horizontal divergence and H the diabatic heating due to ocean-land contrast.



(a)



(b)

Fig. 2.1 (a) Horizontal geometry of β -plane model.

(b) Vertical geometry of β -plane model.

The horizontal velocity field \underline{V} is geostrophic: $\underline{V} = \hat{k} \times \nabla \psi$ where \hat{k} is a unit vector in the vertical direction. The static stability is assumed to be constant. Equations (2.1)-(2.4) are the quasi-geostrophic vorticity equation, the thermodynamic equation, the hydrostatic equation and the continuity equation respectively. The boundary conditions are:

$$v = 0 \quad \text{at} \quad y = \pm \frac{1}{2} Y_0$$

$$\omega = 0 \quad \text{at} \quad p = 0, \quad \text{the top of the model atmosphere}$$

$$\omega = \frac{1}{2} g \cdot \nabla p_g - \frac{p_0 F}{2 f_0} b_g \quad \text{at} \quad p = p_0, \quad \text{the bottom of the model atmosphere}$$

ζ is the geostrophic vorticity and quantities with subscript g denote values at the bottom of the atmosphere. The first contribution to the surface vertical velocity is due to flow of air over surface topography where the standard pressure is p_g . The second contribution is due to viscosity in the Ekman layer which is taken into account by the use of a friction coefficient F , forcing a surface vertical velocity which balances Ekman convergence (Charney and Eliassen, 1949).

In the vertical direction, the atmosphere is divided into two layers of equal mass. As shown in Fig. 2.1b, we carry ψ , δ at levels 1 and 3; T , ω at level 2 and ω at the top and bottom of the atmosphere. Applying Eqs. (2.1) and (2.4) at levels 1 and 3, Eqs. (2.2) and (2.3) at level 2 and using linear interpolation for ψ_2 , we have

$$\frac{\partial}{\partial t} \nabla^2 \psi_1 + J(\psi_1, \nabla^2 \psi_1 + f) + f_0 \delta_1 = 0 \quad (2.5)$$

$$\frac{\partial}{\partial t} \nabla^2 \psi_3 + J(\psi_3, \nabla^2 \psi_3 + f) - f_0 \delta_3 = 0 \quad (2.6)$$

$$\frac{\partial}{\partial t} (\psi_1 - \psi_3) + J\left(\frac{\psi_1 + \psi_3}{2}, \psi_1 - \psi_3\right) - \frac{R}{f_0} \sigma_2 \omega_2 = \frac{R}{f_0 c_p} H \quad (2.7)$$

The boundary conditions become

$$v_1 = v_3 = 0 \quad \text{at} \quad y = \pm \frac{1}{2} Y_0$$

$$\omega_0 = 0 \quad \text{at} \quad p = 0$$

$$\omega_4 = \underline{V}_3 \cdot \underline{\nabla} p_3 - \frac{p_4 F}{2 f_0} b_4 \quad \text{at} \quad p = p_4$$

Linear extrapolation is used to give $b_4 = \nabla^2 \psi_4 = \nabla^2 \left(\frac{3}{2} \psi_3 - \frac{1}{2} \psi_1 \right)$ in the frictional component of the surface vertical velocity. It can be shown that \underline{V}_3 , rather than an extrapolated \underline{V}_4 , must be used in the topography component so that topography does not make a net contribution to the time rate of change of total energy.

We introduce the mean and thermal streamfunctions $\psi = \frac{1}{2} (\psi_1 + \psi_3)$, $\psi_T = \frac{1}{2} (\psi_1 - \psi_3)$. Adding and subtracting Eqs. (2.5) and (2.6) and rewriting in terms of ψ and ψ_T , we get

$$\frac{\partial}{\partial t} \nabla^2 \psi + J(\psi, \nabla^2 \psi + f) + J(\psi_T, \nabla^2 \psi_T) - \frac{f_0}{2 p_2} \omega_4 = 0 \quad (2.8)$$

$$\frac{\partial}{\partial t} \nabla^2 \psi_T + J(\psi, \nabla^2 \psi_T) + J(\psi_T, \nabla^2 \psi + f) - \frac{f_0}{2 p_2} (2\omega_2 - \omega_4) = 0 \quad (2.9)$$

Eliminate ω_2 between Eqs. (2.9) and (2.7) and let $\mu^2 = 2f_0^2 / R \sigma_2 p_2$ (μ^{-1} is the radius of deformation). We then obtain

$$\frac{\partial}{\partial t} (\nabla^2 - \mu^2) \psi_T + J(\psi, (\nabla^2 - \mu^2) \psi_T) + J(\psi_T, \nabla^2 \psi + f) + \frac{f_0}{2p_2} \omega_4 + \frac{f_0 H}{9 \sigma_2 p_2} = 0 \quad (2.10)$$

Equations (2.8) and (2.10), together with the appropriate boundary conditions, are the equations of interest.

In order to derive an energy equation for an adiabatic and frictionless atmosphere, it is more convenient to write Eqs. (2.8) and (2.10) in the following form:

$$\left\{ \frac{\partial}{\partial t} + J(\psi_1, \cdot) \right\} (\nabla^2 \psi_1 + f - \frac{1}{2} \mu^2 (\psi_1 - \psi_3)) = 0 \quad (2.11)$$

$$\left\{ \frac{\partial}{\partial t} + J(\psi_3, \cdot) \right\} (\nabla^2 \psi_3 + f + \frac{1}{2} \mu^2 (\psi_1 - \psi_3) - \frac{f}{p_2} p_3) = 0 \quad (2.12)$$

The above equations express the conservation of potential vorticity for each layer, with the effect of surface topography in the lower layer.

Multiplying Eq. (2.11) by ψ_1 and Eq. (2.12) by ψ_3 and adding, we get

$$\frac{d_1}{dt} (KE_1 + PE_1) + \frac{d_3}{dt} (KE_3 + PE_3) = \nabla \cdot \left\{ \psi_1 \frac{d_1}{dt} \nabla \psi_1 + \psi_3 \frac{d_3}{dt} \nabla \psi_3 - \frac{1}{2} (\psi_1^2 + \psi_3^2) \hat{k} \times \nabla (\beta y) + \frac{f}{2p_2} \psi_3^2 \hat{k} \times \nabla p_3 \right\} \quad (2.13)$$

where $\frac{d_i}{dt} = \frac{\partial}{\partial t} + J(\psi_i, \cdot)$ is the material derivative, $KE_i = \frac{1}{2} (\psi_{ix}^2 + \psi_{iy}^2)$ is the kinetic energy and $PE_i = \frac{1}{8} \mu^2 (\psi_i - \psi_3)^2 = PE_3$ is the potential energy for each layer ($i=1, 3$). For a bounded atmosphere with zero

normal velocity on the boundary, integration of Eq. (2.13) shows that the total energy of the bounded atmosphere is conserved:

$$\frac{\partial}{\partial t} \iint (KE_1 + KE_3 + PE_1 + PE_3) dx dy = 0$$

II-2. Free solutions of the basic equations

In the absence of friction, topography and diabatic forcing ($\omega_y = 0 = H$) solutions to Eqs. (2.8) and (2.10) exist of the form

$$\psi = -Uy + B \sin k(x-ct) \tag{2.14}$$

$$\psi_T = -U_T y + B_T \sin k(x-ct) \tag{2.15}$$

This solution describes zonally propagating Rossby waves in a zonal flow. Because of its simple structure, it is an exact solution to the governing nonlinear equations. The resulting dispersion relation is

$$\frac{k^2}{\beta}(U-c) = \frac{(2k^2+1) \pm (1+4k^2(k^2-1)\left(\frac{k^2 U}{\beta}\right)^2)^{1/2}}{2k^2(k^2+1)} ; \quad K^2 = \frac{k^2}{k^2} \tag{2.16}$$

The ratio of wave amplitudes is also determined:

$$\frac{B_T}{B} = \frac{1 - K^2 \frac{k^2}{\beta}(U-c)}{K^2 \frac{k^2 U}{\beta}} = \frac{1 - (K^2+1) \frac{k^2}{\beta}(U-c)}{(K^2-1) \frac{k^2 U}{\beta}} \tag{2.17}$$

For the Rossby waves to be non-growing, c must be real. This in turn requires the zonal shear not to exceed the "critical shear" for the 2-level model:

$$\frac{\mu^2 U_T}{\beta} \leq \frac{1}{2k^2 \sqrt{1-k^2}} = \left(\frac{\mu^2 U_T}{\beta} \right)_{\text{critical}} \quad (2.18)$$

This is shown in Fig. 2.2. The short waves ($1 < k^2$) do not have a critical shear and are always stable. However, the 2-level model is not really valid at such short wavelengths. Analysis of continuous analog of the 2-level model (Green, 1960) shows that the critical shear expressed by Eq. (2.18) actually represents a transition between conditions where the dominant unstable waves are long, deep waves and conditions where the dominant unstable waves are short, shallow waves. The 2-level model is capable of resolving only the former unstable modes. Held (1978), using scaling arguments, has shown that the vertically integrated kinetic energy and eddy sensible heat flux of a baroclinic wave are proportional to the cube of the wave height. Thus the long, deep waves, which are resolved by the 2-level model, are much more efficient at transporting heat poleward than the short, shallow waves.

Eqs. (2.16) and (2.17) provide two equations for the four quantities $\frac{\mu^2}{\beta}(U-c)$, $\frac{\mu^2 U_T}{\beta}$, k and B_T/β . The first two describe the zonal flow while the last two describe the Rossby wave. Specifying any two of these four quantities determine the other two, with an overall wave amplitude being arbitrary. In Figs. 2.3 and 2.4, we show the variation of the zonal flow for different wave properties, i.e., variation of

$$\frac{\mu^2}{\beta}(U-c) \quad \text{and} \quad \frac{\mu^2 U_T}{\beta} \quad \text{as a function of } B_T/\beta \quad \text{for}$$

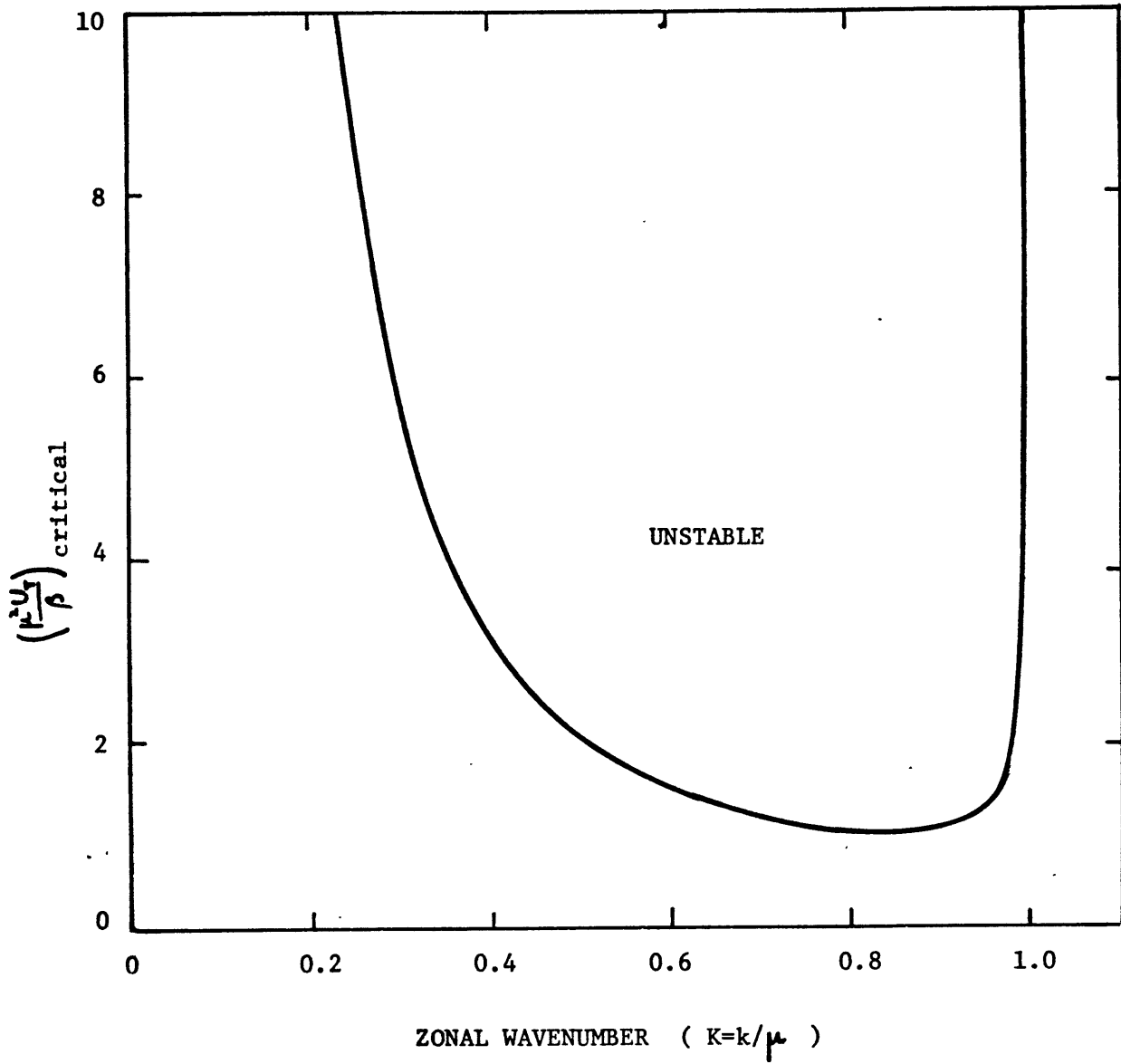


Fig. 2.2 Critical shear of the 2-level model as a function of zonal wavenumber.

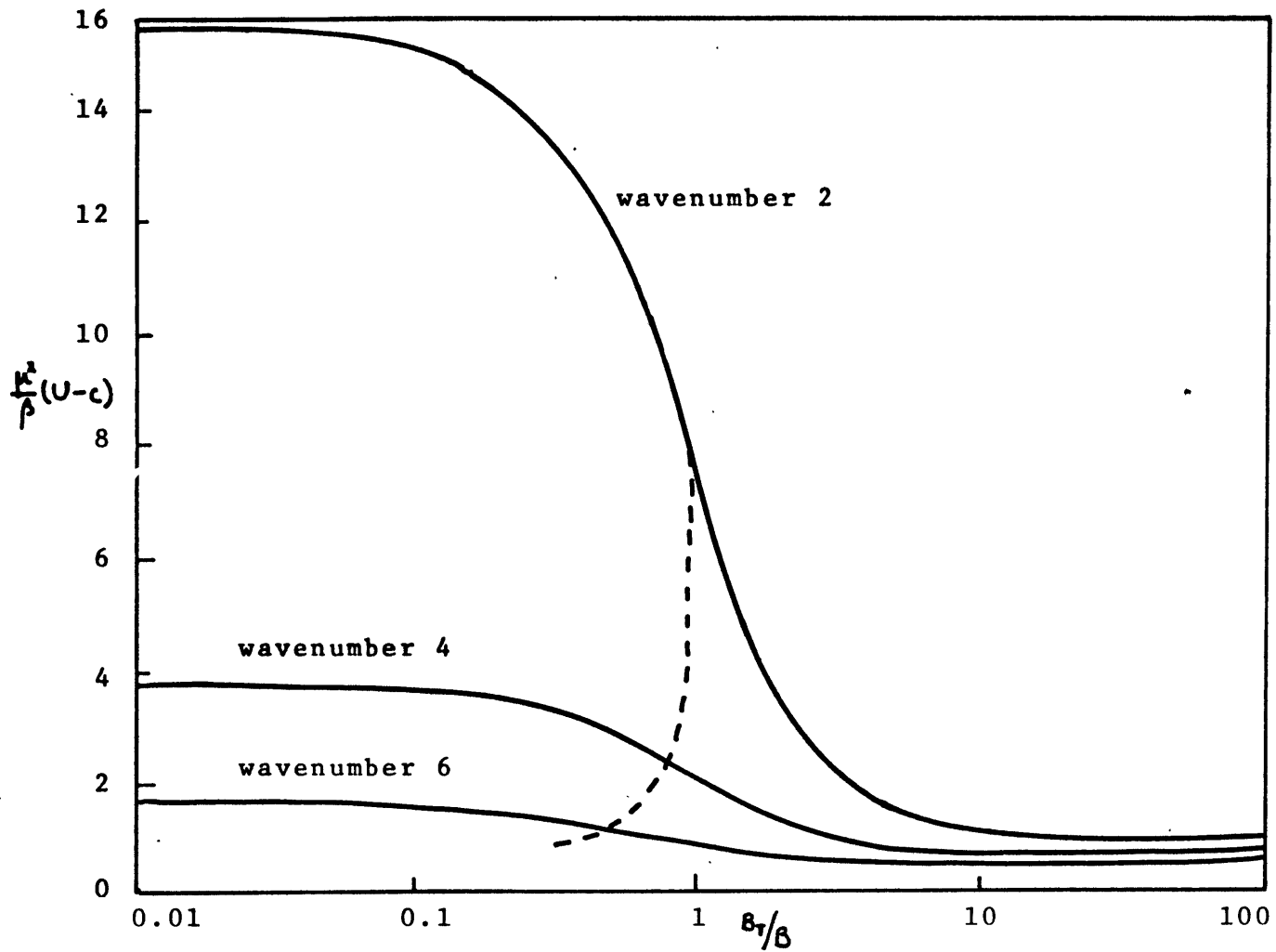


Fig. 2.3 The barotropic zonal flow ($\frac{K^2}{\rho}(U-c)$) as a function of B_1/B for Rossby waves of wavenumbers 2,4,6. The dashed curve represents critical conditions for different wavenumbers.

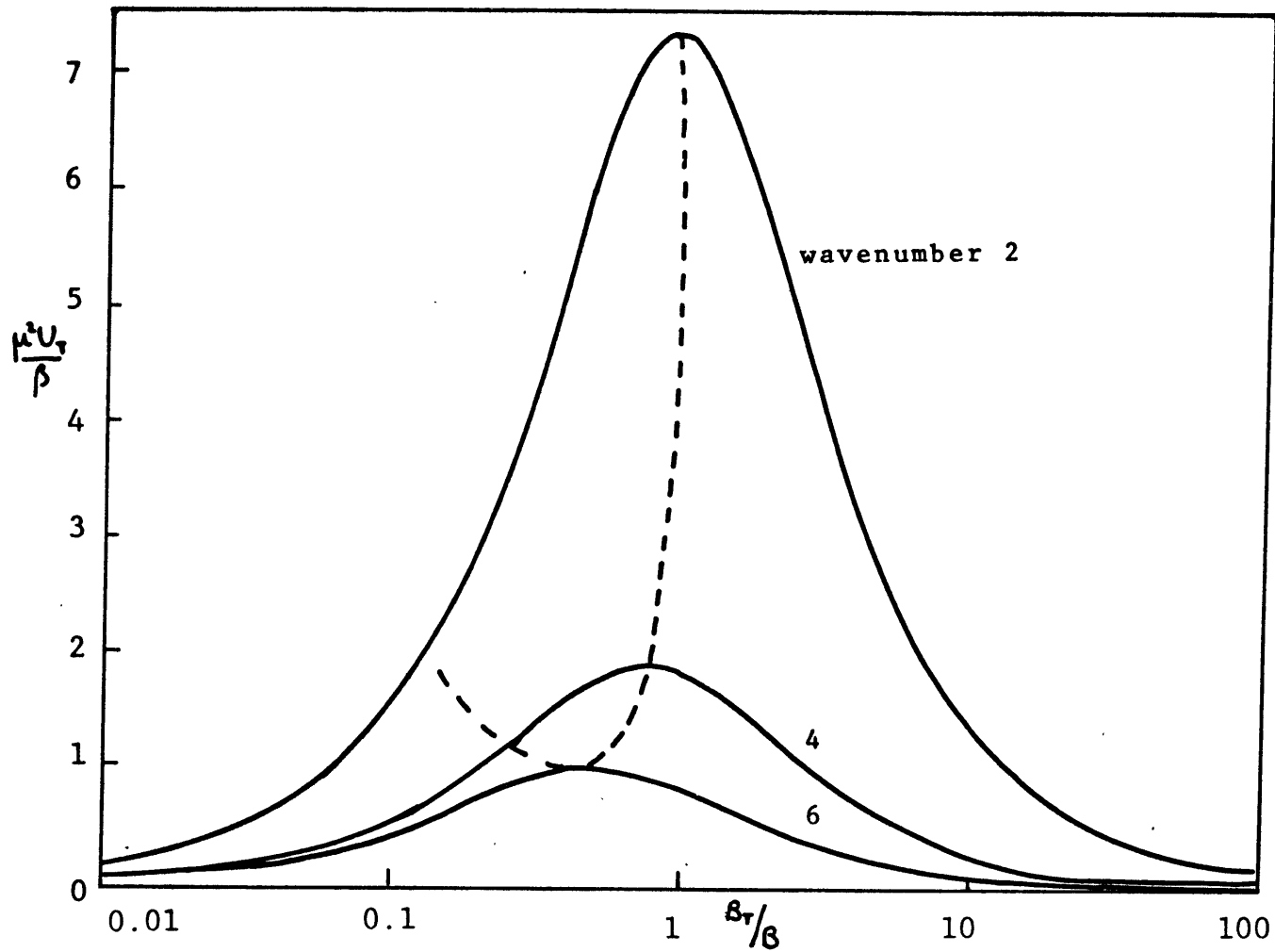


Fig. 2.4 The zonal shear ($\frac{u}{\beta}$) as a function of B_T/β for Rossby waves of wavenumbers 2,4,6. The dashed curve represents critical conditions for different wavenumbers.

different values of K . The three values of K shown correspond to wavenumbers 2,4,6 at midlatitudes. The value of the ordinate at the critical condition given by Eq. (2.18) for each wavenumber is shown by the dashed lines. Note for our choice of β_T/β and K as independent variables, the ordinate is a single-valued function of the abscissa. We see that for each wavenumber, the zonal shear is bounded by the corresponding critical shear, in order that the wave be stable to small perturbations. In the limits $\frac{\beta_T}{\beta} \rightarrow 0$ and $\frac{\beta_T}{\beta} \rightarrow \infty$, $\frac{k^2}{\beta}(U-c) \rightarrow \frac{1}{K^2}$ and $\frac{k^2}{\beta}(U-c) \rightarrow \frac{1}{K^2+1}$ respectively, while $\frac{k^2 U_T}{\beta} \rightarrow 0$ for both limits. These are the limiting pure barotropic and pure baroclinic Rossby waves respectively. Dimensionally, they are described by $\beta_T=0$, $U-c = \beta/k^2$ and $\beta=0$, $U-c = \beta/k^2 \cdot \mu^2$ respectively, and both have $U_T=0$. For non-zero values of the zonal shear, the wave consists of both barotropic and baroclinic components.

Condition (2.18) is identical to the condition for convergence of the expansion of the radical in Eq. (2.16). Thus for stable waves, we have from Eq. (2.16) for the negative and positive roots:

$$\frac{k^2}{\beta}(U-c) = \begin{cases} \frac{1}{K^2+1} + K^2(1-K^2)\left(\frac{k^2 U_T}{\beta}\right)^2 \dots\dots\dots (-) \\ \frac{1}{K^2} - K^2(1-K^2)\left(\frac{k^2 U_T}{\beta}\right)^2 \dots\dots\dots (+) \end{cases} \quad (2.19)$$

while Eq. (2.17) gives

$$\frac{\beta}{\beta_T} = K^2(K^2+1)\frac{k^2 U_T}{\beta} \dots\dots\dots (-)$$

$$\frac{\beta_T}{\beta} = K^2(1-K^2)\frac{k^2 U_T}{\beta} \dots\dots\dots (+) \quad (2.20)$$

With no zonal shear, the negative and positive roots correspond to the pure baroclinic and barotropic Rossby waves respectively. Thus in general, we may term the negative root as the baroclinic mode and the positive root as the barotropic mode. Eqs. (2.19) and (2.20) give the corrections to the pure baroclinic and barotropic modes due to zonal shear, to lowest order in zonal shear.

Fig. 2.5 shows the variation of $\frac{k^2}{\beta}(U-c)$ with k according to Eq. (2.16), for fixed values of the zonal shear. The heavy curve labelled "critical" corresponds to the zonal shear being the critical shear. This curve separates the baroclinic mode (negative root) and the barotropic mode (positive root). The two modes for $\frac{k^2 U}{\beta} = 0$ and $\frac{k^2 U}{\beta} = 1$ are also shown, together with the lowest order approximation given by Eq. (2.19) for the case $\frac{k^2 U}{\beta} = 1$. The case $\frac{k^2 U}{\beta} = 1$ corresponds to the zonal shear being the minimum critical shear. It is of special interest as the atmosphere has a zonal shear close to this value (Moura and Stone, 1976). Fig. 2.6 shows B_T/β versus k for the baroclinic and barotropic modes of $\frac{k^2 U}{\beta} = 1$, together with the critical curve which separates the two modes. The lowest order approximations given by Eq. (2.20) are also shown. Note that except for short wavelengths $k \approx 1$, the baroclinic and barotropic modes have $\frac{B_T}{\beta} > 1$ and $\frac{B_T}{\beta} < 1$ respectively, thus justifying the classifications "baroclinic" and "barotropic". The lowest order approximations work well, especially for low wavenumbers. Thus Eqs. (2.19) and (2.20) may be regarded as longwave expansions.

Lindzen et al (1968) studied the effects of the upper boundary condition $\omega = 0$ at some finite height in continuous and finite difference

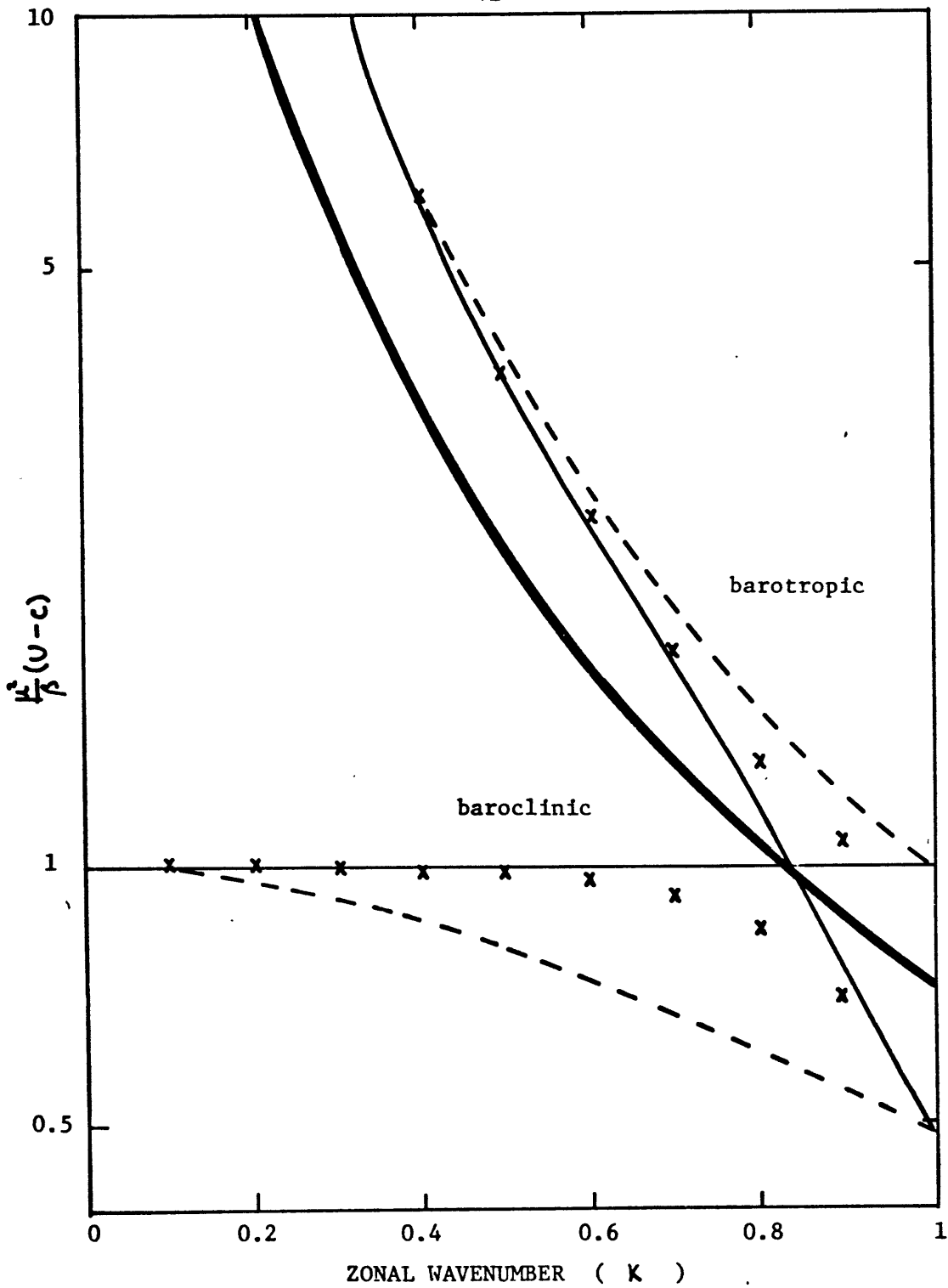


Fig. 2.5 $K^2(u-c)/\beta$ as a function of zonal wavenumber (K) of Rossby wave, for zonal shears $K^2u/\beta = 0$ (dashed) and $K^2u/\beta = 1$ (solid). Both baroclinic and barotropic modes are shown. Crosses denote lowest order approximation for the case $K^2u/\beta = 1$. Heavy curve corresponds to critical conditions and separates baroclinic and barotropic modes.

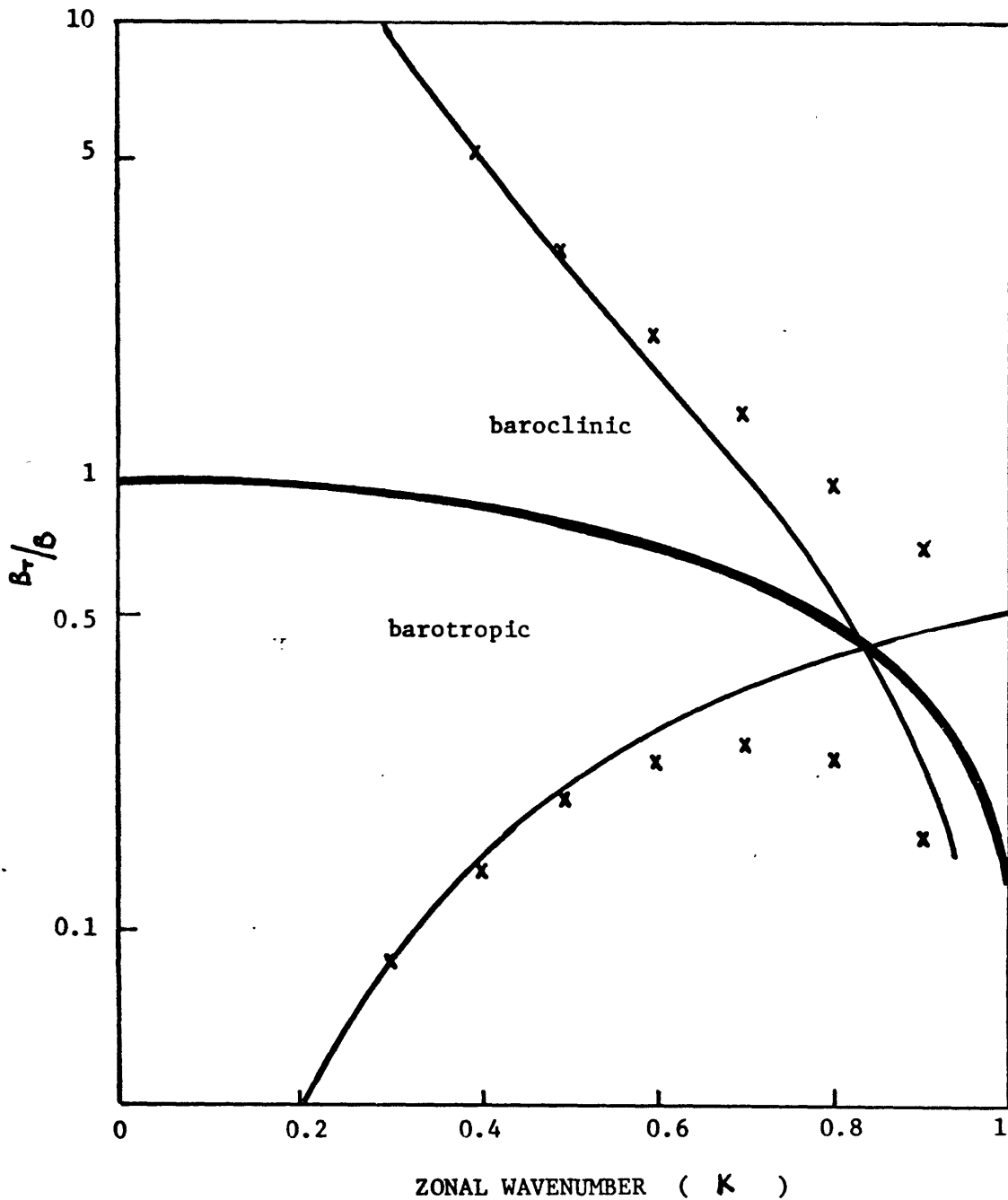


Fig. 2.6 B_T/B as a function of zonal wavenumber (K) of Rossby wave, for zonal shear $\mu^2 U_1/\beta = 1$. Crosses denote lowest order approximation. Heavy curve corresponds to critical conditions.

models of free and forced linear oscillations. Their basic atmosphere was rotating, isothermal and quiescent. Comparisons with results obtained from an unbounded atmosphere with the radiation condition or boundedness as upper boundary condition indicated spurious oscillations were generated due to reflection at the upper boundary. In particular, for the 2-level model, the only non-spurious free oscillation was found to be the pure barotropic Rossby wave. However, Charney and Drazin (1961) showed that stationary, small amplitude, adiabatic and quasi-geostrophic waves in a uniform zonal flow can propagate energy vertically only when the zonal flow is westerly and less than some critical velocity. Thus the use of realistic atmospheric zonal winds, instead of the resting basic state used by Lindzen et al (1968) may prevent forced waves from reaching the upper boundary. Kirkwood and Derome (1977) investigated this problem by examining the forced wavenumber 1 response in a high resolution reference model (200 vertical levels) with radiation condition at a finite height as upper boundary condition, and a layer model (101 to 6 levels) with the upper boundary condition $\omega = 0$ at $p = 0$ (the P model). Realistic vertical zonal wind profiled for different seasons, together with Newtonian cooling which varied with height and which had a maximum at 50 km, were used. For winter, it was found that the strong upper level westerlies acted as a reflecting medium and results of the sufficiently high resolution P model agreed well with those of the reference model. In other words, as long as the upper level westerlies were resolved, the rigid lid upper boundary condition did not have much effect as little energy was able to penetrate up to that level anyway. For spring, the weak, westerly zonal winds did not inhibit the vertical propagation of energy, but the damping effect of Newtonian cooling prevented the wave from reaching the

top boundary with significant amplitude. Thus the P model with adequate resolution again minimized the effects of the upper rigid lid.

Our model has only two vertical levels and is not able to model the stratospheric westerlies or the Newtonian cooling maximum. However, the use of a rigid lid as an upper boundary condition may be thought of as a strongly reflecting or dissipative winter stratosphere. Indeed, more refined calculations than the 2-level model have shown the existence of the counterpart of the baroclinic Rossby wave of the 2-level model.

Fullmer (1979) examined the baroclinic instability of one dimensional basic states using a β -plane quasi-geostrophic model. His model had 48 levels in the vertical with the troposphere extending from 1000 to 250 mb and the stratosphere from 250 to 0 mb. The upper boundary condition used is vanishing perturbation streamfunction amplitude at the top of the model atmosphere. Slowly growing, long wave modes, first discovered by Green (1960), were found using a basic state with the static stability of the stratosphere fifty times of the troposphere and a linear shear zonal wind which vanished at the ground and reached 24 m/sec at 250 mb. The ratio of static stabilities of the stratosphere and troposphere is realistic for mid-latitude winter conditions; the zonal wind profile is also realistic in the troposphere. The doubling time of these

"Green modes" is over 10 days. Fig. 2.7 shows the phase speed of these modes as a function of zonal wavenumber, together with the phase speed of the baroclinic Rossby wave in the 2-level model with the corresponding values of tropospheric static stability and barotropic and baroclinic zonal flow components. We see that the phase speeds agree well for long wavelengths. The vertical structure of the streamfunction phase for the fastest growing Green mode is shown in Fig. 2.8. There is an abrupt

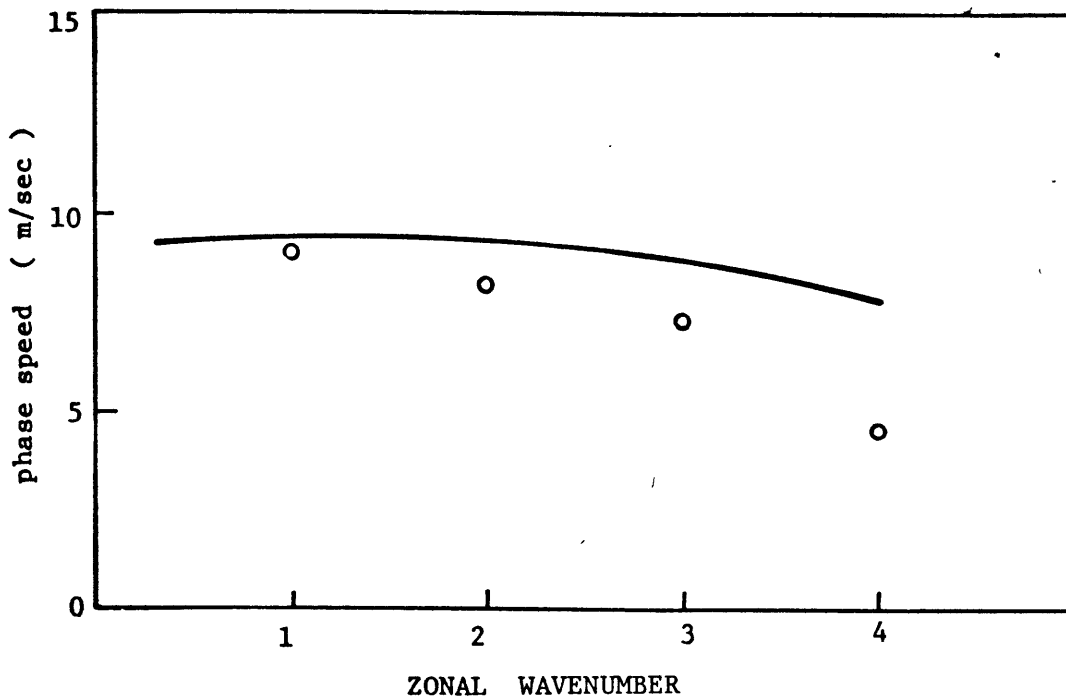


Fig. 2.7 Comparison of phase speeds of Green modes obtained with linear vertical shear of basic zonal wind and stratospheric static stability fifty times that of the troposphere (o ; from Fullmer, 1979), and phase speeds of the neutral baroclinic Rossby wave in the two level model with comparable basic flow parameters (curve).

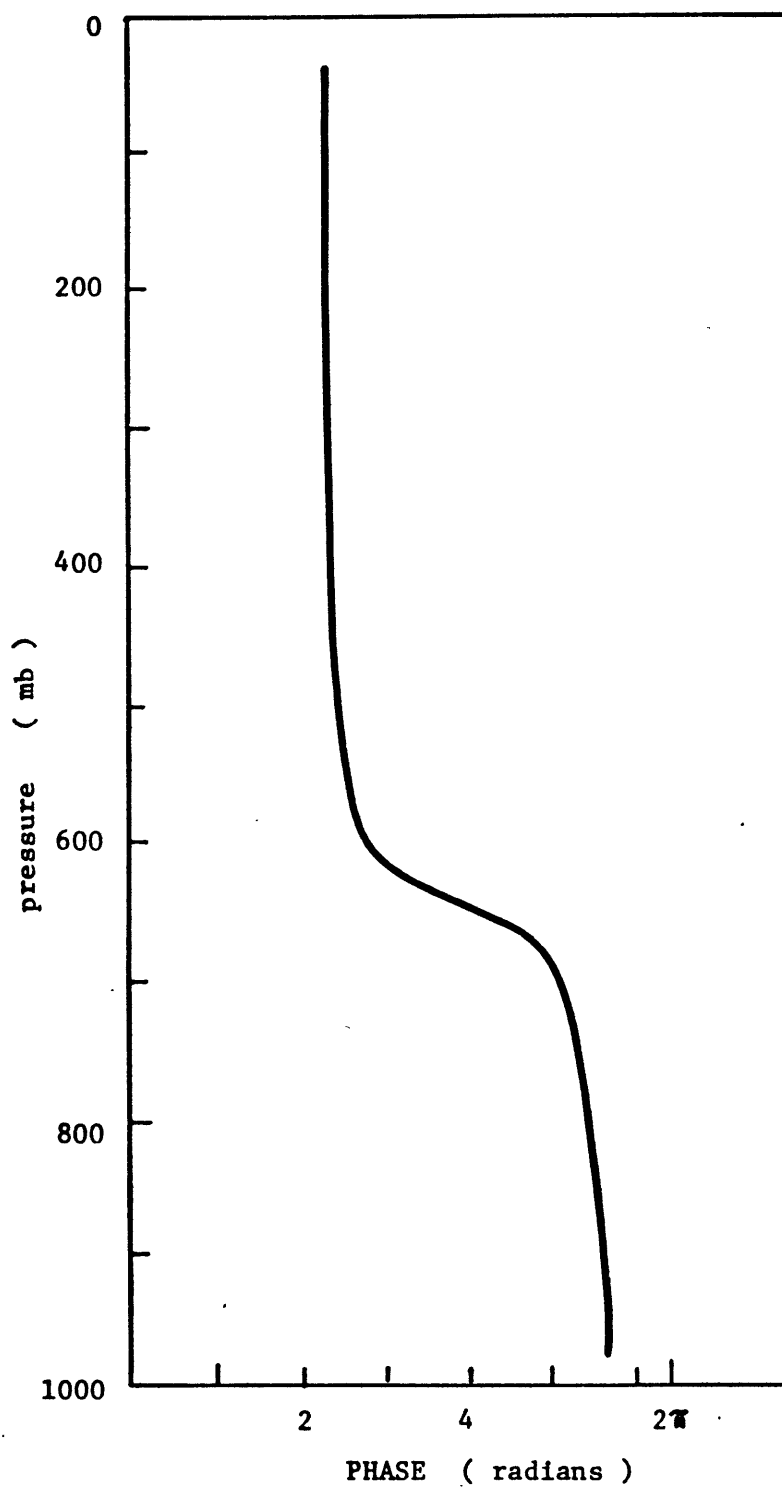


Fig. 2.8 Vertical structure of streamfunction phase for the fastest growing Green mode. Basic flow parameters as in Fig. 2.7. (from Fullmer, 1979)

phase shift of approximately π radians at 650 mb, much like the baroclinic Rossby wave which has the upper and lower level streamfunctions out of phase with each other by 180° .

The 2-level model is not able to model the stratosphere but as we discussed earlier, the use of a rigid lid as an upper boundary condition is analogous to a strongly reflecting or dissipative winter stratosphere. The good agreement of the phase speed and vertical structure of the Green mode in a high vertical resolution model and the baroclinic Rossby wave in a 2-level model suggests that the latter can be identified with a Green mode.

III. HEAT TRANSPORT BY STATIONARY WAVES

In this section, we examine the energetics and heat transport properties of stationary waves forced by realistic topography and diabatic forcing in winter. The latter are taken from Derome and Wiin-Nielsen (1971), hereafter referred to as DWN, who Fourier analyzed Berkofsky and Bertoni's (1955) topographic field and Brown's (1964) heating field. These were shown in Fig. 1.4. DWN found topographically forced waves do not transport heat, while diabatically forced waves transport heat only when friction is present. Quasi-resonance resulted when the zonal scale of the topographic forcing was close to the wavelength of stationary Rossby waves, which are a solution to the unforced problem. Taking winter conditions, the calculated perturbation heights of the 250, 500 and 750 mb surfaces agreed well with observations. Following DWN, we represent the forced stationary waves by Fourier series in the zonal direction with a sinusoidal meridional structure. The heating (H), standard pressure due to surface topography (P_g), mean and thermal streamfunctions (Ψ, Ψ_T) which consist of a zonal flow and forced waves, are expressed as:

$$H = \cos \lambda y \sum_{n=1}^N (Q_n \cos k_n x + T_n \sin k_n x) \quad (3.1a)$$

$$P_g = \cos \lambda y \sum_{n=1}^N (R_n \cos k_n x + S_n \sin k_n x) \quad (3.1b)$$

$$\Psi = -U_y + \bar{\Psi} = -U_y + \cos \lambda y \sum_{n=1}^N (A_n \cos k_n x + B_n \sin k_n x) \quad (3.1c)$$

$$\Psi_T = -U_T y + \bar{\Psi}_T = -U_T y + \cos \lambda y \sum_{n=1}^N (A_{Tn} \cos k_n x + B_{Tn} \sin k_n x) \quad (3.1d)$$

$k_n = n/a \cos \varphi_0$ is the zonal wavenumber, a and φ_0 being the radius of the earth and 45°N respectively; λ is the meridional wavenumber, x and y represent linear distance to the east and north respectively. The meridional wavelength is taken to be 60° latitude. Wavenumbers 1 through 18 are kept in the summation, i.e. $N = 18$. Substituting eqs. (3.1) into eqs. (2.8) and (2.10), we obtain upon linearization about the zonal flow a system of algebraic equations for the amplitudes A_n B_n A_{Tn} and B_{Tn} . It may formally be written as:

$$\begin{pmatrix} M_n & N \\ N & -M_n \end{pmatrix} \begin{pmatrix} X_n \\ Y_n \end{pmatrix} = \begin{pmatrix} G_n \\ H_n \end{pmatrix} \quad (3.2)$$

where

$$M_n = Uk_n \begin{pmatrix} m_{11} & m_{12} \\ m_{21} & m_{22} \end{pmatrix} = Uk_n \begin{pmatrix} \beta/k_n^2 + \lambda^2 - 1 & -U \\ U(1 - \frac{\lambda^2}{k_n^2 + \lambda^2}) & 1 - \frac{\beta/k_n^2 + \lambda^2}{U} + \frac{\lambda^2}{k_n^2 + \lambda^2} \end{pmatrix}$$

$$N = \frac{1}{2}F \begin{pmatrix} 1 & -2 \\ 1 & -2 \end{pmatrix} \quad X_n = \begin{pmatrix} A_n \\ A_{Tn} \end{pmatrix} \quad Y_n = \begin{pmatrix} B_n \\ B_{Tn} \end{pmatrix}$$

$$G_n = \mathcal{A}_n \begin{pmatrix} \sin \theta_{Tn} \\ \sin \theta_{Tn} - r_n \cos \theta_{Hn} \end{pmatrix} \quad H_n = \mathcal{A}_n \begin{pmatrix} -\cos \theta_{Tn} \\ -\cos \theta_{Tn} - r_n \sin \theta_{Hn} \end{pmatrix}$$

$a_{Hn} = \sqrt{Q_n^2 + T_n^2}$ and $\theta_{Hn} = \tan^{-1}(Q_n/T_n)$ are the amplitude and phase of each wavenumber of the diabatic forcing; similarly, $a_{Tn} = \sqrt{R_n^2 + T_n^2}$ and $\theta_{Tn} = \tan^{-1}(R_n/S_n)$ are the amplitude and phase of the

topographic forcing; $A_n = \frac{f_0}{2\rho_2} (U - U_T) \frac{k_n}{k_n^2 + \lambda^2} a_{Tn}$ is a measure of the vertical velocity forced by topography alone; $B_n = \frac{2a_{Hn}/c_p \sigma_2}{(U - U_T) k_n a_{Tn}}$ is a measure of the ratio of vertical velocities forced by diabatic heating and topography. Eqs. (3.2) are identical to those solved by DWN, except we have used an energy-conserving extrapolation for the topographic surface vertical velocity; DWN used an extrapolation obtained from the hydrostatic equation. DWN did not evaluate the heat transport and energetics of the forced stationary waves.

If we assume the determinant of M_n does not vanish, i.e. free frictionless Rossby waves are suppressed, then solutions to Eqs. (3.2) can be written as

$$Y_n = M_n^{-1} (D_n^2 + I)^{-1} (D_n G_n - H_n) \quad (3.3a)$$

$$X_n = M_n^{-1} (D_n^2 + I)^{-1} (D_n H_n + G_n) \quad (3.3b)$$

where $D_n = N M_n^{-1}$. Note D_n has dimension of F/Uk_n which is dimensionless. Let $\Delta_n = m_{11} m_{22} - m_{12} m_{21} = \frac{1}{Uk_n}$ determinant (M_n). Then eqs. (3.3) become

$$\underline{J}_{Tn} = \begin{pmatrix} A_{Tn} \\ B_{Tn} \end{pmatrix} = \underline{I}_{Tn} + \underline{H}_{Tn} \quad (3.4a)$$

$$\underline{J}_n = \begin{pmatrix} A_n \\ B_n \end{pmatrix} = \underline{I}_n + \underline{H}_n \quad (3.4b)$$

where

$$\underline{I}_{Tn} = \frac{\alpha_n}{Uk_n} \frac{m_{11} - m_{21}}{f^2(d_1 + d_2)^2 + \Delta_n^2} \left\{ \begin{pmatrix} -f(d_1 + d_2) \\ \Delta_n \end{pmatrix} \cos \theta_{Tn} + \begin{pmatrix} \Delta_n \\ f(d_1 + d_2) \end{pmatrix} \sin \theta_{Tn} \right\}$$

$$\underline{H}_{Tn} = \frac{\alpha_n \Delta_n}{Uk_n} \frac{1}{f^2(d_1 + d_2)^2 + \Delta_n^2} \left\{ \begin{pmatrix} -m_n \Delta_n - (d_1 + d_2) f^2 \\ (-m_{11} + m_{21}) f d_2 \end{pmatrix} \cos \theta_{Hn} + \begin{pmatrix} (-m_n + m_{21}) f d_2 \\ m_{11} \Delta_n + (d_1 + d_2) f^2 \end{pmatrix} \sin \theta_{Hn} \right\}$$

$$\underline{I}_n = \frac{\alpha_n}{Uk_n} \frac{m_{22} - m_{12}}{f^2(d_1 + d_2)^2 + \Delta_n^2} \left\{ \begin{pmatrix} -f(d_1 + d_2) \\ \Delta_n \end{pmatrix} \cos \theta_{Tn} + \begin{pmatrix} \Delta_n \\ f(d_1 + d_2) \end{pmatrix} \sin \theta_{Tn} \right\}$$

$$\underline{H}_n = \frac{\alpha_n \Delta_n}{Uk_n} \frac{1}{f^2(d_1 + d_2)^2 + \Delta_n^2} \left\{ \begin{pmatrix} m_n \Delta_n - 2(d_1 + d_2) f^2 \\ (-m_{22} + m_n) f d_2 \end{pmatrix} \cos \theta_{Hn} + \begin{pmatrix} (-m_{22} + m_n) f d_2 \\ -m_{22} \Delta_n + 2(d_1 + d_2) f^2 \end{pmatrix} \sin \theta_{Hn} \right\}$$

In the above $f = \frac{1}{2} F / Uk_n$, $d_1 = m_{22} + 2m_{21}$, $d_2 = -m_{12} - 2m_{11}$.

The non-dimensional parameter f is a measure of the ratio of advective time scale to dissipative time scale. The solutions \underline{J}_m and \underline{I}_n are composed of a topographic component (\underline{I}_{Tn} , \underline{I}_n) and a diabatic component (\underline{H}_{Tn} , \underline{H}_n). They are additive because eqs. (3.2) are linear. Aside from the factor α_n / Uk_n , all the variables are non-dimensional. Friction keeps the solution finite even in the limit $\Delta_n \rightarrow 0$, i.e. resonance is not achieved. Changing the phase of the forcing for a particular wavenumber rotates the vectors \underline{I}_{Tn} , \underline{H}_{Tn} , \underline{I}_n and \underline{H}_n and leaves their amplitude unchanged.

The meridional heat transport by the stationary waves is

$$[\bar{v}^* \bar{T}^*] = \frac{f_0}{R} \cos^2 \lambda_y \sum_{n=1}^M k_n (B_n A_{Tn} - A_n B_{Tn}) \quad (3.5)$$

We see that there is non-zero heat transport only if the streamlines tilt with height. For a single wavenumber k_n , the magnitude of the transport depends on the quantity

$$|B_n A_{Tn} - A_n B_{Tn}| = |\underline{J}_{Tn} \times \underline{J}_n| = |\underline{J}_{Tn}| \cdot |\underline{J}_n| \cdot |\sin \gamma_n|$$

where γ_n is the angle between \underline{J}_{Tn} and \underline{J}_n . Note $|\sin \gamma_n|$ is the absolute value of the correlation coefficient for meridional heat transport; its sign depends on the direction of $\underline{J}_{Tn} \times \underline{J}_n$: it is positive if $\underline{J}_{Tn} \times \underline{J}_n$ is along the positive z-direction. As \underline{I}_{Tn} is always parallel to \underline{I}_n , $\underline{I}_{Tn} \times \underline{I}_n$ vanishes and thus topographic waves transport no heat. For diabatic waves, $f = 0$ (no friction) gives \underline{H}_{Tn} parallel to \underline{H}_n , i.e. no heat transport. Thus heat transport by diabatic waves is frictionally induced. The phase of the forcing does not affect this heat transport, as it depends only on $|\underline{H}_{Tn}|$, $|\underline{H}_n|$ and the angle between \underline{H}_{Tn} and \underline{H}_n .

In Figs. 3.1 and 3.2, we show the effect of friction on wave amplitude vectors for topographic and diabatic waves for zonal wavenumber 2 and realistic winter values for the other parameters. The phase of the forcing is 0° and non-dimensional amplitudes are shown. For topographic waves,

\underline{I}_{T_2} is parallel to \underline{I}_2 , as noted earlier. Increasing friction decreases the wave amplitude. This is because topographic forcing, like friction, is a surface forcing; thus a large friction implies topography is negligible and it acts as a purely dissipative mechanism. For diabatic waves, increasing friction actually increases the wave amplitude until an asymptotic value is reached. This is due to the non-surface nature of the diabatic forcing in the 2-level model. A particular value of the friction maximizes $|\underline{H}_{T_2} \times \underline{H}_2|$, i.e. the heat transport; for the values of parameters chosen, this occurs when $F/uk_2 \approx 12$. However, this may not be realistic in view of the wave amplitude behavior at large friction.

In Fig. 3.3, we show heat flux as a function of longitude of stationary waves forced by realistic topographic and winter diabatic fields (shown in Fig. 1.4). For comparison, the observed stationary wave heat flux distribution for the troposphere, averaged over January 1973, 1974 and 1975 is shown in Fig. 3.4. The latter was calculated from National Meteorological Center (NMC) data at the Goddard Institute of Space Studies. The observed distribution is characterized by three zones of strong northward heat transport: eastern Asia (90°E - 150°E), central and eastern Pacific (175°E - 135°W) and eastern North America and the Atlantic (90°W - 10°W). The positions of the first two zones are reproduced well, but the third is displaced about 10° latitude to the south. The intensity of each zone is modelled poorly: the first zone is much stronger than observed while the other two are weaker; agreement is better for the third zone. Areas of large negative (southward) heat flux present in the model calculation are not present in the

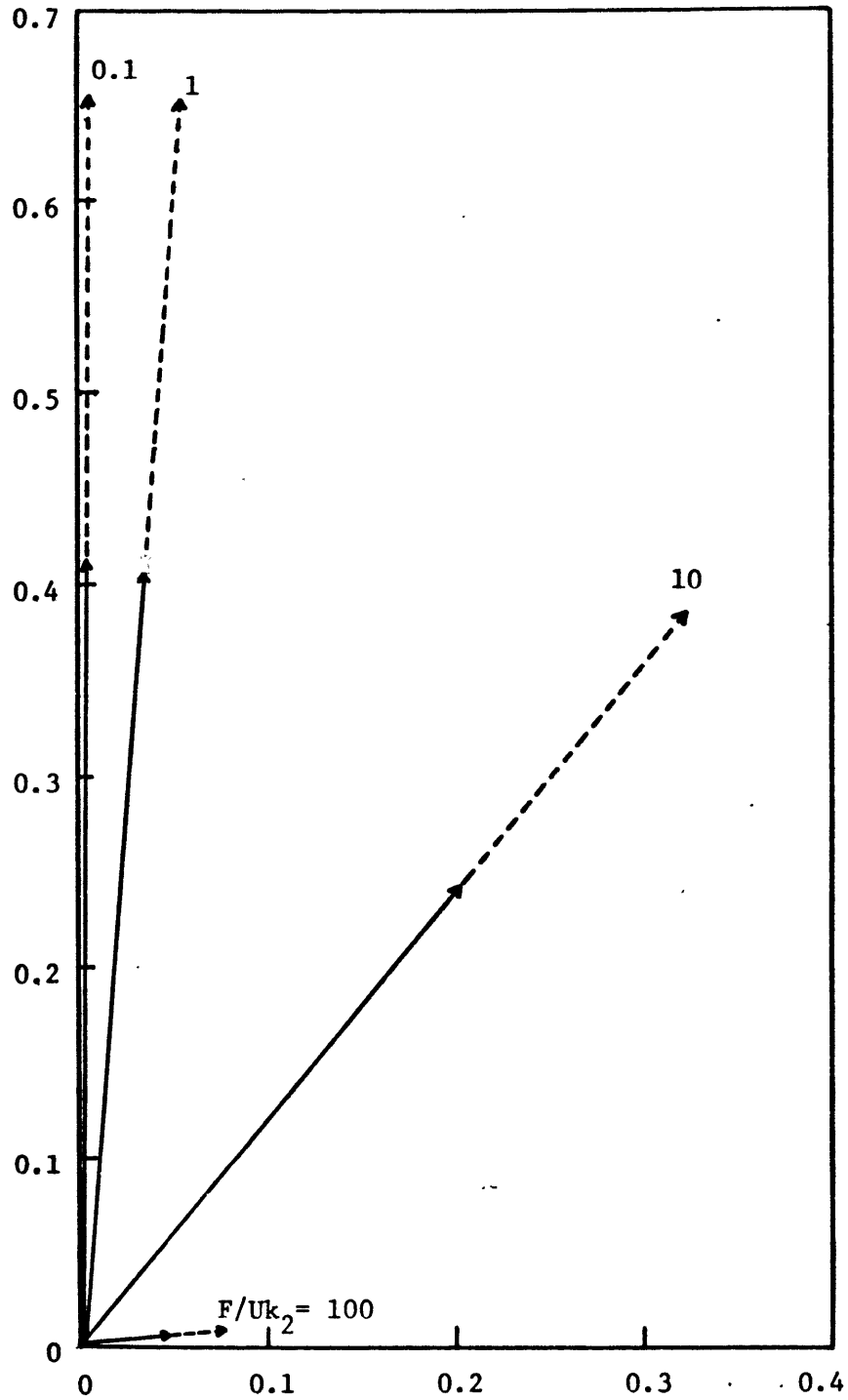


Fig. 3.1 Effects of friction ($F/Uk_2 = 0.1, 1, 10, 100$) on non-dimensional topographic wavenumber $2.2 U k_2 I_T / A_2$ denoted by solid line, $U k_2 I / A_2$ denoted by dashed line. Parameter values are $U = 15 \text{ m/sec}$, $U_T = 5 \text{ m/sec}$, $\lambda = k_2$, $\mu^2 = 3 \times 10^{-12} \text{ m}^{-2}$.

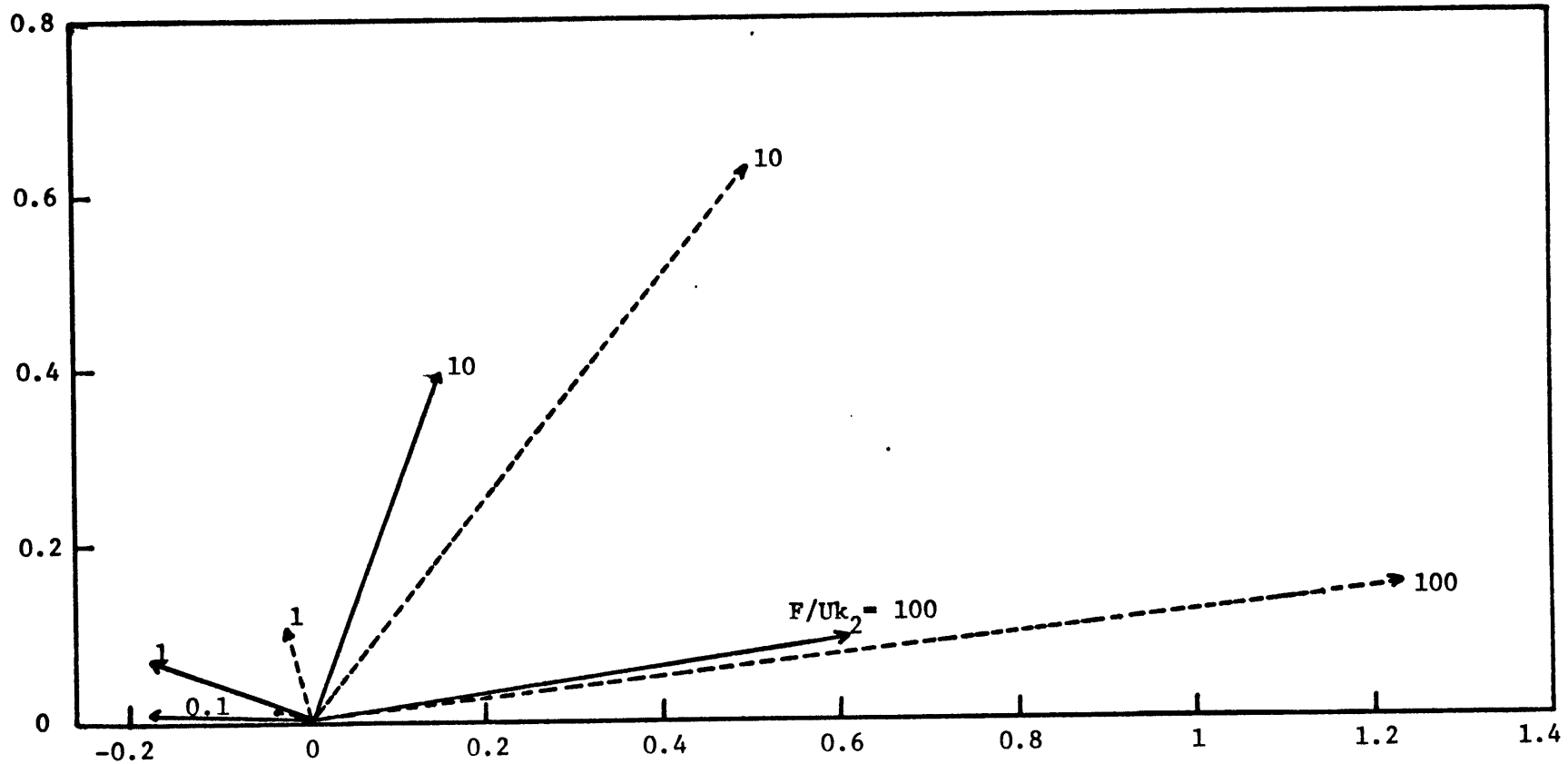


Fig. 3.2 Effects of friction ($F/Uk_2 = 0.1, 1, 10, 100$) on non-dimensional diabatic wavenumber 2. $Uk_2 H_T / N_2 S_2$ denoted by solid line, $Uk_2 H / N_2 S_2$ denoted by dashed line. Parameter values as in Fig. 3.1.

observed distribution. The latitudes of maximum heat transport agree only for the Asian and Pacific zones. The NMC data are for January only and may not be representative of a typical winter. Haines and Winston (1963) examined the spatial distribution of monthly mean meridional sensible heat flux for a period of 3 1/2 years. They found the poleward heat flux across latitude 45°N (where the zonally averaged flux is maximum) in winter is dominated by the above zones also. However, for each of the four winters examined, they found the eastern Asia zone to be the most intense, which agrees with our results. The theoretical and observed zonally averaged heat transport are shown in Fig. 3.5. The latter is taken from Oort and Rasmusson (1971). The transport is underestimated at all latitudes especially poleward of 45°N. The maximum heat transport is about a factor of two smaller than the observed value and is located about 8° too far south.

The spectra of the northward heat transport ($[\bar{v}'\bar{T}']$) and the correlation coefficient ($\rho = [\bar{v}'\bar{T}'] / \sqrt{[\bar{v}'^2]} \cdot \sqrt{[\bar{T}'^2]}$) are shown in Fig. 3.6. For ease of visualisation, absolute values of negative values are shown. The calculated transport is dominated by wavenumber 2. This is not surprising as the forcing is strongest at that scale. The agreement with the observations at 850 mb, 40°N is good for wavenumber 1, fair for wavenumber 2 and poor for wavenumber 3. The correlation coefficient is generally small (≤ 0.5), except for wavenumbers 8 and 13, which transport almost no heat. The overall correlation of the 18 wavenumbers is 0.17. The observed value is 0.59 at 50°N and is above 0.50 in mid-latitudes in winter (Oort and Rasmusson, 1971). Thus the model stationary waves are much less efficient at

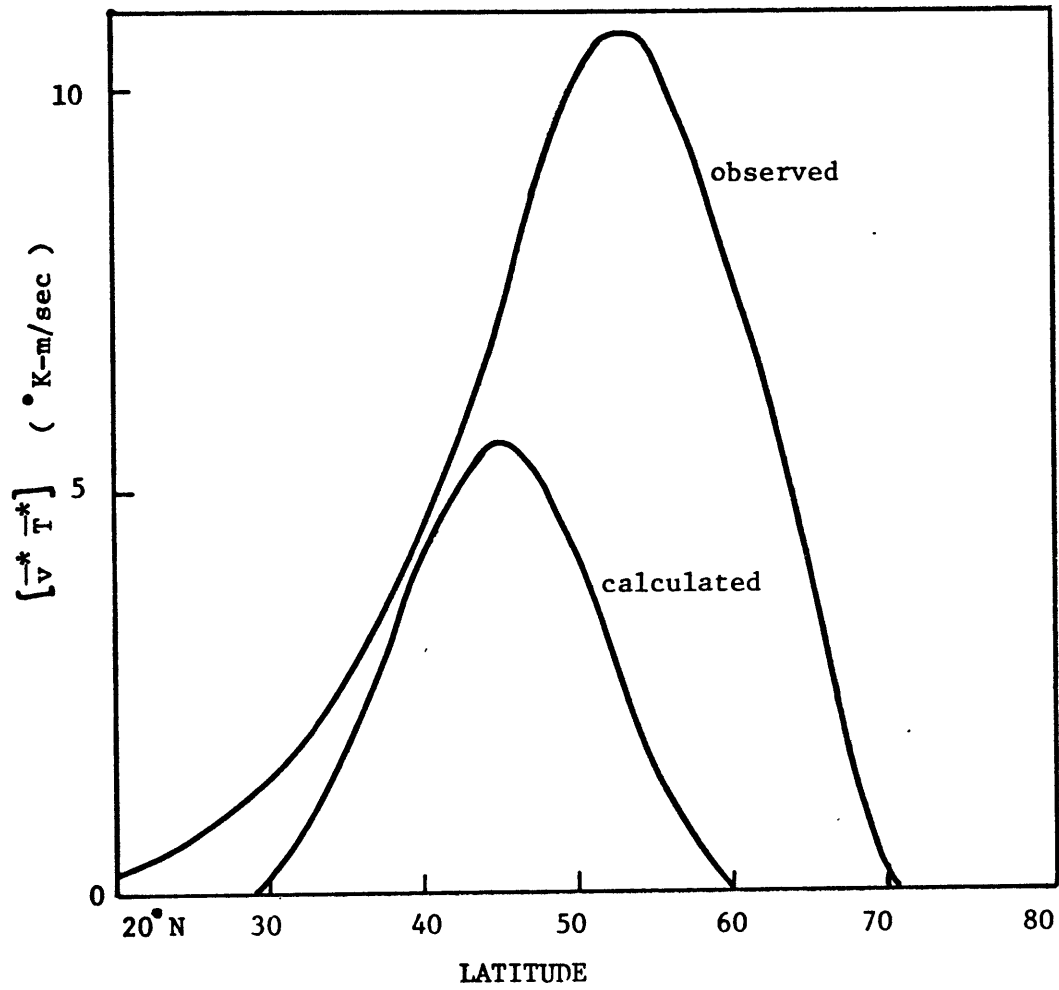


Fig. 3.5 Calculated and observed (from Oort and Rasmusson, 1971) zonally averaged stationary eddy heat transport $[\overline{v^* T^*}]$ for winter, as a function of latitude.

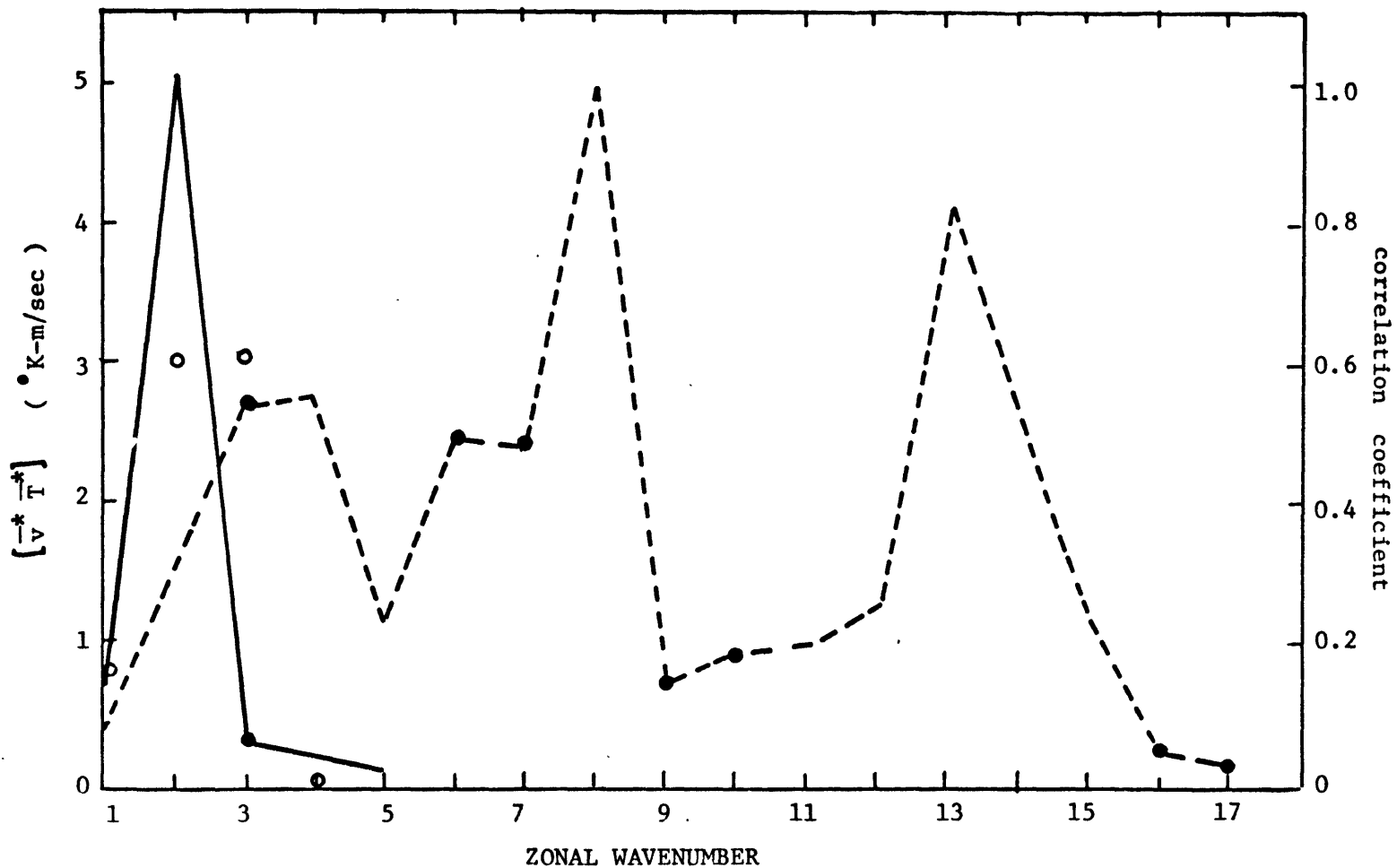


Fig. 3.6 Calculated spectra of northward stationary eddy heat transport ($[\overline{v^* T^*}]$, solid) and correlation coefficient (ρ , dashed). Dots indicate negative values. Open circles are from observations at 850 mb, 40°N (from Kao and Sagendorf, 1970).

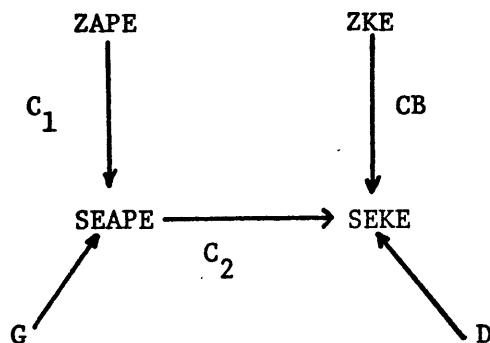
transporting heat than the atmospheric waves.

From eqs. (2.8) and (2.10), we may derive the energy equation for stationary waves:

$$\begin{aligned}
 0 &= -\frac{f_0}{2\rho_2} (U-U_T) \left[\Psi_3 \frac{\partial \rho_2}{\partial x} \right] + \frac{1}{2} F [\Psi_3 b_4] - \frac{f_0}{\rho_2} [\omega_2 \Psi_T] \\
 &= \text{CB(ZKE, SEKE)} + \text{D(SEKE)} + C_2(\text{SEAPE, SEKE}) \quad (3.6)
 \end{aligned}$$

$$\begin{aligned}
 0 &= \mu^2 U_T [\Psi_T \Psi_x] + \frac{f_0}{c_p \sigma_2 \rho_2} [\Psi_T H] + \frac{f_0}{\rho_2} [\omega_2 \Psi_T] \\
 &= C_1(\text{ZAPE, SEAPE}) + \text{G(SEAPE)} - C_2(\text{SEAPE, SEKE}) \quad (3.7)
 \end{aligned}$$

Recall Ψ , Ψ_T , Ψ_3 are the barotropic, baroclinic and level 3 components of the stationary wave field. Eqs. (3.6) and (3.7) are the steady state eddy kinetic energy and eddy available potential energy equations respectively for stationary waves. CB(ZKE, SEKE) is a conversion from ZKE to SEKE due to the mountain torque arising from the pressure difference between the western and eastern sides of the mountain; D(SEKE) is the dissipation of SEKE by surface friction; $C_2(\text{SEAPE, SEKE})$ is a conversion of SEAPE to SEKE due to rising of warm air and sinking of cold air at the same latitude; $C_1(\text{ZAPE, SEAPE})$ is a conversion of ZAPE to SEAPE by the northward transport of heat by SE's; G(SEAPE) is the generation of SEAPE by diabatic heating. The energy diagram is sketched below (directions of energy flow are for positive values of the conversions):



The sum of eqs. (3.6) and (3.7) gives the total SEKE and SEAPE equation. The conversion C_2 drops out because it is a conversion between the two forms of eddy energy.

The generation, dissipation and conversions of the various forms of eddy energy are shown as a function of wavenumber in Fig. 3.7. As before, absolute values of negative conversions are shown. We see that wavenumber 2 dominates all the conversions (note the ordinate is a logarithmic scale). Surface frictional dissipation (D) is always negative, and is almost entirely balanced by the conversion CB. For the dominant planetary scale wavenumbers 1-2, SEAPE is destroyed by diabatic processes ($G < 0$); SEAPE is thus maintained by conversion C_1 , resulting in a northward transport of heat. Since the waves are steady, the approximate balance between CB and D, C_1 and G for the planetary scale wavenumbers means that the conversion C_2 between SEAPE and SEKE is small. The energy diagram for all 18 wavenumbers, averaged over 30°N to 60°N, is shown below (conversions are in units of $10^{-5} \text{ m}^2/\text{sec}^2/\text{sec}$):

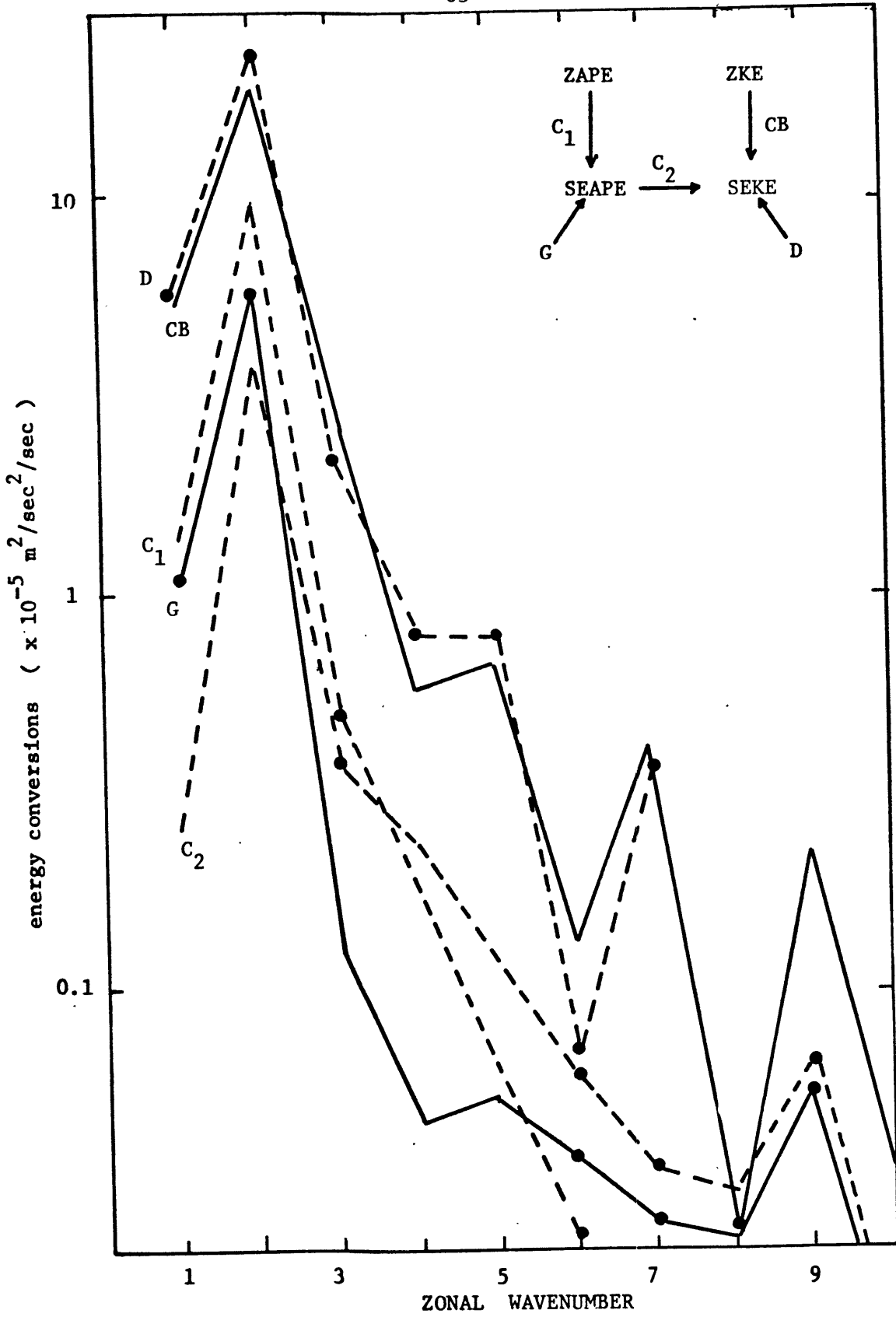
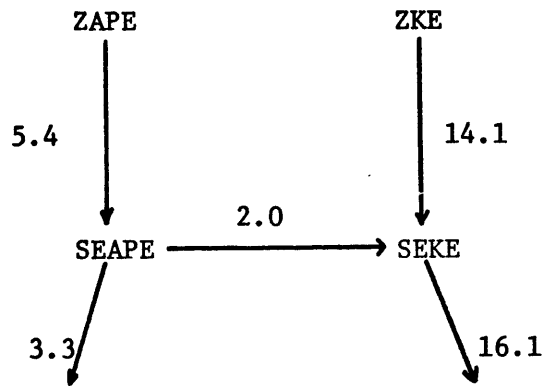
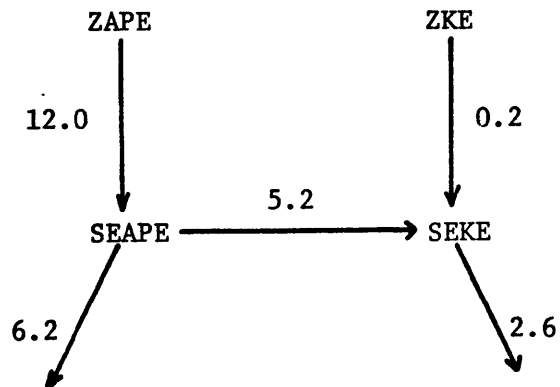


Fig. 3.7 Calculated spectra of energy conversions of stationary waves in winter. Dots indicate negative values.



Holopainen (1970) examined the energetics of stationary waves using observational data. The energy diagram, for winter averaged over 15°N to 90°N and 100 to 1000 mb, he found was (conversions in units of $10^{-5} \text{ m}^2/\text{sec}^2/\text{sec}$) :



The above is not an exact steady state because Holopainen included the effects of transient waves, but their effects were not large. We see the model gives the correct directions of energy conversions, but the magnitudes of the transfer are not reproduced well. The destruction of SEAPE and the baroclinic conversion $\text{ZAPE} \rightarrow \text{SEAPE}$ are underestimated

by about a factor of 2. The effects of surface friction and topography are overestimated drastically. A linear extrapolation for the surface variables has also been tried, instead of the energy-conserving extrapolation used in the above results. The linear extrapolation gives weaker surface winds and thus should reduce the surface energy conversions. This is indeed the case: the conversions CB and D are reduced by a factor of 3, which are still larger than the observed values. However, the generation and baroclinic conversions (G, C_1, C_2) are also reduced by a factor of 2. Thus the overall energetics is not improved.

We have shown that the 2-level model reproduces qualitatively the main features of heat transport and energetics of atmospheric stationary waves. The most severe defect is in the estimate of the surface energy terms, due probably to inadequate vertical resolution of surface phenomena. The heat transport, correlation coefficient and baroclinic conversion $\Sigma APE \rightarrow \Sigma EAPE \rightarrow \Sigma EKE$ are underestimated systematically. However, in our simple model, several of the specified parameters are not known accurately. The most uncertain are probably the friction coefficient (F), the meridional wavenumber of the stationary waves (λ) and the amplitude of the diabatic forcing. Table 3.1 shows the sensitivity of the results to variations of these parameters by a factor of two. This table shows the maximum zonally averaged heat transport ($[\bar{v}^* \bar{T}^*]_{max}$), the correlation coefficient for heat transport (ρ), the root-mean-square meridional eddy velocity ($\langle \bar{v}^{*2} \rangle^{1/2}$; $\langle \rangle$ denotes an area average) and the various energy conversions.

From Table 3.1, we see that increasing friction reduces the maximum heat transport. A realistic value of the maximum transport is obtained by halving the friction coefficient, but ρ remains small.

Increasing friction also reduces the eddy velocity; it remains smaller than the amplitude of the zonal flow ($U = 15 \text{ m/sec}$). Thus the linearization assumption is satisfactory. The dependence on λ is expected to be sensitive, as this parameter is important in determining which zonal wavenumber attains resonance. DWN showed that quasi-resonance resulted when the nondivergent Rossby wave is excited. This is consistent with the fact that wavenumber 4 has the largest eddy amplitude for the case of 0.5λ , while it is wavenumber 2 for the case of λ . The maximum heat transport is negative (southward) for the 0.5λ case while the transport and eddy velocity are all small for the 2λ case. Increasing the amplitude of the diabatic heating increases the maximum heat transport and eddy amplitude, but the correlation coefficient remains small. The signs of all energy conversions remain the same when F is varied; however, the dissipation decreases as F is increased. This unrealistic behavior is due to the use of an interpolated surface velocity in order to compute the surface velocity. In fact, an increase of F by a factor of 5 results in $D > 0$, i.e. a positive dissipation, which is clearly unrealistic. The conversions due to topography and friction are large compared to Holopainen's (1970) results. The energetics are sensitive to the value of λ . For the case of 0.5λ , $C_1 < 0$ (southward heat transport) and $G > 0$ (positive generation by diabatic processes) are opposite to observational results. The magnitudes of all conversion terms are reduced for the 2λ case compared to the λ case. Increasing the amplitude of the diabatic heating increases the magnitudes of all conversions; the topographic and fric-

parameter	$[\bar{v}^* \bar{T}^*]_{\max}$	ρ	$\langle \bar{v}^{*2} \rangle^{1/2}$	C_1	G	C_2	CB	D
F, λ , Q	5.6 K $\frac{m}{\text{sec}}$	0.17	5.6 $\frac{m}{\text{sec}}$	54	-33	20	141	-161
0.5F	9.8	0.14	8.5	94	-56	36	181	-217
2F	2.8	0.16	3.7	27	-17	10	100	-110
0.5 λ	-4.6	-.07	8.7	-44	56	14	69	-83
2 λ	0.3	0.46	0.7	3	9	13	19	-31
0.5Q	2.5	0.11	5.0	24	-15	9	129	-138
2Q	13.8	0.20	7.0	133	-79	51	165	-216

-67-

Table 3.1 Sensitivity to variations of the parameters F (friction coefficient), λ (meridional wavenumber) and Q (diabatic heating). First row indicates values with parameters of DWN. Second to fourth columns show the maximum heat transport, correlation coefficient and meridional eddy velocity amplitude respectively; last five columns show the energy conversions in units of $10^{-6} \text{ m}^2/\text{sec}^2/\text{sec}$.

tional conversions are still much larger than observed.

We see from Table 3.1 that the results are most sensitive to the parameter λ , because of the quasi-resonance phenomenon. The linearization assumption is found to be satisfactory. A value of the maximum zonally averaged heat transport close to the observed value of 10.8°K m/sec can be obtained by reducing F by a factor of two or by doubling the diabatic heating amplitude. In both cases, the correlation coefficient remains small compared to the observed value of 0.59. For the most "realistic" choices of the parameters F , λ and diabatic heating amplitude, we have seen that the efficient heat transport of winter SE's is not well reproduced. The underestimation of the heat transport by SE's also occurs in much more sophisticated models: in a simulation of January conditions, the general circulation model of the Goddard Institute of Space Studies underestimated the SE sensible heat flux by about 45%, while the TE flux was simulated relatively accurately (Stone et al, 1975). The deficit occurred almost entirely in wavenumbers 1-3, as shown by the calculations of baroclinic conversion (Tenenbaum, 1976). Our results lend support to the idea that stationary forcing alone is not sufficient to explain the efficient heat transporting long stationary waves of the atmosphere in winter.

IV. LINEAR STABILITY PROBLEM OF ROSSBY WAVES IN BAROCLINIC ZONAL FLOW

VI-1. Preliminary considerations

In the Introduction, we formulated a hypothesis where baroclinic instability of stationary waves may lead to efficient heat transporting planetary scale waves. In Chapter III, we found with a simple model that heat transport of stationary waves forced by realistic topography and diabatic heating and the efficiency of the transport were smaller than observed. In this chapter and the next, we present the next step in the examination of our hypothesis: a parameter study of the stability of the baroclinic Rossby wave in a zonal shear flow. This model includes a scale selection mechanism via eddy-eddy interaction which may lead to realistic kinetic energy and heat transport spectra in the planetary scales. As we discussed in the Introduction, this model can provide insight into the problem of the stability of forced stationary waves, and is also of interest because the basic wave may be identified with Green modes. These modes will affect the baroclinic stability problem once they reach finite amplitude. Thus our stability study is of direct interest for the atmosphere.

In Chapter II, we found a dispersion relation for the baroclinic Rossby wave which relates the following four quantities: the ratio of radius of deformation to wave scale ($K = k/\mu$); the ratio of baroclinic wave component to barotropic wave component (B_T/B); the barotropic zonal flow component ($\mu^2(U-c)/\beta$); and the baroclinic zonal flow component ($\mu^2 U_T/\beta$). In our stability analysis, we will specify the parameters K and B_T/B which describe the

basic wave and let the zonal flow parameters ($\mu^2(U-c)/\beta$, $\mu^2 U_T/\beta$) be specified by the dispersion relation. As we discussed in Chapter II, the limits $B_T/\beta \rightarrow 0$ and $B_T/\beta \rightarrow \infty$ correspond to the barotropic and baroclinic Rossby waves respectively. Both exist with no shear in the zonal flow. The stability of these waves have been examined by Lorenz (1972) and Kim (1975) respectively. More generally, the zonal shear will not be zero and the wave will consist of a barotropic and baroclinic part ($U_T \neq 0$, $B_T \neq 0$, $\beta \neq 0$) . Another limit of interest is $B_T \rightarrow 0$, $\beta \rightarrow 0$ with B_T/β fixed. For values of B_T/β which give an unstable zonal flow, this limit corresponds to the baroclinic instability of a two-level atmosphere first investigated by Phillips (1954). Our study will unify the studies of Phillips (1954), Lorenz (1972) and Kim (1975) and their results will be recovered in appropriate regions of parameter space.

IV-2. Linearized perturbation equations

The basic flow whose stability we wish to study is described by eqs. (2.14) and (2.15). We note that the basic streamfunctions are independent of time in a co-ordinate system moving with the basic wave. Thus we let $x_0 = x - ct$ and treat t , x_0 and y as the independent variables. We impose small perturbations on this flow by linearizing the adiabatic and frictionless governing equations

(eqs. (2.8) and (2.10) with $\omega_4 = H = 0$). We let $\bar{\psi} = -Uy + \beta \sin kx_0$

and $\bar{\psi}_T = -U_T y + \beta_T \sin kx_0$ denote the barotropic and baroclinic components of the basic flow respectively;

ψ' and ψ'_T will denote the barotropic and baroclinic components of the perturbation.

The linearized equations are

$$\left(\frac{\partial}{\partial t} - c \frac{\partial}{\partial x_0}\right) \nabla^2 \psi' = -J(\bar{\psi}, \nabla^2 \psi') - J(\psi', \nabla^2 \bar{\psi} + f) - J(\bar{\psi}_T, \nabla^2 \psi'_T) - J(\psi'_T, \nabla^2 \bar{\psi}_T) \quad (4.1)$$

$$\begin{aligned} \left(\frac{\partial}{\partial t} - c \frac{\partial}{\partial x_0}\right) (\nabla^2 - \mu^2) \psi'_T &= -J(\bar{\psi}, (\nabla^2 - \mu^2) \psi'_T) - J(\psi', (\nabla^2 - \mu^2) \bar{\psi}_T) \\ &\quad - J(\bar{\psi}_T, \nabla^2 \psi') - J(\psi'_T, \nabla^2 \bar{\psi} + f) \end{aligned} \quad (4.2)$$

Eqs. (4.1) and (4.2) are two linear, coupled partial differential equations with x_0 -dependent coefficients. Solutions exist of the form:

$$\psi' = \Psi'(x_0) e^{i(\ell y + \sigma t)} \quad (4.3a)$$

$$\psi'_T = \Psi'_T(x_0) e^{i(\ell y + \sigma t)} \quad (4.3b)$$

Substituting the above into eqs. (4.1) and (4.2) and letting $\bar{\psi} = \beta \sin k x_0$,

$\bar{\psi}_T = \beta_T \sin k x_0$ denote the stationary wave of the basic flow,

we get

$$\begin{aligned} 0 &= (i\sigma \ell^2 + i\ell(\ell^2 - k^2) \bar{\psi}_{x_0}) \Psi' + (U - c)\ell^2 - \beta) \Psi'_x - (i\ell \bar{\psi}_{x_0} + i\sigma) \Psi'_{x_0 x_0} - (U - c) \Psi'_{x_0 x_0 x_0} \\ &\quad + i\ell(\ell^2 - k^2) \bar{\psi}_{Tx_0} \Psi'_T + U_T \ell^2 \Psi'_{Tx_0} - i\ell \bar{\psi}_{Tx_0} \Psi'_{Tx_0 x_0} - U_T \Psi'_{Tx_0 x_0 x_0} \end{aligned} \quad (4.4)$$

$$\begin{aligned} 0 &= (i\sigma(\ell^2 + \mu^2) + i\ell(\ell^2 - k^2 + \mu^2) \bar{\psi}_{x_0}) \Psi'_T + (U - c)(\ell^2 + \mu^2) - \beta) \Psi'_{Tx_0} - (i\ell \bar{\psi}_{x_0} + i\sigma) \Psi'_{Tx_0 x_0} \\ &\quad - (U - c) \Psi'_{Tx_0 x_0 x_0} + i\ell(\ell^2 - k^2 - \mu^2) \bar{\psi}_{Tx_0} \Psi' + U_T(\ell^2 - \mu^2) \Psi'_{Tx_0} \\ &\quad - i\ell \bar{\psi}_{Tx_0} \Psi'_{x_0 x_0} - U_T \Psi'_{x_0 x_0 x_0} \end{aligned} \quad (4.5)$$

Eqs. (4.4) and (4.5) constitute the system to be solved for the eigenvalue σ . If σ has a negative imaginary part, the basic flow is unstable. Periodic boundary conditions in x_0 will be imposed for the perturbations. This requires Ψ' and Ψ_T' to be unchanged if x_0 is increased by a multiple of a certain distance, which will be taken to be the basic wavelength $2\pi/k$. A similar condition applied in the y direction will result in discrete values of the meridional wavenumber l . However, we will not impose this condition and thus allow for a continuous spectrum of l values. The simplest solutions of eqs. (4.4) and (4.5) satisfying the boundary condition in x_0 assume the form

$$\Psi' = \sum_n \chi_n e^{inkx_0} \quad (4.6a)$$

$$\Psi_T' = \sum_n \gamma_n e^{inkx_0} \quad (4.6b)$$

Note n denotes the order of the harmonic of basic wavenumber. We substitute eqs. (4.6) in (4.4) and (4.5), and express trigonometric quantities in terms of complex exponents. Putting the resulting equations in non-dimensional form, we obtain

$$(\lambda + a_n)\chi_n + c_{n-1}\chi_{n-1} + c_{n+1}'\chi_{n+1} + t_n\gamma_n + s_{n-1}\gamma_{n-1} + s_{n+1}'\gamma_{n+1} = 0 \quad (4.7a)$$

$$(\lambda + e_n)\gamma_n + g_{n-1}\gamma_{n-1} + g_{n+1}'\gamma_{n+1} + f_n\chi_n + t_{n-1}\chi_{n-1} + t_{n+1}'\chi_{n+1} = 0 \quad (4.7b)$$

where

$$\lambda = \frac{\sigma/k}{U-c}, \quad L = \frac{l}{k}, \quad M = \frac{k}{k}$$

$$a_n = \frac{n(n^2 + L^2 - \frac{\beta}{(U-c)k^2})}{n^2 + L^2}$$

$$e_n = \frac{n(n^2 + L^2 + M^2 - \frac{\beta}{(U-c)k^2})}{n^2 + L^2 + M^2}$$

$$c_n = \frac{1}{2} \frac{Bk}{U-c} L \frac{n^2 + L^2 - 1}{(n+1)^2 + L^2}$$

$$g_n = \frac{1}{2} \frac{Bk}{U-c} L \frac{n^2 + L^2 + M^2 - 1}{(n+1)^2 + L^2 + M^2}$$

$$c_n' = \frac{1}{2} \frac{Bk}{U-c} L \frac{n^2 + L^2 - 1}{(n-1)^2 + L^2}$$

$$g_n' = \frac{1}{2} \frac{Bk}{U-c} L \frac{n^2 + L^2 + M^2 - 1}{(n-1)^2 + L^2 + M^2}$$

(4.7c)

$$b_n = n \frac{U_T}{U-c}$$

$$f_n = n \frac{U_T}{U-c} \frac{n^2 + L^2 - M^2}{n^2 + L^2 + M^2}$$

$$s_n = \frac{1}{2} \frac{B_T k}{U-c} L \frac{n^2 + L^2 - 1}{(n+1)^2 + L^2}$$

$$t_n = \frac{1}{2} \frac{B_T k}{U-c} L \frac{n^2 + L^2 - M^2 - 1}{(n+1)^2 + L^2 + M^2}$$

$$s_n' = \frac{1}{2} \frac{B_T k}{U-c} L \frac{n^2 + L^2 - 1}{(n-1)^2 + L^2}$$

$$t_n' = \frac{1}{2} \frac{B_T k}{U-c} L \frac{n^2 + L^2 - M^2 - 1}{(n-1)^2 + L^2 + M^2}$$

The physical interpretations of the various non-dimensional parameters are as follows:

$$M = \frac{k}{k} \sim \frac{\text{zonal scale of basic wave}}{\text{radius of deformation}}$$

$$\frac{B_T k}{U - c} = \frac{\text{velocity amplitude of baroclinic basic wave}}{\text{barotropic component of zonal flow relative to basic wave}}$$

$$\frac{B k}{U - c} = \frac{\text{velocity amplitude of barotropic basic wave}}{\text{barotropic component of zonal flow relative to basic wave}}$$

$$\frac{U_T}{U - c} = \frac{\text{baroclinic component of zonal flow}}{\text{barotropic component of zonal flow relative to basic wave}}$$

$$\frac{\beta / k^2}{U - c} = \frac{\text{barotropic Rossby phase speed}}{\text{barotropic component of zonal flow relative to basic wave}}$$

$$L = \frac{l}{k} = \frac{\text{zonal scale of basic wave}}{\text{meridional scale of perturbation}}$$

$$\lambda = \frac{c / k}{U - c} = \frac{\text{phase speed of perturbation}}{\text{barotropic component of zonal flow relative to basic wave}}$$

Note the above non-dimensionalization is equivalent to measuring distance and velocity in units of k^{-1} and $U - c$ respectively. We will specify the first three parameters (U/k , $B_T k / U - c$, $B k / U - c$) independently. This determines the other parameters describing the basic flow $U_T / U - c$, $\beta / k^2 (U - c)$ using the dispersion relation, eqs. (2.16)

and (2.17). The non-dimensional eigenvalue λ is then solved as a function of the nondimensional meridional wavenumber $L = l/k$.

This is done by restricting the integral values of n in eqs.

(4.7) to $|n| \leq N$, thus obtaining a sequence of finite, linear, homogeneous algebraic equations. Eqs. (4.7) truncated to $|n| \leq N$

involve the $4N+2$ unknowns $X_0, X_{\pm 1}, \dots, X_{\pm N}; Y_0, Y_{\pm 1}, \dots, Y_{\pm N}$.

The set of $4N+2$ linear, homogeneous equations involving these unknowns is shown below:

$$\begin{bmatrix}
 \lambda+a_{-N} & b_{-N} & c_{-N+1} & d_{-N+1} & 0 & 0 & \dots & 0 & 0 \\
 f_{-N} & \lambda+c_{-N} & h_{-N+1} & g_{-N+1} & 0 & 0 & \dots & 0 & 0 \\
 c_{-N} & d_{-N} & \lambda+a_{-N+1} & b_{-N+1} & c_{-N+2} & d_{-N+2} & \dots & 0 & 0 \\
 h_{-N} & g_{-N} & f_{-N+1} & \lambda+c_{-N+1} & h_{-N+2} & g_{-N+2} & \dots & 0 & 0 \\
 0 & 0 & c_{-N+1} & d_{-N+1} & \dots & \dots & \dots & 0 & 0 \\
 0 & 0 & h_{-N+1} & g_{-N+1} & \dots & \dots & \dots & 0 & 0 \\
 \vdots & \vdots & \vdots & \vdots & \vdots & \vdots & \vdots & \vdots & \vdots \\
 0 & 0 & \dots & \dots & 0 & 0 & c_{N-1} & d_{N-1} & \lambda+a_N & b_N \\
 0 & 0 & \dots & \dots & 0 & 0 & h_{N-1} & g_{N-1} & f_N & \lambda+c_N
 \end{bmatrix}
 \begin{bmatrix}
 X_{-N} \\
 Y_{-N} \\
 X_{-N+1} \\
 Y_{-N+1} \\
 \vdots \\
 X_N \\
 Y_N
 \end{bmatrix}
 = \underline{0}$$

(4.8)

In order for non-trivial solutions to exist the $(4N+2) \times (4N+2)$ coefficient matrix has to have vanishing determinant. For the lowest truncation ($N=1$), the 6×6 determinant can be calculated analytically. Setting it equal to zero, we obtain a sixth order polynomial equation for the eigenvalue λ . There is a pair of zeros and the remaining four roots are of the form $\pm i\lambda_a$ and $\pm i\lambda_i$ of $\pm i\lambda_i'$ and $\pm i\lambda_i''$. The unstable mode will be termed propagating or non-propagating, relative to the basic wave, according to whether $\lambda_a \neq 0$ or $\lambda_a = 0$ respectively. Henceforth, propagation of unstable modes will be relative to the basic wave. For $N \geq 2$, eqs. (4.8) are solved numerically by a FORTRAN version of the ALGOL routines developed by Wilkinson et al (1971). At each stage of truncation, there are $4N+2$ eigenvalues, not all of which correspond to instability generally. For a particular unstable mode, λ_N is solved for as a function of L . When N is so large that $\lambda_N(L)$ has converged, a good approximation to the "true" solution will have been obtained. Physically, this truncation process corresponds to retaining more and more modes, with progressively decreasing zonal scales with wavenumbers consisting of multiples of the basic wavenumber. Convergence is attained when the smallest significant scale has been resolved. We anticipate two important scales: the scale of the basic wave and the radius of deformation. The former is important because it is present as an explicit scale while the latter is the natural response scale of a perturbation in a baroclinic zonal flow. Thus we expect the behavior of the perturbation to depend significantly on their ratio, r/k

The zonal structure of our perturbations consists of harmonics of the basic wavenumber (eqs. 4.6). For a perturbation with all possible integral wavenumbers, eqs. (4.7) decouple into two sets: the first set has perturbations consisting of only zonal harmonics of the basic wavenumber, while perturbations of the second set has all other wavenumbers. For our hypothesis, the basic wave will be of planetary scale. For basic wavenumber 1, harmonics of the basic wavenumber give all integral wavenumbers, thus the decoupling does not occur. For basic wavenumber 2, the decoupling gives perturbations consisting of even and odd wavenumbers. In Chapter VI, where we apply the stability analysis to the atmosphere, we show that the growth rate of the most unstable mode of the latter perturbation is smaller than the former. Thus the most unstable mode has a zonal structure given by harmonics of the basic wavenumber. This zonal structure of the perturbation streamfunction is the only one which will generate a zonally symmetric perturbation component ($n = 0$ component) via interaction between the basic wave and the perturbation. For the other perturbations, all components are zonally asymmetric. This means that these perturbations possess a larger meridional velocity component. As this velocity component is always subject to the stabilizing β -effect, it is reasonable to expect these perturbations to have smaller growth rates than the one consisting of harmonics of the basic wavenumber.

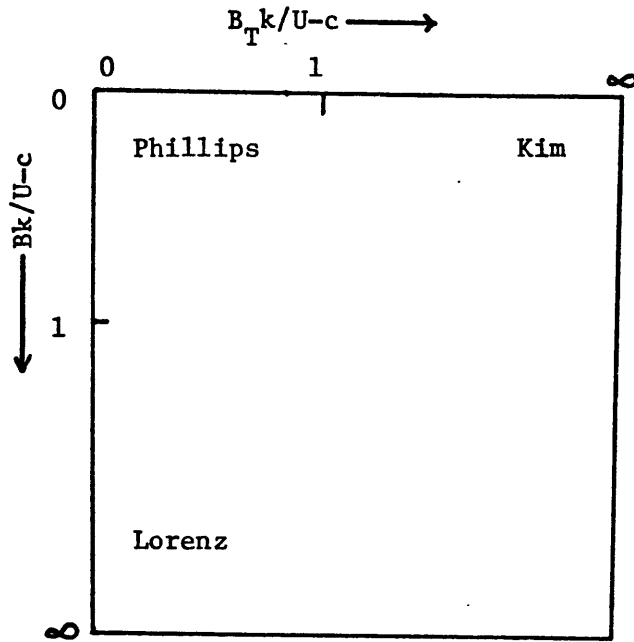
IV-3. Some properties of unstable modes.

We note that the coefficients $c_n, c'_n, q_n, q'_n, S_n, S'_n, t_n, t'_n$ all vanish if $L = 0$. This in turn means that modes with different values of n are decoupled (see eqs. 4,7), i.e. modes with different zonal scales do not interact. Closer examination of eqs. (4,7) shows that this corresponds to the stability problem of a baroclinic zonal flow to perturbations with no y variation. All basic wave effects vanish for this perturbation. Physically, this is because this perturbation has no y structure and since the basic wave has only x structure, there is no advection of perturbation vorticity by the basic wave nor advection of basic wave vorticity by the perturbation. The only advection that remains is that of perturbation vorticity by the zonal flow. A non-zero value of L allows for interaction between the perturbation and the basic wave. Since the basic wave is zonally asymmetric, this interaction generates further harmonics, i.e. modes with different zonal scales are now coupled. Thus with the presence of a basic wave, if the corresponding zonal flow by itself is unstable to the $L = 0$ perturbation, the most unstable mode has a growth rate greater than or equal to that of this mode.

We noted earlier that there are three independent non-dimensional parameters in the stability problem: $\mu/k, B_{rk}/U-c, B_k/U-c$.

The limit of small wave amplitude, $B_{rk}/U-c \rightarrow 0, B_k/U-c \rightarrow 0$ with B_T/β fixed at values for which the zonal flow is baroclinic, gives Phillips (1954) problem. In this case, $c_n, c'_n, q_n, q'_n, S_n, S'_n, t_n, t'_n$ all vanish and modes with different values of n decouple, as before. Thus the perturbation consists of a single zonal scale and is

stable or unstable depending on its wavelength and the zonal shear. We shall term this regime, where the zonal flow dominates, the Phillips regime. For values of B_r/β which give a stable zonal flow, instabilities at the small wave amplitude limit correspond to a resonantly interacting triad, consisting of the basic wave and two perturbation waves (Gill, 1974; Pedlosky, 1975a; Yamagata, 1977). The limit $B_{rk}/U-c \rightarrow 0$, $B_k/U-c > 0$ gives a barotropic wave with no shear in the zonal flow as the basic flow. The unstable modes decouple into pure barotropic or pure baroclinic modes (Yamagata, 1976), with the former modes always growing faster than the latter. The former instability was first investigated by Lorenz (1972). Accordingly, we term this region of parameter space where the barotropic basic wave dominates, the Lorenz regime. Similarly, the limit $B_k/U-c \rightarrow 0$, $B_{rk}/U-c > 0$ gives a baroclinic wave with no zonal shear as the basic flow. The unstable perturbations decouple into two sets of mixed barotropic-baroclinic modes (Kim, 1975). This regime, where the baroclinic basic wave dominates, will be termed the Kim regime. The three regimes may be sketched in two-dimensional parameter space $(B_{rk}/U-c, B_k/U-c)$ for fixed μ/k , as follows:

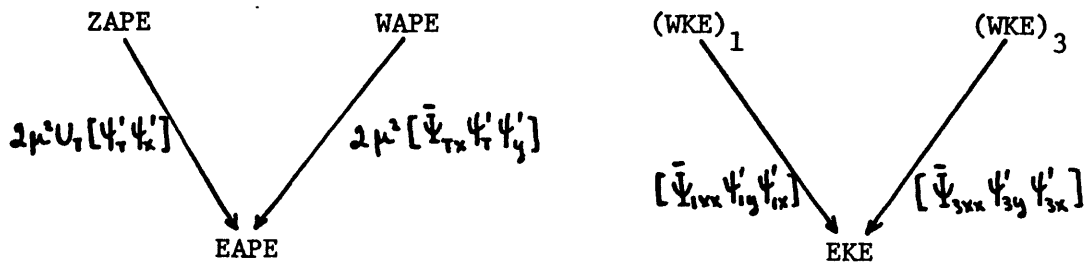


An energy equation for the perturbation may be derived by multiplying eqs. (4.1) and (4.2) by ψ' and ψ'_T respectively and adding. Integrating the resulting equation over one wavelength in the x_0 and y directions yields

$$\frac{\partial}{\partial t} \iint_{\text{cycle}} \left\{ \nabla \psi' \cdot \nabla \psi' + \nabla \psi'_T \cdot \nabla \psi'_T + \mu^2 (\psi'_T)^2 \right\} dx_0 dy = 2\mu^2 \iint_{\text{cycle}} \left\{ U_T \psi'_T \psi'_{x_0} + \bar{\Psi}_{Tx_0} \psi'_T \psi'_y \right\} dx_0 dy$$

$$+ \iint_{\text{cycle}} \left\{ \bar{\Psi}_{1x_0} \psi'_{iy} \psi'_{1x_0} + \bar{\Psi}_{3x_0} \psi'_{3y} \psi'_{3x_0} \right\} dx_0 dy \quad (4.9)$$

The first two terms on the left hand side represent the rate of change of perturbation KE while the third is the rate of change of perturbation APE. The right hand side describes the baroclinic and barotropic conversions. The first two terms consist of the product of the vertical shear of the zonal flow and the perturbation meridional heat transport, and the product of the vertical shear of the basic wave and the perturbation zonal heat transport respectively. These represent conversions of APE of the basic flow to perturbation APE and are termed baroclinic conversions. The third and fourth terms are barotropic conversions and are written in terms of levels 1 and 3 quantities. They consist of the product of horizontal shear of the basic wave meridional velocity and the Reynolds stress at each level. They represent conversions of basic wave KE to perturbation KE. A sketch of the energy diagram is as follows:



In the above, quantities denoted Z, W, E represent zonal flow, basic wave and eddy quantities respectively; $()_1$ and $()_3$ are levels 1 and 3 quantities respectively. Square brackets denote an area

average. For all the unstable modes we examined, there is a conversion from perturbation APE to perturbation KE.

The perturbation energy equation may be put in non-dimensional form by defining non-dimensional variables x'_0, y', t' as kx_0, ly, Ukt respectively. If at the same time we substitute for the basic wave quantities, we get: (overbar denotes area average)

$$\frac{\partial}{\partial t'} \left\{ \overline{(\psi'_{x'_0})^2} + \frac{l^2}{k^2} \overline{(\psi'_{y'})^2} + \overline{(\psi'_{Tx'_0})^2} + \frac{l^2}{k^2} \overline{(\psi'_{Ty'})^2} + \frac{\mu^2}{k^2} \overline{(\psi'_T)^2} \right\} = \frac{\mu^2}{k^2} \frac{U_T}{U-c} \overline{\psi'_T \psi'_{x'_0}}$$

$$+ \frac{\mu^2}{k^2} \frac{B_T k}{U-c} \frac{l}{k} \overline{\cos x'_0 \psi'_T \psi'_{y'}} - \frac{B_1 k}{U-c} \frac{l}{k} \overline{\sin x'_0 \psi'_{1y'} \psi'_{1x'_0}} - \frac{B_2 k}{U-c} \frac{l}{k} \overline{\sin x'_0 \psi'_{3y'} \psi'_{3x'_0}} \quad (4.10)$$

The perturbation streamfunctions are also non-dimensionalized in the above. For a basic wave with large zonal scale $\mu^2/k^2 \gg 1$, the baroclinic conversions dominate. This is because for a large scale wave, vertical shears are more important than horizontal shears. Also, the last three conversion terms involving the basic wave on the right hand side of eq. (4.10) vanish when $l/k = 0$, i.e. the perturbation with $l = 0$ does not feel the presence of the basic wave, as we discussed earlier. The three conversions are also proportional to the scaled velocity amplitude of the appropriate basic wave component.

V. RESULTS OF STABILITY ANALYSIS

V-1. Stability of a planetary scale basic wave.

In this chapter, we analyze the stability of three basic flows consisting of a basic wave of planetary scale ($\frac{k}{k} > 1$), very large scale ($\frac{k}{k} \gg 1$) and synoptic scale ($\frac{k}{k} \approx 1$). In each case, both wave amplitudes ($\frac{B_1 k}{U-c}$, $\frac{B_2 k}{U-c}$) are specified independently within the range (0.1, 10) and the corresponding zonal flow is given by the Rossby wave dispersion relation. The growth rates, structures and energetics of the unstable modes will be examined.

We take as a typical planetary scale wave, wavenumber 2 at mid-latitudes. This gives $\frac{k}{k} = 3.9$ for a typical value of the radius of deformation in winter. The growth rate of the most unstable mode is shown as a function of basic wave amplitudes ($\frac{B_1 k}{U-c}$, $\frac{B_2 k}{U-c}$) for the lowest truncation $N=1$ in Fig. 5.1. We see the presence of the Phillips, Lorenz and Kim regimes of instability. The wave regimes (Lorenz, Kim) are marked by increasing growth rates with increasing basic wave amplitude, for values of the latter larger than order unity. In the Phillips regime, the wave amplitudes are smaller than order unity and the contours are distorted by the zonal shear. For comparable wave amplitudes, the growth rates are larger in the Kim regime than in the Lorenz regime. This is because the large horizontal extent of the basic wave makes vertical shear more important than horizontal shear. Propagating modes (relative the basic wave) exist for a band of wave amplitudes where the baroclinic wave component is comparable to the barotropic component ($\frac{B_1 k}{U-c} \approx \frac{B_2 k}{U-c}$). Away from this band, the most unstable

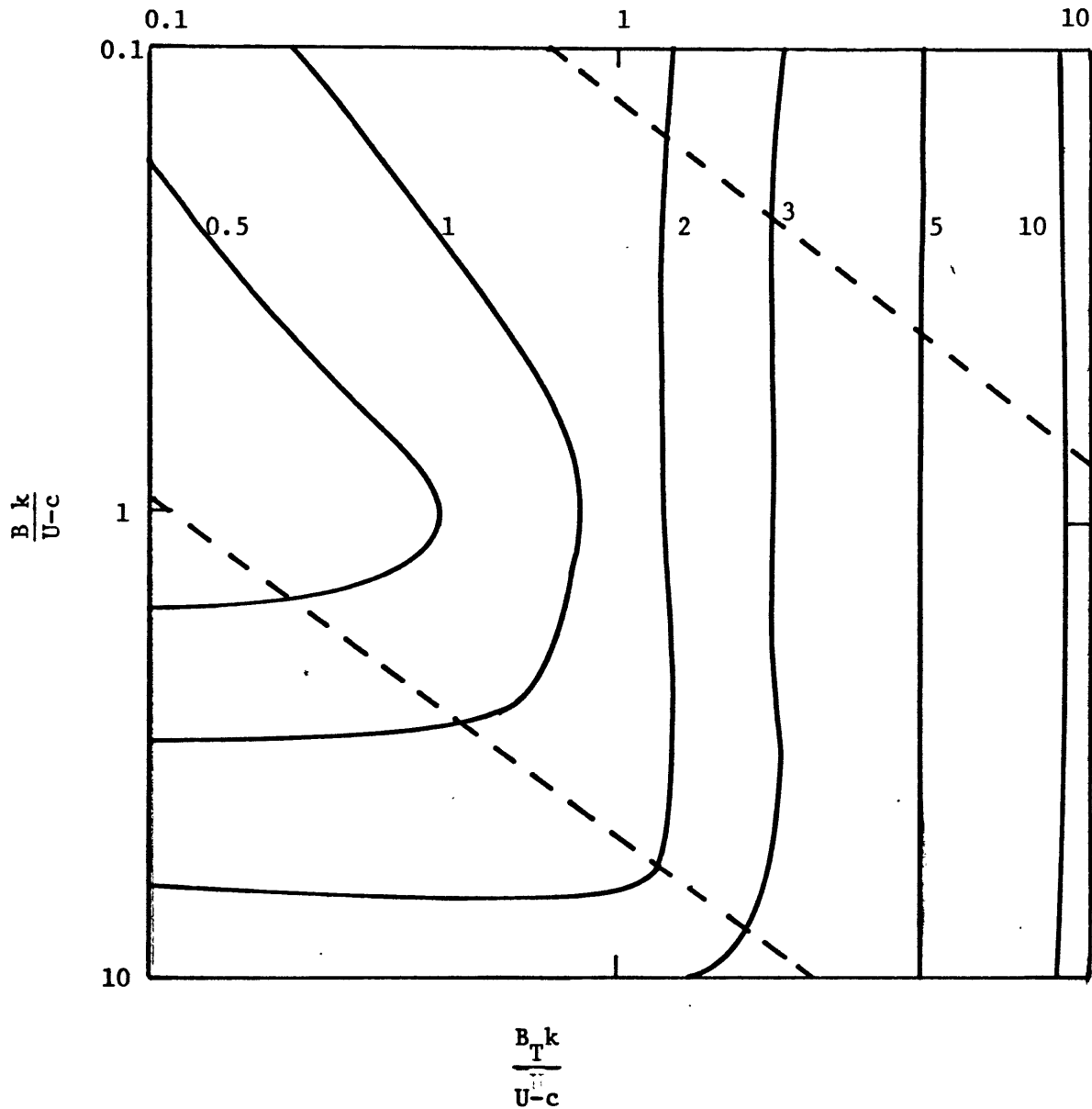


Fig. 5.1 Contours of constant growth rate $\left| \frac{\sigma_i/k}{U-c} \right|$ of most unstable mode for planetary scale basic wave ($\mu/k = 3.9$) and lowest truncation, $N=1$. The coordinates are the non-dimensional amplitudes of the basic wave on a logarithmic scale. Dotted lines enclose region of propagating unstable modes, relative to basic wave.

modes are non-propagating. This agrees with the results of Lorenz (1972) and Kim (1975), who found unstable modes are stationary relative to the basic wave. This provides a means of classifying the Lorenz and Kim wave regimes: an unstable mode belongs to these wave regimes if it does not propagate relative to the basic wave and if the basic wave amplitude is larger than order unity. For the latter smaller than order unity, the zonal shear dominates (Phillips regime) and the unstable modes are propagating. The wave regimes may also be classified as regions in parameter space where basic wave amplitudes exceed order unity and the zonal shear is less than the minimum critical shear. In that case, absence of the basic wave leads to stability. These two classifications of the Lorenz and Kim wave regimes are similar.

We can identify the dominant instability mechanism in each regime more clearly by scanning the parameter space along the baroclinic wave path ($\frac{Bk}{U-c} = 0.1, 0.1 \leq \frac{B_T k}{U-c} \leq 10$), barotropic wave path ($\frac{B_T k}{U-c} = 0.1, 0.1 \leq \frac{Bk}{U-c} \leq 10$) and the mixed baroclinic-barotropic wave path ($0.1 \leq \frac{B_T k}{U-c} = \frac{Bk}{U-c} \leq 10$). The growth rates for each of these paths are compared with the corresponding non-dimensional zonal shear $U_T/U-c$ in Fig. 5.2. The abscissa is either $\frac{B_T k}{U-c}$ or $\frac{Bk}{U-c}$ depending on the path taken. For values of the abscissa less than unity the growth rate curves for the three paths have slopes similar to those of the zonal shear curves, i.e. in the Phillips regime where wave amplitudes are smaller than order unity, the zonal shear is dominant. For values of the abscissa larger than unity, wave effects become more important and the growth rate increases monotonically with wave amplitudes. The growth rates for the mixed case lie in between those of the baroclinic and barotropic cases, closer to the former. The

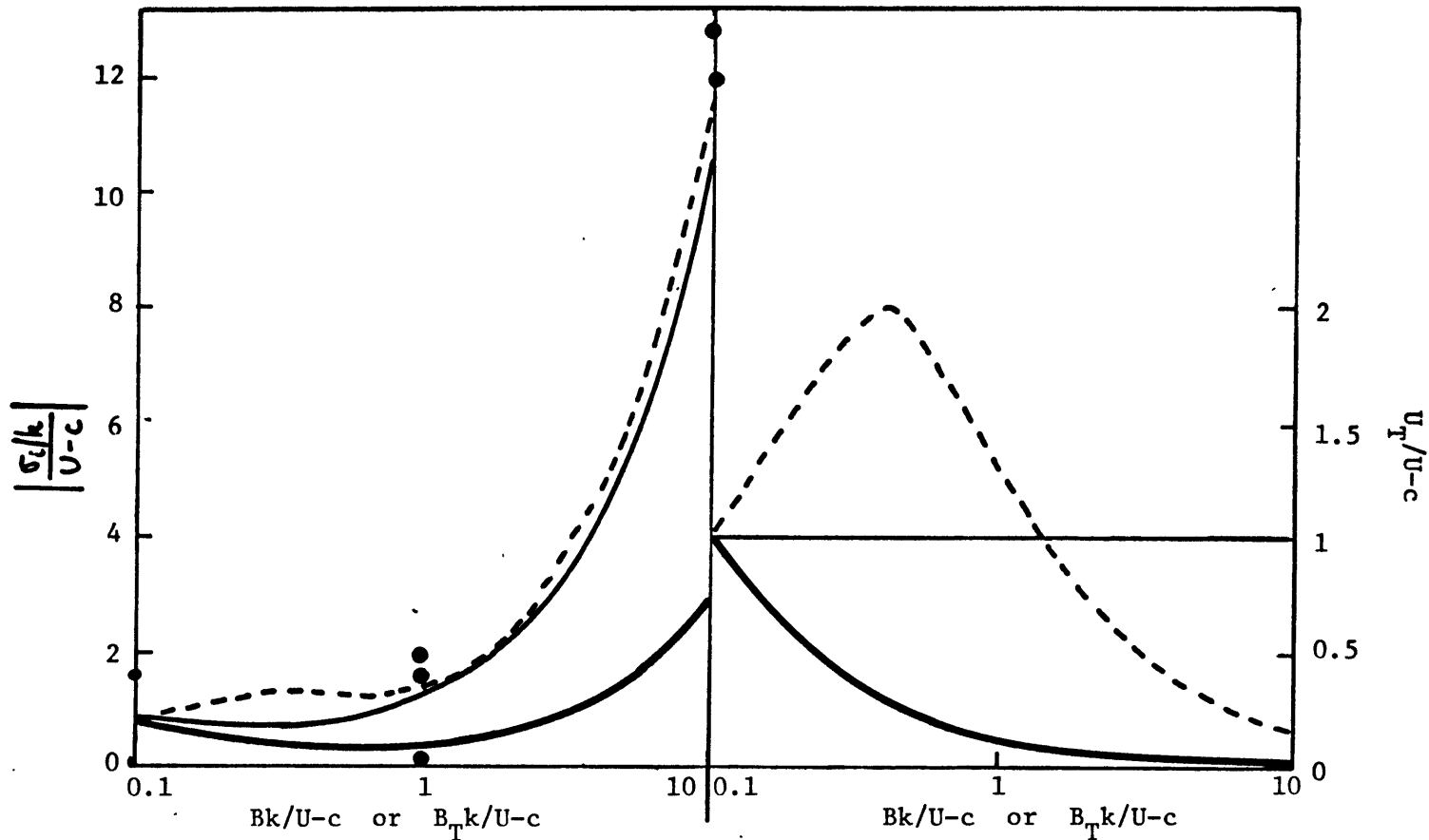


Fig. 5.2 Growth rate $\left| \frac{\sigma_i/k}{U-c} \right|$ and zonal shear $\frac{u_T}{U-c}$ for $N=1$ along the baroclinic path (----, $\frac{Bk}{U-c}=0.1$, $0.1 \leq \frac{B_Tk}{U-c} \leq 10$), barotropic path (—, $\frac{B_Tk}{U-c}=0.1$, $0.1 \leq \frac{Bk}{U-c} \leq 10$) and mixed baroclinic-barotropic path (—, $0.1 \leq \frac{Bk}{U-c} = \frac{B_Tk}{U-c} \leq 10$). Abscissa is either $\frac{Bk}{U-c}$ or $\frac{B_Tk}{U-c}$ depending on the path. $H/k = 3.9$. Dots are for $N=6$.

growth rates for $N=6$ truncation, when convergence has been obtained, are also shown for several values of the abscissa. We see the $N=1$ results are a good approximation, especially in the wave regimes. In the Phillips regime where the zonal shear is dominant, the lowest truncation results are not expected to be accurate, because the radius of deformation is an important scale. To resolve this scale, N must be at least three.

The rate of convergence of an unstable mode reflects the extent to which harmonics of the basic wavenumber are excited. This can be examined by considering the barotropic and baroclinic perturbation amplitudes as a function of n , i.e. the spectra $|X_n|$, $|Y_n|$. They are shown in Fig. 5.3 for the most unstable mode for $N=6$ and $\frac{B_1 k}{U-c}$, $\frac{B_2 k}{U-c} = 0.1, 1, 10$ together with the meridional wavenumber of the most unstable mode, $L_0 = 1/k$. The spectra are normalized by taking $|X_0| = 1$. We refer to the nine cases by the ordered pair $(\frac{B_1 k}{U-c}, \frac{B_2 k}{U-c})$. For (0.1,0.1) and (1,1), the spectra consist of a spike at $n=3$, which corresponds to a zonal scale of the radius of deformation, and $L_0 = 0$. This is because the zonal shear is the dominant instability mechanism and the most unstable mode is identical to that of the corresponding baroclinic zonal flow only - recall the $L=0$ perturbation does not feel the presence of the basic wave. This mode is poorly approximated until the radius of deformation is resolved. No other harmonics are generated because interaction between the basic wave and the perturbation is absent. This is not the case for (0.1,1) and (1,0.1) even though these represent weaker wave amplitudes than (1,1). This is because $\frac{k^2 U}{\beta} = 7.5$ for (1,1) while $\frac{k^2 U}{\beta} = 1.59$ and 1.39 for (0.1,1) and (1,0.1) respectively. The larger magnitude

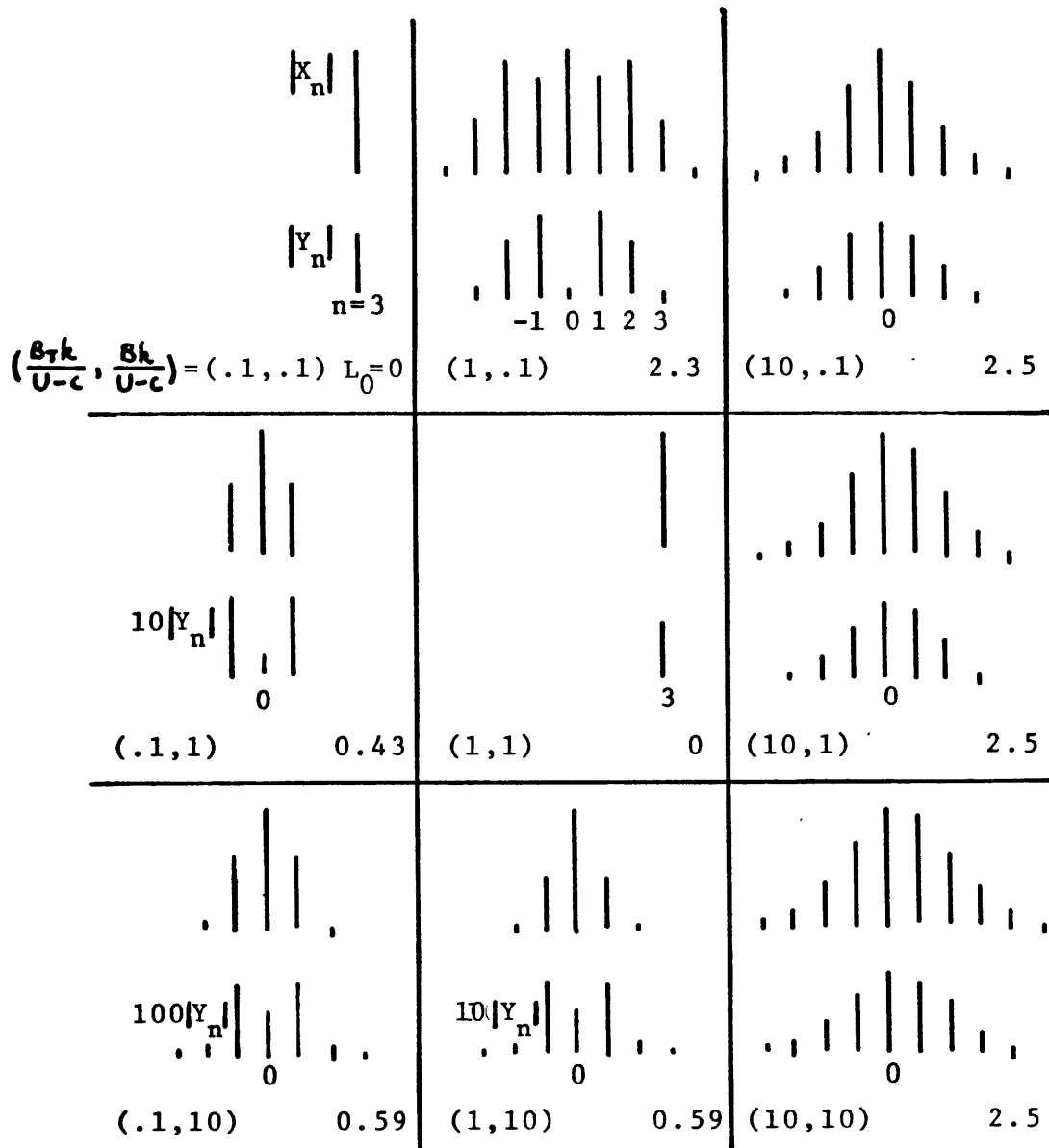


Fig. 5.3 Spectra of barotropic and baroclinic perturbation wave amplitude ($|X_n|, |Y_n|$) for the most unstable mode; L_0 is the meridional wavenumber. n denotes order of harmonic of basic wavenumber. $\tau/k = 3.9$ $N=6$.

of the zonal shear for (1,1) means zonal shear effects are more important there. However, we can see effects of the zonal shear in (1,0.1): the $n=2$ mode has significant amplitude in $|X_n|$ and $|Y_n|$.

This perturbation feels the presence of the zonal shear and has significant response in a scale close to the radius of deformation, smaller than the basic wave scale. The spectra for (0.1,1), (0.1,10) and (1,10) have significant amplitudes only in $n=0$ and $n=\pm 1$ modes. The baroclinic amplitudes $|Y_n|$ are much smaller than the barotropic amplitudes $|X_n|$ especially for the second case. This is expected as this mode is in the Lorenz regime. The convergence for (1,0.1), (10,0.1) and (10,1) is slower - the spectra are fairly broad. For strong basic wave amplitudes (10,10), several harmonics of the basic wavenumber are excited. The spectrum is also slightly skewed. For non-propagating modes in the Lorenz and Kim regimes, the spectra are symmetrical about $n=0$ because the stationary mode consists of two waves of equal amplitudes travelling in opposite directions. For the propagating modes in the Phillips and mixed barotropic-baroclinic wave regime, the spectra are skewed. We have shown the spectra for these cases for $\lambda_{real} < 0$, which corresponds to an eastward propagating wave for positive n . For the $\lambda_{real} > 0$ mode, the spectra are reflected about $n=0$. For (0.1,1), (0.1,10) and (1,10), we have $L_0 \approx 0.5$. Here, the barotropic basic wave dominates

$\frac{Bk}{U-c} \gg \frac{B_T k}{U-c}, \frac{Bk}{U-c} \gg \frac{U_T}{U-c}$ and as a result of the quasi-two dimensional nature of the basic flow, $\frac{L}{k} < 1$ for kinetic energy

and enstrophy transfer to take place (Fjortoft, 1953; Lorenz, 1972). The Phillips regime is characterized by $L_0 = 0$ unstable modes, as we discussed earlier. For the remaining cases, $L_0 \approx 2.5$, which means

the meridional scale is slightly larger than the radius of deformation.

The kinetic energy and meridional heat transport spectra of the perturbation for the nine cases examined are shown in Fig. 5.4. Each spectrum is normalized by the component with the largest amplitude. The two spectra are similar, except there is no heat transport by the $n=0$ component. Except for (0.1,0.1), (1,0.1) and (1,1) all the spectra peak at either $n=0$ or $n=1$. For (0.1,0.1) and (1,1), only the perturbation with zonal scale the radius of deformation is excited. For (1,0.1), the maximum response is in a scale smaller than the basic wave scale, close to the radius of deformation. This reflects the influence of the zonal shear. Southward heat transport is found for (0.1,10), indicating a conversion of eddy APE to zonal APE. However, this case lies in the Lorenz regime and the baroclinic component of the perturbation is much smaller than the barotropic component (Fig. 5.3), i.e. the temperature perturbation is small. Thus this conversion is not expected to be significant in the overall energetics. This can be seen from the energetics of the unstable modes, shown in Fig. 5.5. The barotropic conversions $(WKE)_1, (WKE)_3 \rightarrow EKE$ dominate in (0.1,10) and to a lesser extent in (0.1,1) and (1,10). We let Λ denote the ratio of basic wave APE to KE, this parameter depends on the scale of the basic wave and the relative amplitudes of the baroclinic and barotropic basic wave components. For (0.1,10), (0.1,1) and (1,10), $\Lambda \ll 1$, thus the importance of barotropic conversion is to be expected. For (10,0.1), (10,1) and (10,10), $\Lambda \gg 1$ and the baroclinic interaction with the basic wave $WAPE \rightarrow EAPE$ dominates. In the Phillips regime (0.1,0.1) and (1,1), only one conversion $ZAPE \rightarrow EAPE$ exists. For (1,0.1), the baroclinic interactions with both zonal flow and basic wave are equally significant.

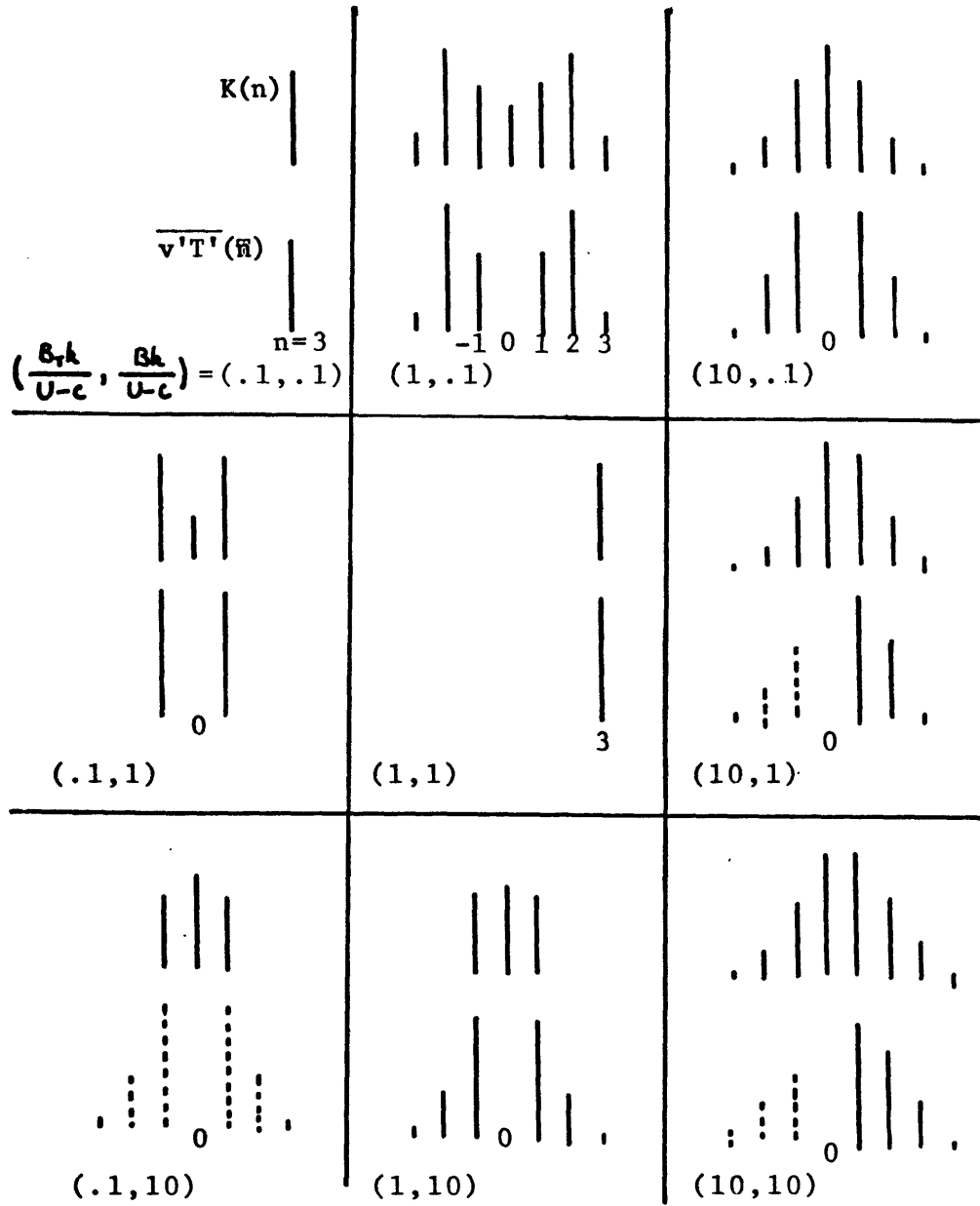


Fig. 5.4 Kinetic energy and heat transport spectra $(K(n), \overline{v'T'}(n))$ for the most unstable mode. Dashed lines indicate southward transport. n denotes order of harmonic of basic wavenumber.
 $k/h = 3.9, N=6.$

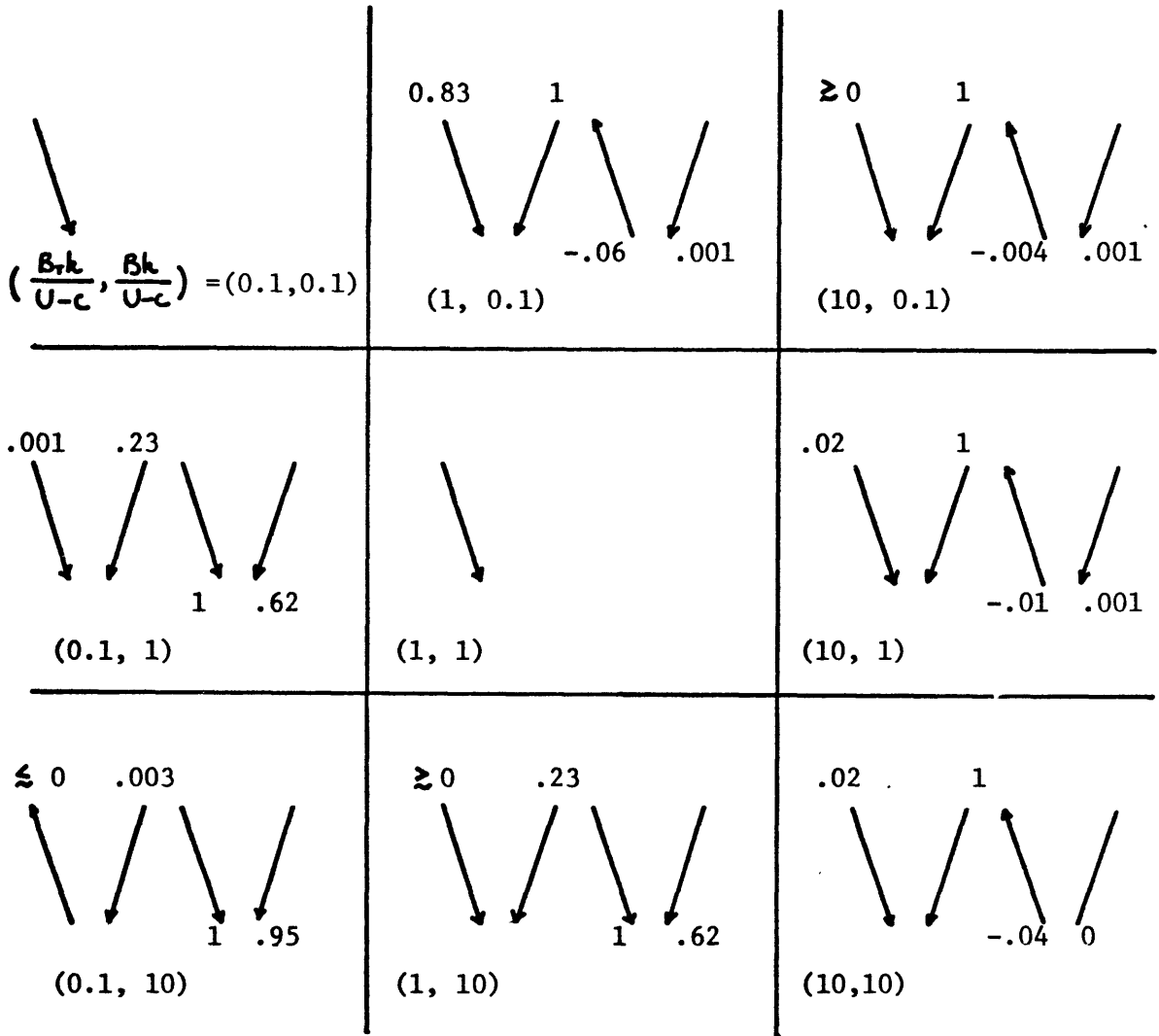
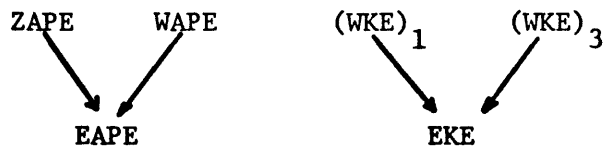


Fig. 5.5 Energetics of the most unstable mode. $V/k = 3.9$, $N=6$.



We conclude this section by presenting a brief summary. The Phillips, Lorenz and Kim regimes of instability are identified, depending on the amplitude of the basic wave and the zonal shear. A fourth regime, where barotropic and baroclinic basic wave amplitudes are both larger than order unity and are comparable, is also identified. As a result of the presence of two different zonal scales, the radius of deformation and the larger basic wave scale, higher harmonics of the latter can be excited depending on the type of instability. Even though the basic wave lacks meridional structure, the most unstable modes have in general a non-zero meridional wavenumber which maximizes advections between the basic wave and the perturbation. The perturbation may be propagating or non-propagating relative to the basic wave.

V-2. Stability of a very large scale basic wave

In this section, we consider the stability of a basic wave with $\frac{K}{k} = 10$. This means the basic wave scale is much larger than the radius of deformation. Thus we expect significant harmonics of the basic wave to be excited away from the Lorenz regime, and results from the lowest truncation may not be accurate. The Lorenz regime is quasi-barotropic and should be largely independent of vertical stratification. In Fig. 5.6, we show the growth rate as a function of basic wave amplitudes for the lowest truncation. They are generally larger than those of the $\frac{K}{k} = 39$ case examined earlier. The Phillips, Lorenz and Kim regimes are discernible. The Kim regime has much larger growth rates than the Lorenz regime for comparable wave amplitudes due to the large basic wave scale: vertical shears are much more important than horizontal shears. Most of the unstable

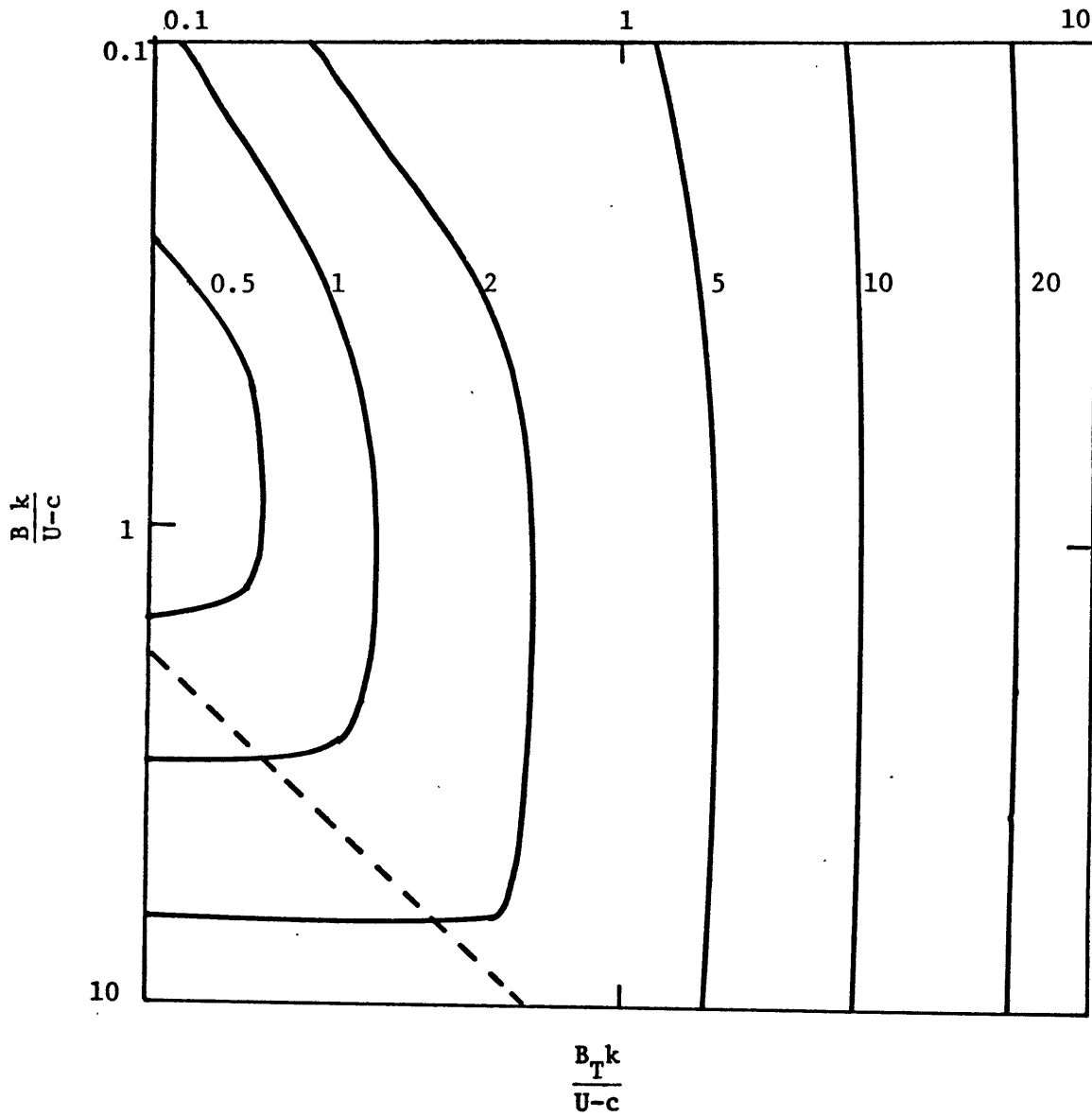


Fig. 5.6 As in Fig. 5.1 but for $\mu/k = 10$. Propagating modes are to the right of dashed line.

modes are propagating. The dominant instability mechanism can be identified by scanning along the baroclinic, barotropic and mixed baroclinic-barotropic wave paths as before. This is shown in Fig. 5.7. For wave amplitudes less than order unity, the zonal shear is dominant; for larger wave amplitudes, the growth rate increases monotonically. The results for $N=13$ when convergence is attained, is also shown. As we expected, the lowest order approximation does not work as well as before except in the Lorenz regime.

The distributions of $|X_n|$, $|Y_n|$, $K(n)$ and $\overline{v'T'(n)}$ are shown in Figs. 5.8 and 5.9 together with the meridional wavenumber L_0 of the most unstable mode. As before, we identify each case by the pair $(\frac{Bk}{U-c}, \frac{Bk}{U-c})$. The $l=0$ mode is the most unstable mode for $(0.1,0.1)$, $(1,0.1)$, (1.1) , and the spectra consist of a spike at the radius of deformation $n=6$. $(0.1,1)$ has fairly broad spectra, peaked at a scale intermediate between the radius of deformation and the basic wave scale. Its spectra are strongly asymmetric about $n=0$ indicating the perturbation propagates. As a matter of fact, all modes propagate except for the ones in the Lorenz regime. For the latter cases, $(0.1,10)$, $(1,10)$ the modes are almost barotropic, with little amplitudes outside the $n=0$ and $n=\pm 1$ harmonics. $(10,0.1)$, $(10,1)$ and $(10,10)$ all have broad spectra, showing the importance of the radius of deformation, especially in $(10,1)$. The kinetic energy and heat transport spectra are similar except for $n=0$ component. The modes in the Lorenz regime have meridional wavenumber less than unity due to the constraint of quasi-two dimensionality. The two-dimensionality is not sufficiently strong for $(0.1,1)$ and the mode there has $L_0=1.9$. For $(10,0.1)$, $(10,1)$ and $(10,10)$, $L_0 \approx 6$, which means the meridional scale is slightly larger

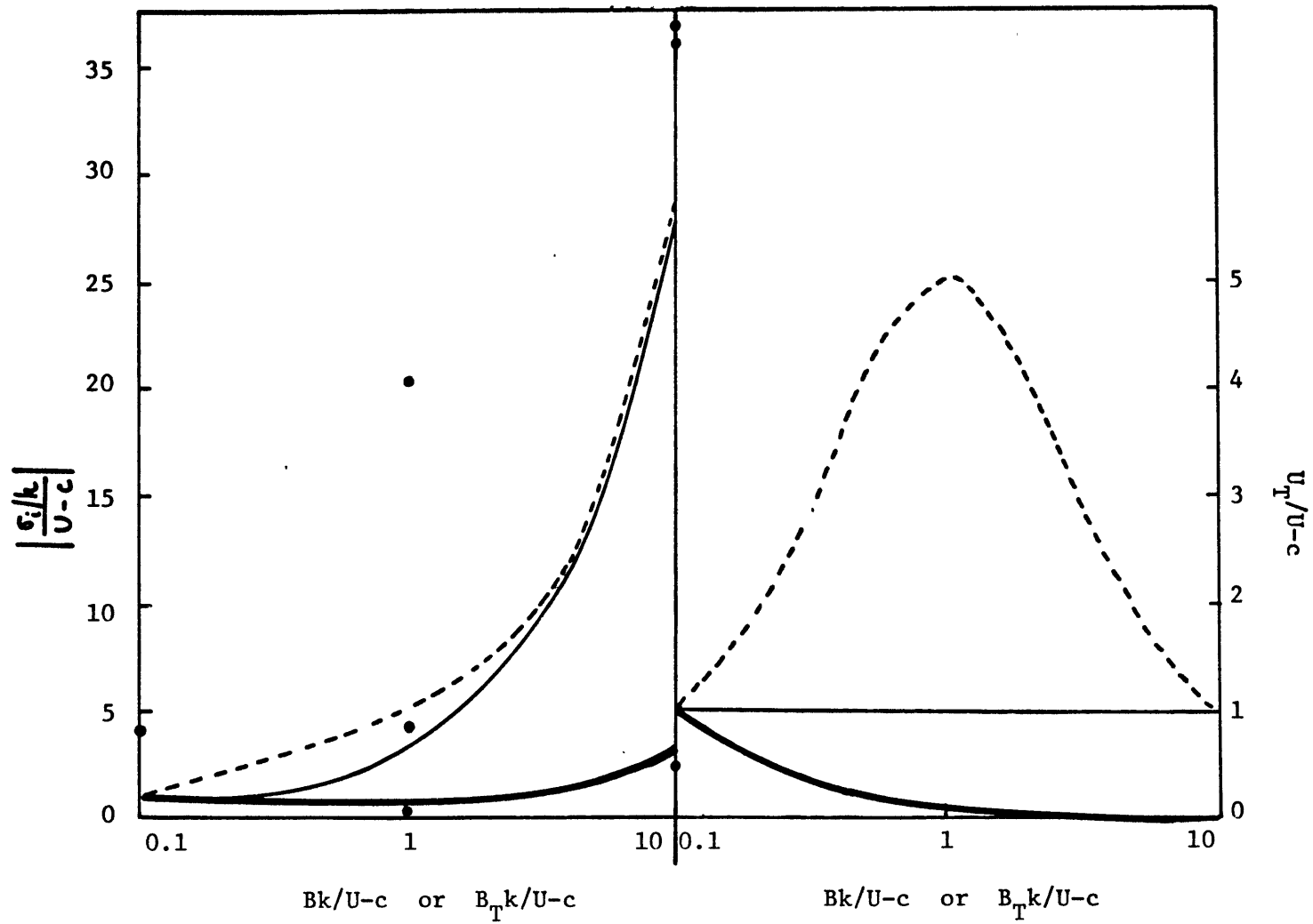


Fig. 5.7 As in Fig. 5.2 but for $\Gamma/k = 10$. Dots are for $N=13$.

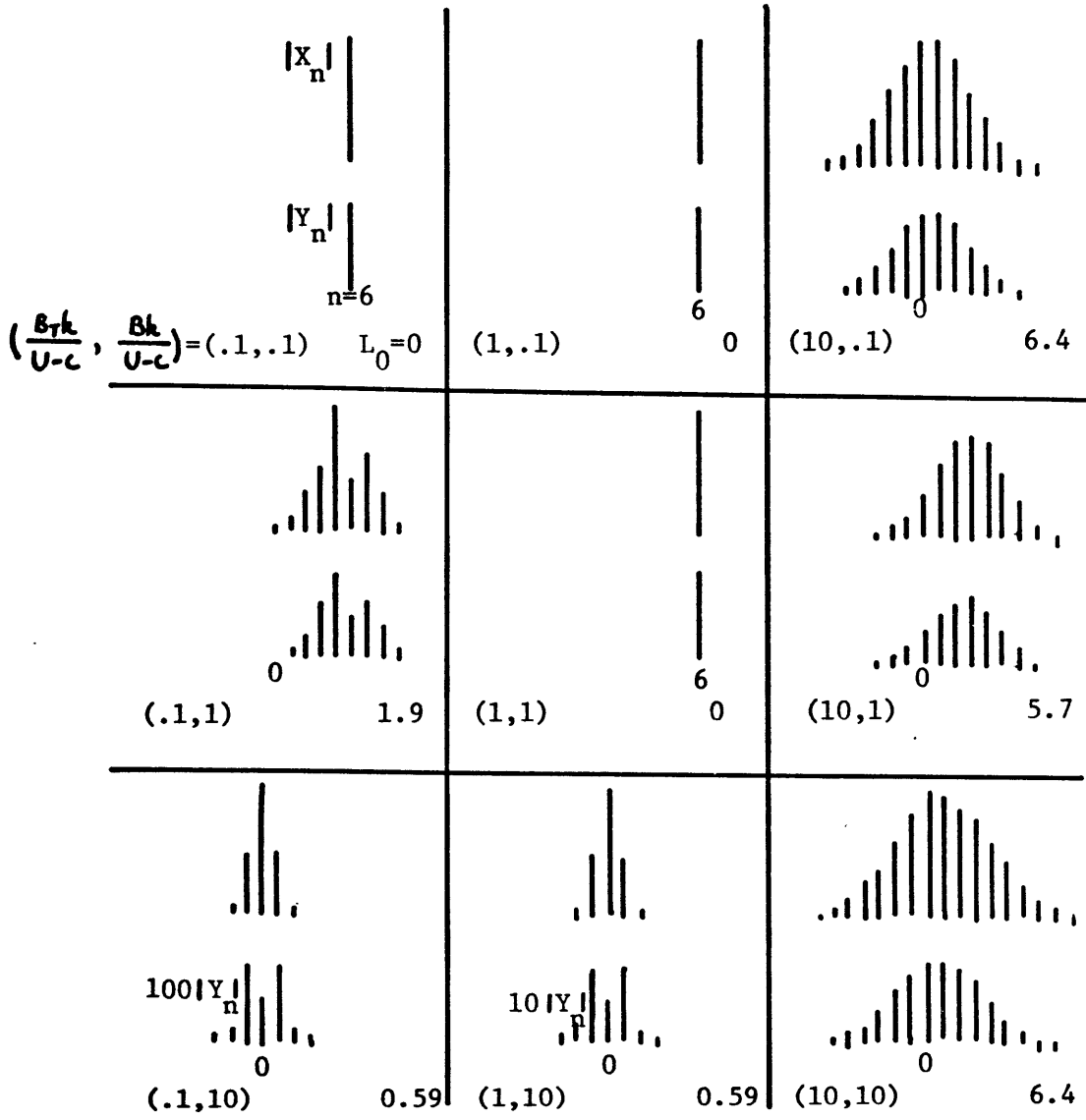


Fig. 5.8 As in Fig. 5.3 but for $k/k = 10$, $N=13$.

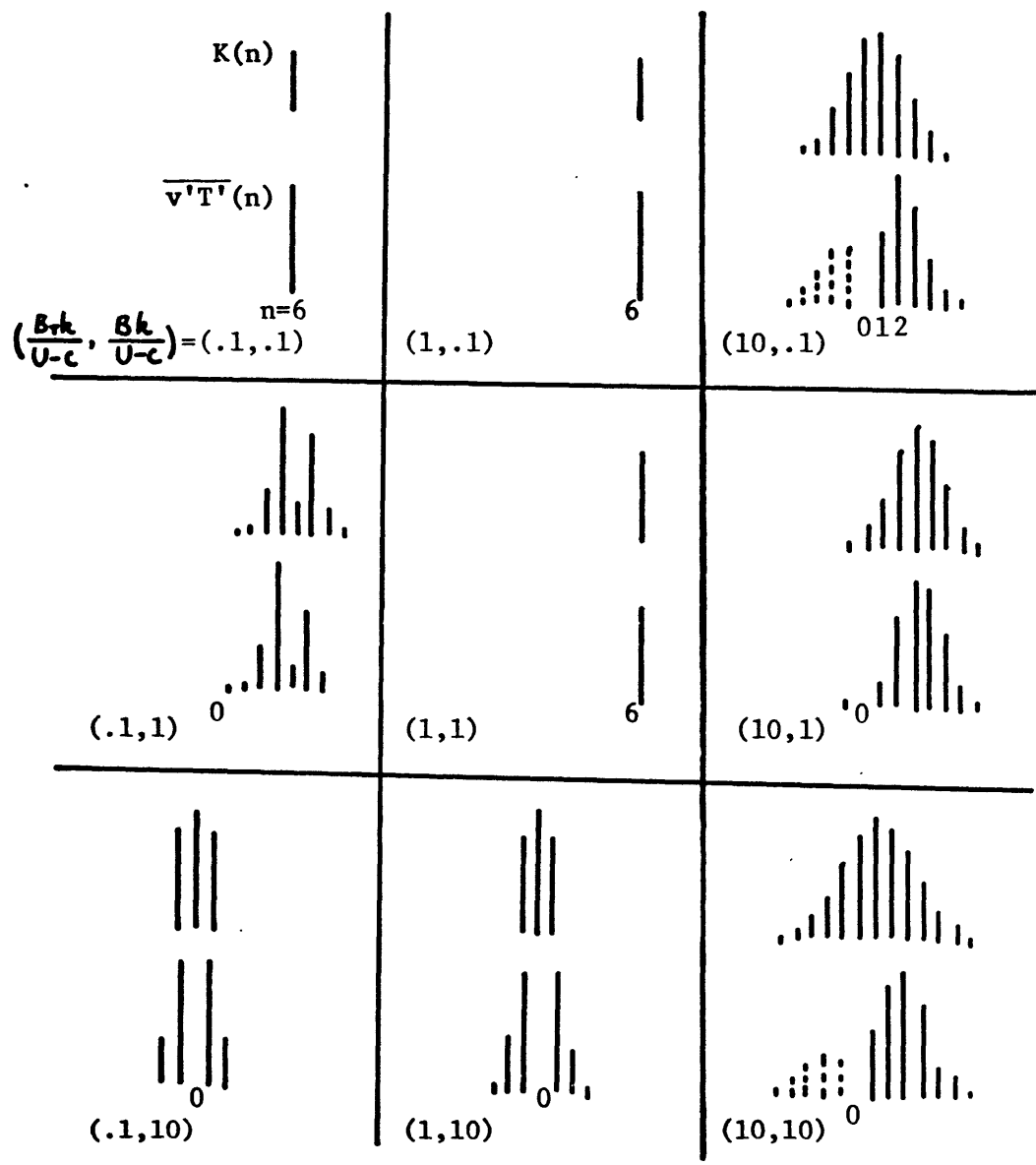


Fig. 5.9 As in Fig. 5.4 but for $k/h = 10$, $N=13$.

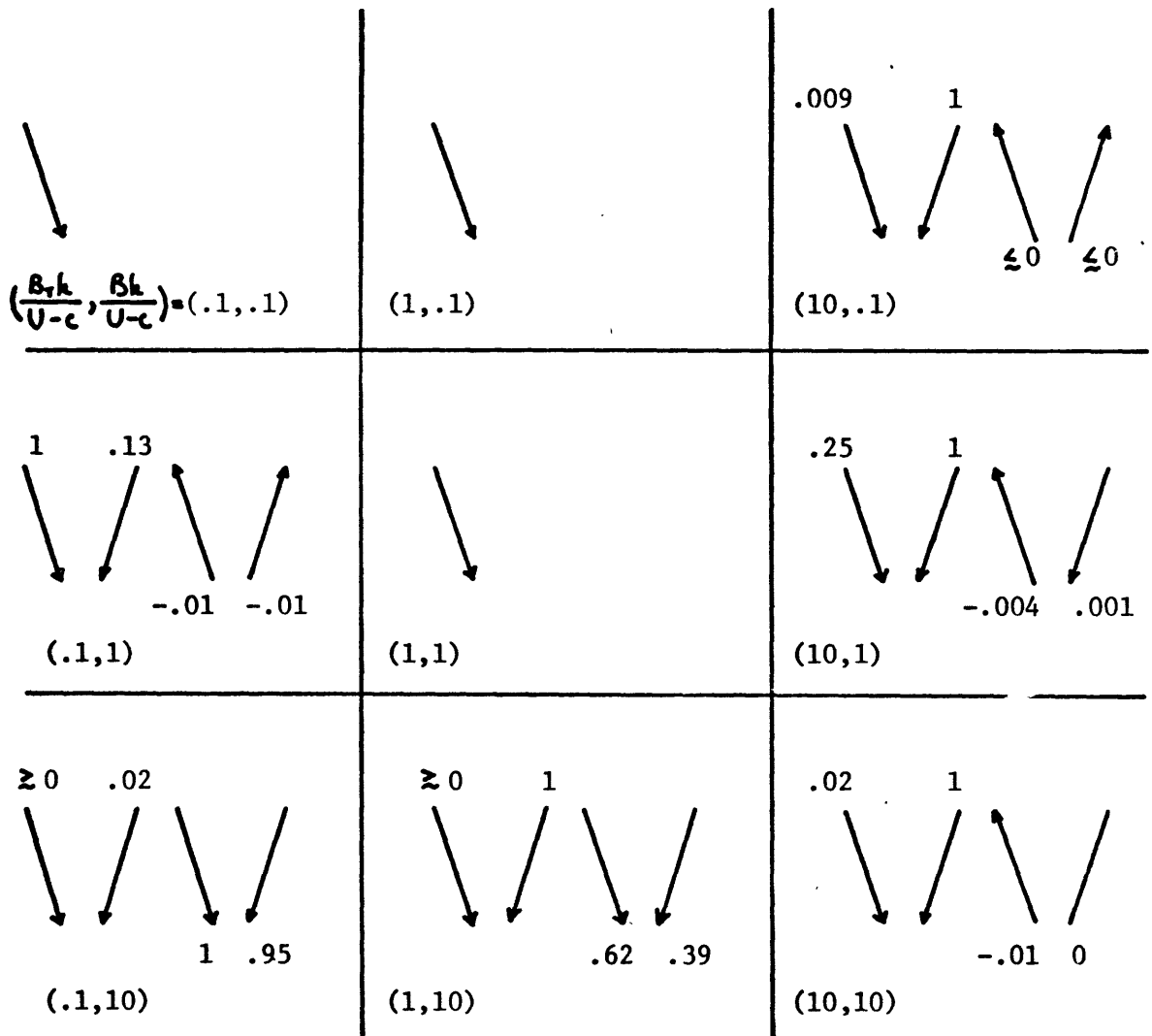


Fig. 5.10 As in Fig. 5.5 but for $r/k = 10$, $N=13$.

than the radius of deformation.

The energetics of the unstable modes is shown in Fig. 5.10. There is only one conversion for the modes in the Phillips regime (0.1,0.1), (1,0.1) and (1,1). The baroclinic interaction with the basic wave dominates in (10,0.1), (10,1) and (10,10); there, the ratio of basic wave APE to KE is larger than 50. For (10,1), the baroclinic interaction with the zonal flow is also significant; $\frac{U_r}{U-c} = 5.03$ is largest there among all three cases. This is consistent with the fact that the spectra for this case peaks at a scale closer to the radius of deformation than the other two cases. Baroclinic interaction with the zonal flow is dominant in (0.1,1), again consistent with the peak of the spectra of that mode near the radius of deformation. The barotropic conversions dominate in (0.1,10) in the Lorenz regime while the baroclinic and barotropic wave interactions are comparable for (1,10).

V-3. Stability of synoptic scale basic wave

We now consider the stability of a synoptic scale basic wave and take $\frac{k}{k_c} = \sqrt{2}$. This value corresponds to the wavelength of maximum instability of a baroclinic zonal flow according to linear theory. From earlier analyses, we do not expect many harmonics of the basic wave scale to be excited as the lowest truncation resolved both the radius of deformation and the basic wave scale. Also, the zonal shear cannot exceed the minimum critical shear $\frac{U_r}{\beta} \leq 1$, in order that the basic wave be stable.

In Fig. 5.11, we see the growth rate as a function of basic wave amplitudes for the most unstable mode, for $N=1$. The Lorenz and Kim regimes are present as before, but now the growth rates in the two regimes are comparable, i.e. horizontal and vertical shears of the basic

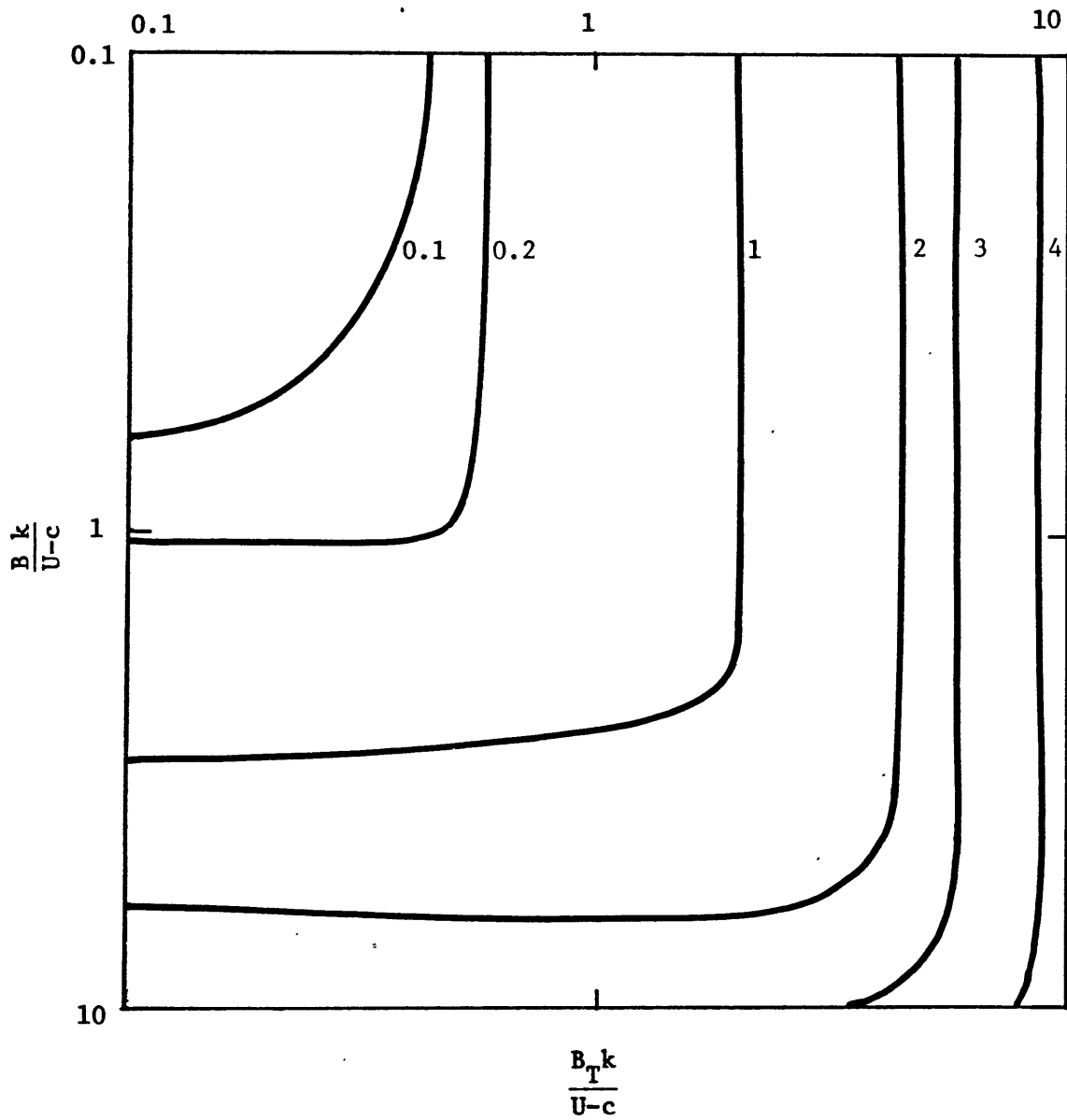


Fig. 5.11 As in Fig. 5.1 but for $\nu/h = 1.2$. All modes are stationary relative to basic wave.

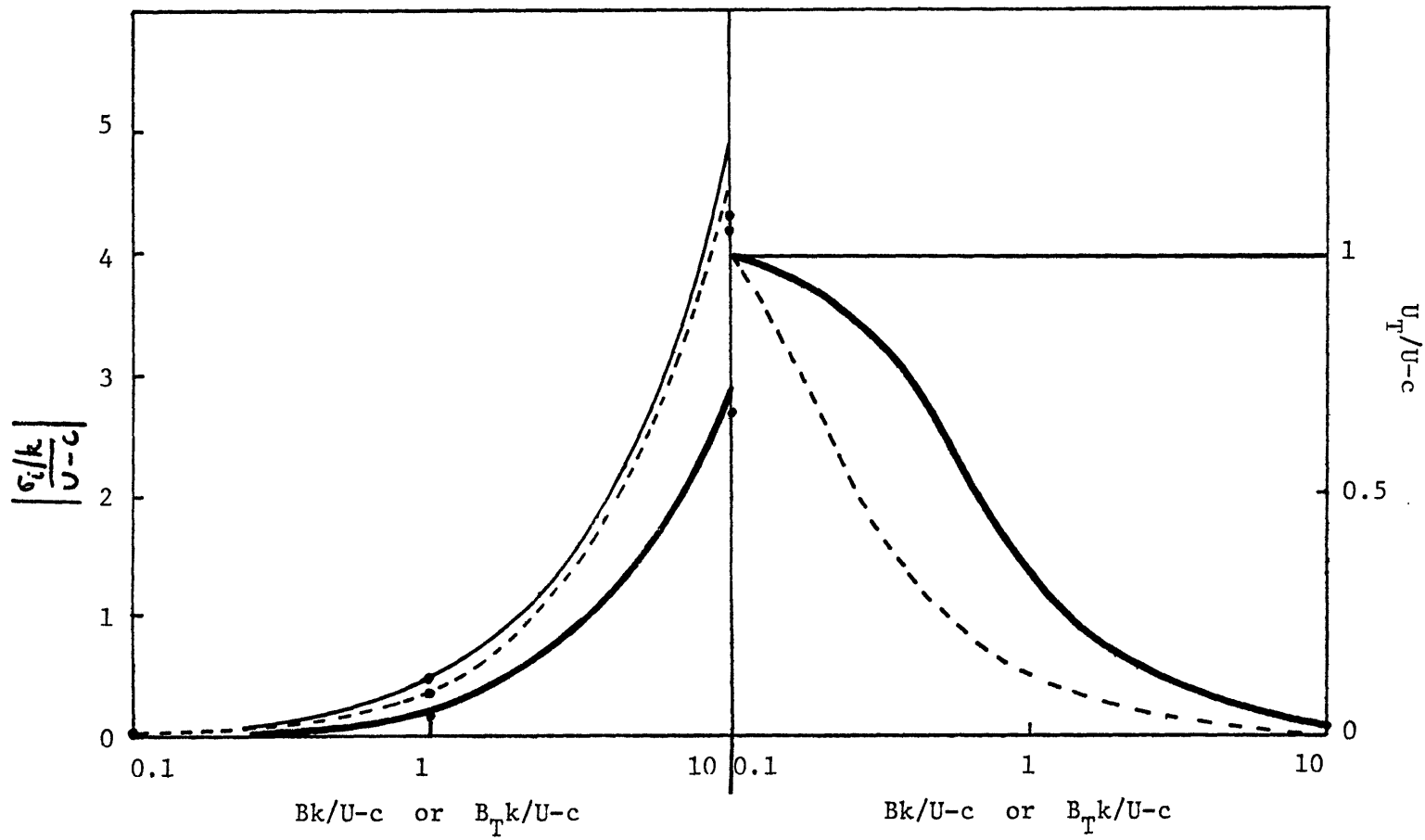


Fig. 5.12 As in Fig. 5.2 but for $r/k = 1.2$. Dots are for $N=6$.

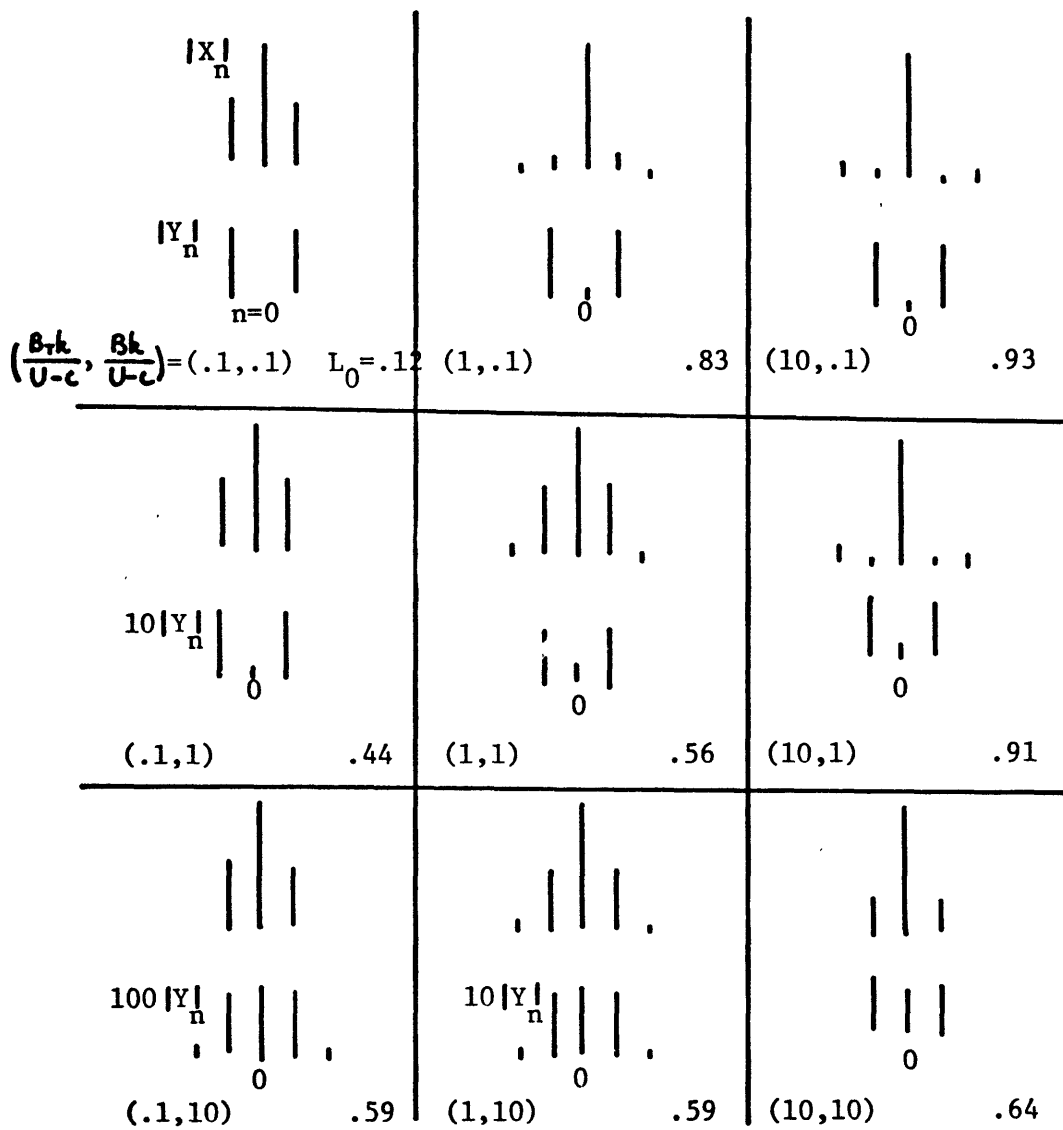


Fig. 5.13 As in Fig. 5.3 but for $\mu/k = 1.2$, $N=6$.

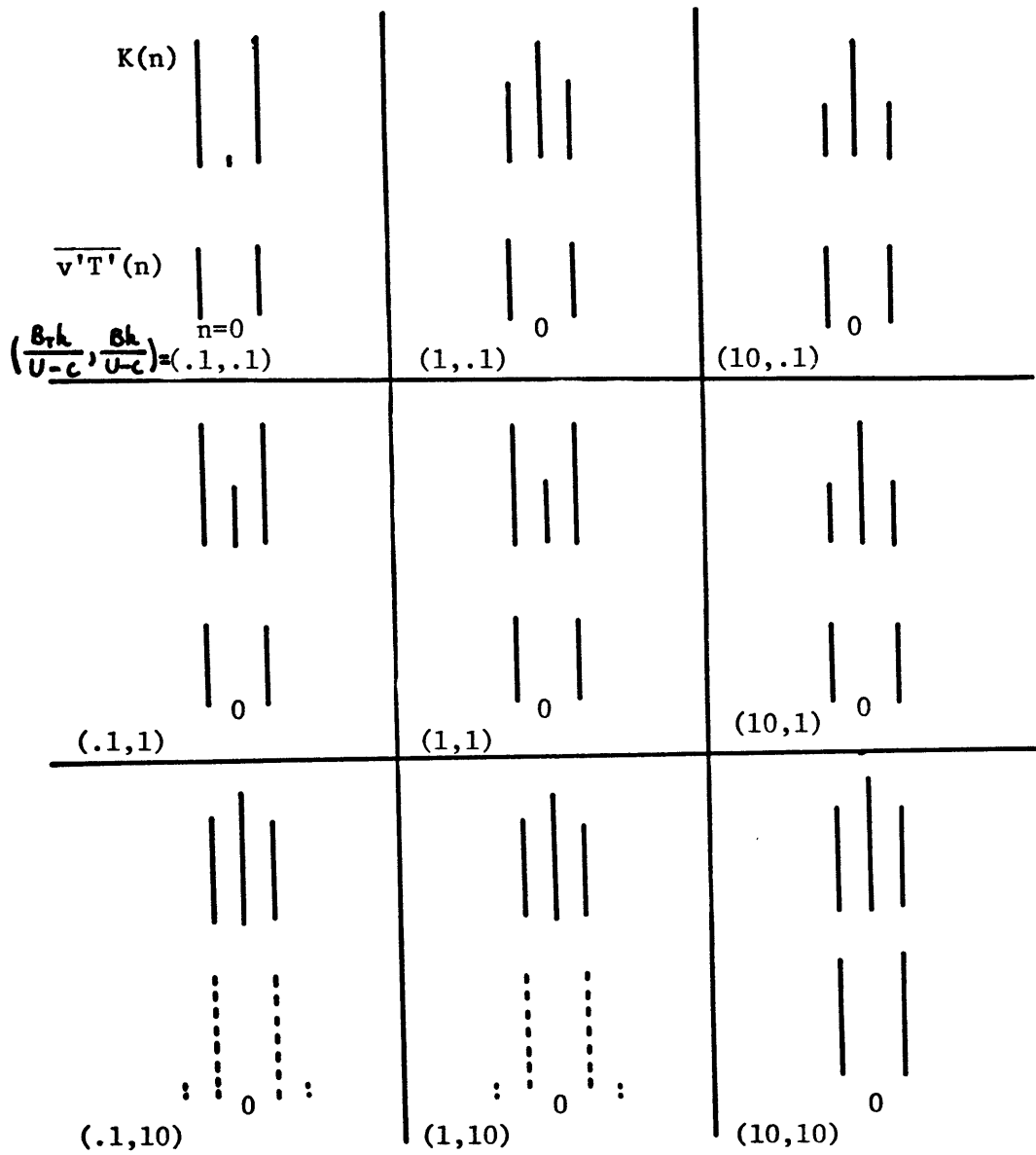


Fig. 5.14 As in Fig. 5.4 but for $\tau/k = 1.2$, $N=6$.

waves are comparable due to the smaller scale of the basic wave. The Phillips regime is not as prominent as before. The value of $u_1/U-c$ does not exceed unity appreciably and all modes are non-propagating, unlike the earlier cases. This reflects the weaker effect of the zonal shear. This fact is also shown in Fig. 5.12, where we proceed along the baroclinic, barotropic and mixed baroclinic-barotropic wave paths. The growth rates increase with wave amplitudes monotonically, even when the latter are less than order unity. The increase is slow in the Phillips regime and much faster in the wave regimes, as expected. The $N=1$ results are good approximations to the $N=6$ results, where convergence has been obtained.

Figs. 5.13 and 5.14 show the spectra $|X_n|$, $|Y_n|$, $K(n)$ and $\overline{v'T'(n)}$. In all cases, convergence has taken place by the second truncation, i.e. there is significant amplitude only in the $n=0$ and $n=\pm 1$ modes. The spectra are all symmetrical as the modes are non-propagating. Except for (0.1,0.1), the meridional wavenumber of the most unstable mode is less than and of order unity, i.e. the meridional scale is of the order of the radius of deformation. The case (0.1,0.1) corresponds to the small basic wave amplitude limit. For the pure barotropic $\frac{\beta_T}{\beta} = 0$ and baroclinic $\frac{\beta_T}{\beta} = \infty$ basic Rossby wave with no shear in the zonal flow, instability for small basic wave amplitudes corresponds to a resonantly interacting triad consisting of the basic wave and two perturbation waves (Gill, 1974; Yamagata, 1977). Pedlosky (1975a) using a 2-level model, examined the small amplitude limit of a marginally stable synoptic scale baroclinic wave in a zonal flow at minimum critical shear. He found the instability is again in the form of a triad resonance and the meridional

scale of the most unstable mode is of the order of the radius of deformation. However, these studies allowed for a more general perturbation zonal wavenumber: instead of multiples of the basic wavenumber, it was taken to be a constant wavenumber plus multiples of the basic wavenumber, i.e. $k_0 + nk$; k_0 , which was constrained to satisfy a resonant condition, was chosen to maximize the growth rate. In our case, $k_0 = 0$ and due to a lack of meridional structure in the basic wave, the resonance condition requires the meridional wavenumber of the perturbation to vanish. This means the basic wavevector and the perturbation wavevector are parallel, which leads to no instability. However, near resonance, L can be small and non-zero and instability is possible. Thus for the most unstable mode of (0.1,0.1), $L_0 = 0.12$ is smaller than the other cases. Pedlosky (1975a) found that for the most unstable mode, the resonant condition required $|k_0/k| = 0.06 \ll 1$. We will be interested primarily in a basic wave of planetary scale when we apply our results to the atmosphere. For such a basic wave, the small value of $|k_0/k|$ means that the perturbation consists of a very large scale component ($n = 0$ component). This component will have a zonal scale many times the basic wave scale, which is unrealistic for our applications to the atmosphere. Thus for our purposes, the restriction $k_0 = 0$ is not a serious one.

The energetics for the nine cases examined are shown in Fig. 5.15. For (0.1,1), (0.1,10) and (1,10), the barotropic conversions dominate as these belong to the Lorenz regime; the ratio of wave APE to KE here is no larger than 0.01. For (1,0.1), (10,0.1) and (10,1) in the Kim regime, the baroclinic interaction with the wave is most important, but the barotropic interactions are significant too. This was not the case for the larger scale basic waves examined earlier where the latter were negligible.

This is because here, the basic wave scale is sufficiently small so that the ratio of wave APE to KE is only slightly larger than unity for these cases. Thus barotropic effects are still significant. For (0.1,0.1), the barotropic interaction with the zonal flow is small. This is because the zonal shear is less than the minimum critical shear and the instability corresponds to a resonant triad, as we discussed earlier. Thus wave conversions dominate. This was not the case for the larger scale basic waves examined earlier because there, the zonal shear by itself was unstable and was the dominant mechanism for instability. In the (1,1) case, zonal flow and wave effects are comparable while for (10,10), the wave interactions dominate, as expected.

V.4 Meridional scale of most unstable mode.

The stability analysis of a non-axisymmetric basic state provides a mechanism for selecting meridional scales. In his study of the instability of the baroclinic Rossby wave, Kim (1975) found the meridional scale of the most unstable mode to be close to the radius of deformation; there is energy transfer from both large and small scales towards this scale. Pedlosky (1975a) considered the stability of a baroclinic wave and a zonal flow at neutral stability as a mechanism for selection of meridional scales of motion in the ocean. The basic wave was of synoptic scale and the limit of small basic wave amplitude was examined. The meridional scale of the most unstable mode was again found to be close to the radius of deformation. In our analysis, the basic wave will be of planetary scale with arbitrary amplitude.

Knowledge of the meridional scale is crucial to finite amplitude

dynamics of baroclinic waves. Pedlosky (1975b) showed that the ratio of that scale to the radius of deformation is important in the equilibration of finite amplitude waves. The eastward velocity (u') and northward velocity (v'), obtained from an earlier analysis (Pedlosky, 1970), of the finite amplitude wave field in the two-level model are

$$u' = -(U^2 - U_c^2)^{1/2} a(t) \cos k(x-ct) \cos ly$$

$$v' = -(U^2 - U_c^2)^{1/2} a(t) \frac{k}{l} \sin k(x-ct) \sin ly$$

In the above, U is the velocity difference between the two layers, U_c is the critical velocity required for instability, $a(t)$ is an oscillatory function of time determined by non-linear theory and is order unity, k and l are the zonal and meridional wavenumbers respectively. We see that the ratio of the magnitudes of fluctuating meridional to zonal velocities is given by k/l . For the most unstable mode from linear theory, $k^2 + l^2 = \sqrt{2}/L_d^2$, where L_d is the radius of deformation (Pedlosky, 1970); thus

$$\frac{k}{l} = \left(\frac{\sqrt{2}}{l^2 L_d^2} - 1 \right)^{1/2}$$

The ratio of fluctuating meridional to mean velocities in Pedlosky's model thus depends on the ratio of the meridional scale of the disturbance

to the radius of deformation. For modes with $\frac{k}{l} \gg 1$, i.e. $l \ll L_n^{-1}$, the fluctuating meridional velocity can greatly exceed the mean velocity, thus such modes are characterized by weak non-linear self-interaction. The meridional scale also appears explicitly in the expression for the steady equilibrium wave amplitude. Pedlosky (1971) examined the finite amplitude baroclinic instability problem with small dissipation and found the streamfunction amplitude ($|A|^2$) reached a steady equilibrium value, independent of the dissipation parameter. This equilibrium value is

$$|A|^2 = \frac{U^2 - U_c^2}{l^2} |a(t=\infty)|^2$$

In the above, $a(t=\infty)$ is an order unity constant. The ratio $\frac{k}{l}$ also plays an important role in parameterizations of heat flux by large scale eddies (Green, 1970; Stone, 1972; Held, 1978). The closure assumptions used in these parameterizations depend on the value of this ratio.

In our stability analysis, the basic wave has no meridional variation. The most unstable perturbation has however a non-zero meridional wavenumber in general; its meridional scale being such that interaction between the basic state and the perturbation is most efficient at extracting energy of the basic flow. We show in the table below the non-dimensional meridional wavenumber (L_0) of the most unstable mode for $(0.1, 0.1) \leq (\beta_{rk}/U-c, \beta^k/U-c) \leq (10, 10)$; for each pair $(\beta_{rk}/U-c, \beta^k/U-c)$, L_0 is shown for the three basic wave scales examined: $M/k = 10, 3.9, 1.2$ respectively.

	$\frac{B_T k}{U - c} = 0.1$	1	10
$\frac{B k}{U - c} = 0.1$	0 0 0.12	0 2.3 0.83	6.4 2.5 0.93
1	1.9 0.43 0.44	0 0 0.56	5.7 2.5 0.91
10	0.59 0.59 0.59	0.59 0.59 0.59	6.4 2.5 0.64

The perturbation has no unique zonal scale as it consists of a superposition of harmonics of the basic wave. Its dominant zonal scale may be estimated by the scale which contains the maximum perturbation KE. Most of the perturbation KE spectra examined peak at $n=0$ indicating the perturbation zonal flow has most KE. This suggests the meridional scale is a good estimate of the scale of the perturbation. From the above table, we see that for sufficiently small basic wave scale, we have $L_0 < 1$, i.e. small scale currents generate perturbations with scales larger than the basic wave scale. This is similar to two dimensional or quasi-geostrophic turbulence where an energy cascade must move preferentially toward small wavenumbers. Also, the value of L_0 varies considerably in parameter space. In this section, we examine the parameter dependence of L_0 by using results of the

lowest truncation. In this case, the dispersion relation can be obtained analytically. However, results of the lowest truncation are accurate when the basic wave scale and the radius of deformation are not widely separated. This is true for the case $\mu/k = 1.2$, and to a lesser extent, for the case when the basic wave corresponds to wavenumber two ($\mu/k = 3.9$).

For the lowest truncation, the dispersion relation for the eigenvalue $\lambda = \frac{\sigma/k}{U-c}$ can be written as

$$f(f^2 + Bf + C) = 0 \quad ; \quad f = \lambda^2 \quad (5.1)$$

$$B = -(a_1^2 + 2b_1f_1 + e_1^2) - 2(s_0t_{-1} + c_0c_{-1} + g_0g_{-1} + t_0s_{-1})$$

$$C = (a_1e_1 - b_1f_1)^2 + 4(c_{-1}g_{-1} - s_{-1}t_{-1})(c_0g_0 - s_0t_0) + 2(s_0t_{-1} + c_0c_{-1})(b_1f_1 + e_1^2) + 2(g_0g_{-1} + t_0s_{-1})(b_1f_1 + a_1^2) - 2b_1(g_0t_{-1} + t_0c_{-1})(a_1 + e_1) - 2f_1(s_0g_{-1} + c_0s_{-1})(a_1 + e_1)$$

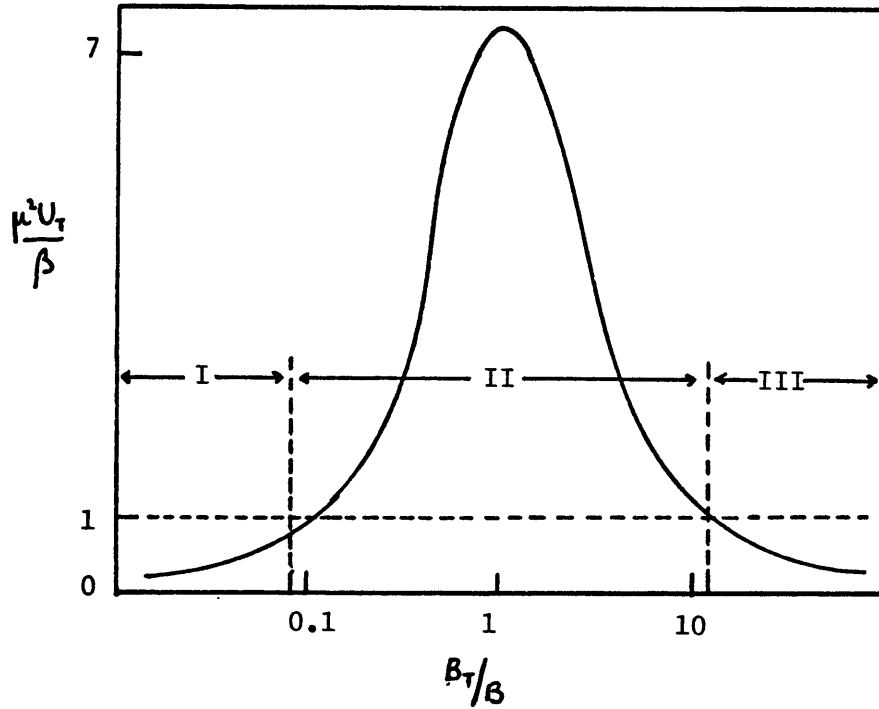
The variables $a_1, e_1,$ etc. are defined in eq. (4.7c). We see non-trivial values of λ are given by a quadratic equation in λ^2 .

The coefficients B and C are complicated functions of the three independent parameters $\beta/\beta, \mu/k, \beta k/U-c$ and the meridional wavenumber $L = \ell/k$.

The algebra proves too cumbersome for an exact analytic solution $\lambda = \lambda(L)$ valid throughout parameter space, but appropriate expressions may be derived for the various regimes.

The meridional wavenumber L_0 may then be found by maximizing the imaginary part of λ with respect to L . To do this,

we need a quantitative classification of the different regimes. We will do this for $k/k_c = 3.9$, the case where the basic wave corresponds to wavenumber 2. We sketch below the zonal shear as a function of B_T/β for a wavenumber 2 basic Rossby wave (see Fig. 2.4).



We have classified the Lorenz and Kim regimes as the regimes where the barotropic and baroclinic component of the basic wave dominates respectively. The Phillips regime is characterized by an unstable zonal flow and a weak basic wave. A fourth regime, where the barotropic and baroclinic components of the basic wave are about equal and both large, will be referred to as the mixed wave regime. With reference to the above sketch, we classify the four regimes quantitatively as follows:

(I) $\frac{B_T}{B} \ll 1$, $\frac{\mu^2 U_T}{\beta} < 1$: Lorenz regime

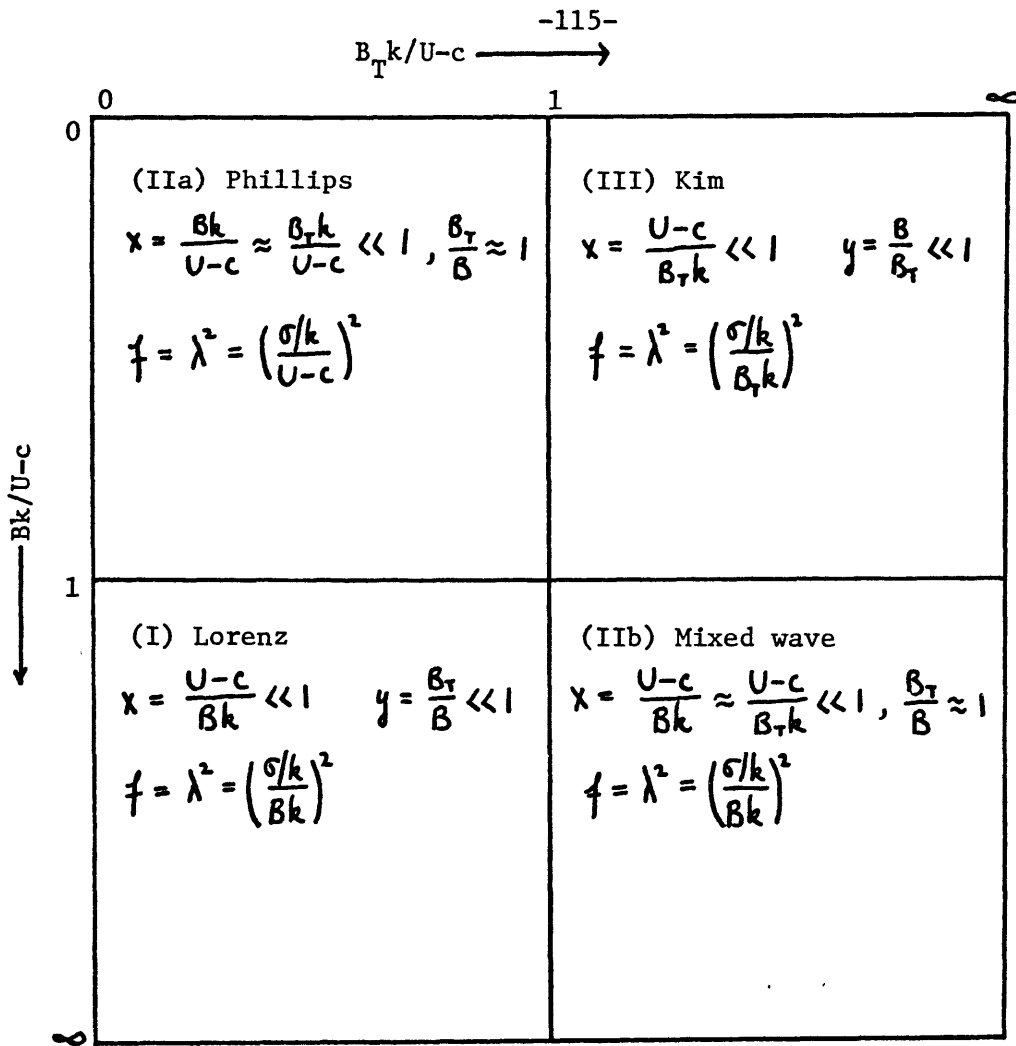
(III) $\frac{B_T}{B} \gg 1$, $\frac{\mu^2 U_T}{\beta} < 1$: Kim regime

(II) $\frac{B_T}{B} \approx 1$, $\frac{\mu^2 U_T}{\beta} > 1$:

(a) Phillips regime if wave amplitude is small: $\frac{Bk}{U-c} \approx \frac{B_T k}{U-c} \ll 1$

(b) Mixed wave regime if wave amplitude is large: $\frac{Bk}{U-c} \approx \frac{B_T k}{U-c} \gg 1$

Due to the dominance of different basic flow components in the different regimes, we rescale the dimensional equations to obtain expressions for the growth rate that are valid locally in each regime. We do this by scaling the dimensional growth rate by the dominant destabilizing mechanism in each regime, so that the non-dimensional growth rate remains order unity. The appropriate non-dimensional equations for the Lorenz, Kim, Phillips and mixed wave regimes are given in eqs. (4.7a,b). The coefficients in eq. (4.7c) are multiplied by $U-c/Bk$, $U-c/B_T k$ and $U-c/Bk$ for the Lorenz, Kim and mixed wave regimes while they remain unchanged for the Phillips regime. The various scalings are illustrated schematically below:



We will examine each of the four regimes separately. In each case, approximations to the solution of eq. (5.1) will be derived analytically.

(i) Lorenz regime

This regime is characterized by a strong barotropic basic wave.

Accordingly, we take $x = \frac{U-c}{Bk} \ll 1, y = \frac{B_T}{B} \ll 1$ and calculate

$f = \left(\frac{\sigma/k}{Bk}\right)^2$ for small x and y . In other words, we do a

two-variable Taylor expansion of $f(\underline{x}) = f(x, y)$ about the

origin $\underline{x}_0 = (0, 0)$. This is done by differentiating eq. (5.1)

implicitly to find the derivative of f , which is then evaluated

at \underline{x}_0 . Two unstable modes exist at \underline{x}_0 ; they consist of

pure barotropic and baroclinic perturbations respectively. The former is the mode investigated by Lorenz (1972) and is more unstable than the latter. For the former mode, we find $f_x(\underline{x}_0)$, $f_y(\underline{x}_0)$ and $f_{xy}(\underline{x}_0)$ all vanish while $f_{xx}(\underline{x}_0) > 0$ and $f_{yy}(\underline{x}_0) < 0$. Thus \underline{x}_0 is a critical point and from the behavior of the second derivatives, we see that it does not represent an extremum. For the latter mode,

$f_x(\underline{x}_0)$, $f_y(\underline{x}_0)$ and $f_{xy}(\underline{x}_0)$ again vanish, but $f_{xx}(\underline{x}_0) > 0$ and $f_{yy}(\underline{x}_0) > 0$. Thus the critical point \underline{x}_0 gives a relative minimum for this mode. This minimum at $f(\underline{x}_0)$ represents a growth rate maximum because $f = \lambda^2 < 0$ for instability. The expansion up to second order for the more unstable mode is shown below:

$$f = \left(\frac{\sigma/k}{\beta k}\right)^2 = \frac{L^2}{L^2+1} \left\{ \frac{1}{2}(L^2-1) + \left(\frac{U-c}{\beta k}\right)^2 \frac{L^2}{L^2+1} + \left(\frac{\beta_T}{\beta}\right)^2 \frac{1}{2} \frac{L^2-1}{M^2(L^2+M^2)} \left[M^2(M^2+L^2) + 2L^2(M^4+1-L^4) \right] \right\} \quad (5.2)$$

We see that f is real, i.e. any possible instabilities are non-propagating. To find the meridional wavenumber of the most unstable mode L_0 , we differentiate eq. (5.2) with respect to L^2 and set the derivative equal to zero. The resulting equation is still difficult to solve analytically and we thus make another approximation. In the problem examined by Lorenz (1972), the two dimensional nature of the motion constrained $L^2 < 1$ for any instability to occur. This can be seen in eq. (5.2) by setting $\beta_T/\beta = 0$. In our problem, the Lorenz regime may be expected to be quasi-two dimensional, thus we may still expect $L^2 < 1$. Thus we carry terms up to

order L^2 and neglect higher order terms in evaluating L_0 . The result is

$$L_0^2 = \frac{1}{2} \frac{1 + (B_T/B)^2}{1 + 2 \left(\frac{U-c}{Bk} \right)^2 - \left(1 + 2 \frac{k^2}{\mu^2} \right) (B_T/B)^2} \quad (5.3)$$

The most unstable meridional wavenumber L_0 as given by eq. (5.3) and the corresponding growth rate are shown for $\mu/k = 3.9$ in Table 5.1. Also shown for comparison are the exact values found numerically. We see that the approximate expression works well in the Lorenz regime.

As a matter of fact, the almost constant value of $L_0 = 0.65$ for $\frac{Bk}{U-c} \geq 4$, $\frac{B_T k}{U-c} \leq 1$ in this regime suggests an even simpler approximation. Setting $\frac{U-c}{Bk} = 0 = \frac{B_T}{B}$ in eq. (5.3), we get for the most unstable mode $L_0 = 1/\sqrt{2} = 0.71$.

An even better approximation can be obtained for this simple case by setting $\frac{U-c}{Bk} = 0 = \frac{B_T}{B}$ in eq. (5.2) and finding L_0 without assuming it is small compared to unity. This gives $L_0 = \sqrt{\sqrt{2}-1} = 0.64$.

Of course, this approximation does not work in as large a region in parameter space as eq.(5.3), but as we can see from the exact values, it works well in the Lorenz regime. The Lorenz regime is quasi-barotropic and is not sensitive to vertical stratification, thus the results are largely independent of μ/k .

	$\frac{B_T k}{U-c}=0.1$	0.4	0.7	1	4	7	10
$\frac{Bk}{U-c}=0.1$	(0.01, .07) (0.77, 1.5)	(0.04, .21) (1.29, 2.0)	(0.14, .41) (1.19, 2.5)	(0.36, .71) (1.34, 2.5)	--- (4.66, 2.5)	--- (8.17, 2.5)	--- (11.7, 2.5)
0.4	(0.04, .20) (0.19, 2.0)	(0.08, .28) (0.82, 1.5)	(0.18, .44) (1.26, 1.5)	(0.38, .71) (1.57, 2.0)	--- (4.39, 2.0)	--- (7.88, 2.5)	--- (11.5, 2.5)
0.7	(0.11, .32) (0.12, 2.5)	(0.15, .37) (0.56, 2.0)	(0.24, .50) (0.97, 2.0)	(0.43, .71) (1.34, 2.0)	--- (4.36, 2.5)	--- (7.47, 2.5)	--- (10.7, 2.0)
1	(0.21, .41) (0.20, .40)	(0.24, .45) (0.49, 2.5)	(0.33, .55) (0.86, 2.5)	(0.50, .71) (1.22, 2.5)	--- (4.41, 2.5)	--- (7.51, 2.5)	--- (10.7, 2.5)
4	(1.34, .67) (1.13, .65)	(1.35, .67) (1.14, .65)	(1.39, .69) (1.16, .65)	(1.46, .71) (1.19, .65)	(8.30, 2.9) (4.30, 2.5)	--- (7.52, 2.5)	--- (10.7, 2.5)
7	(2.43, .69) (2.03, .65)	(2.44, .70) (2.03, .65)	(2.46, .70) (2.05, .65)	(2.50, .71) (2.07, .65)	(3.89, .97) (4.24, 2.5)	(27.7, 5.6) (7.48, 2.5)	--- (10.7, 2.5)
10	(3.50, .70) (2.91, .65)	(3.51, .70) (2.92, .65)	(3.53, .70) (2.93, .65)	(3.55, .71) (2.94, .65)	(4.43, .82) (4.18, 2.5)	(7.27, 1.2) (7.44, 2.5)	(67.1, 9.5) (10.7, 2.5)

-118-

Table 5.1 Non-dimensional growth rate and meridional wavenumber ($|\frac{\sigma_i}{k}|, L_0$) for most unstable mode calculated from a second order expansion valid for the Lorenz regime; --- indicates the expansion is not valid there. The exact values are shown below the approximate values. $\mu/k = 3.9, N=1$.

(ii) Kim regime

This regime is characterized by a strong baroclinic wave. We proceed as in the Lorenz regime by expanding $f(\underline{x}) = f(U-c/\beta_T k, \beta/\beta_T)$ about the origin $\underline{x}_0 = (0, 0)$. There are two unstable modes at \underline{x}_0 with different vertical structure, and one grows faster than the other. \underline{x}_0 is again a critical point for both modes, but the second derivatives are not of one sign, thus \underline{x}_0 is not an extremum. However, for most values of $M = U/k$ and $L = \beta/k$, the faster growing mode does represent a growth rate maximum in parameter space. The Taylor expansion up to second order for this mode is

$$f = \left(\frac{\sigma/k}{\beta_T k}\right)^2 = \frac{L^2}{L^2+M^2+1} \left\{ \frac{1}{2}(L^2-M^2-1) + \left(\frac{U-c}{\beta_T k}\right)^2 \frac{L^2}{L^2+M^2+1} - \left(\frac{\beta}{\beta_T}\right)^2 \frac{1}{2} \frac{(L^4+M^2L^2-1)(L^2-M^2-1)(L^2+M^2) + (L^2-1)(L^4-L^2-M^4)(L^2+M^2+1)}{M^2(M^2+1)} \right\} \quad (5.4)$$

The numerical results indicate that $L_0^2 < 1$ does not hold in general, but it is true that $L_0^2/M^2 < 1$ for all cases examined. Thus we expand in L^2/M^2 and keep only first order terms. The value of L_0^2 found this way is

$$L_0^2 = \frac{1}{2} M^2 (M^2+1)^2 \frac{1 + (\beta_T/\beta)^2}{M^2(M^2+1) + 2M^2 \left(\frac{U-c}{\beta_T k}\right)^2 + (M^6 - M^4 - 1) \left(\frac{\beta}{\beta_T}\right)^2} \quad (5.5)$$

The value of L_0 and the corresponding growth rate and their exact values for $U/k = 3.9$ are shown in Table 5.2. We see they agree

	$\frac{B_T k}{U-c}=0.1$	0.4	0.7	1	4	7	10
$\frac{Bk}{U-c}=0.1$	(0.05, .78) (0.77, 1.5)	(0.36, 1.8) (1.29, 2.0)	(0.81, 2.3) (1.19, 2.5)	(1.27, 2.5) (1.34, 2.5)	(5.61, 2.8) (4.66, 2.5)	(9.87, 2.8) (8.17, 2.5)	(14.1, 2.8) (11.7, 2.5)
0.4	(0.15, .78) (0.19, 2.0)	(0.27, 1.0) (0.82, 1.5)	(0.53, 1.4) (1.26, 1.5)	(0.87, 1.7) (1.57, 2.0)	(5.31, 2.7) (4.39, 2.0)	(9.69, 2.8) (7.88, 2.0)	(14.0, 2.8) (11.5, 2.5)
0.7	(0.26, .78) (0.12, 2.5)	(0.33, .88) (0.56, 2.0)	(0.49, 1.1) (0.97, 2.0)	(0.72, 1.3) (1.34, 2.0)	(4.81, 2.4) (4.37, 2.5)	(9.31, 2.7) (7.47, 2.5)	(13.7, 2.7) (10.7, 2.0)
1	(0.36, .78) (0.20, .40)	(0.42, .83) (0.49, 2.5)	(0.53, .93) (0.86, 2.5)	(0.70, 1.1) (1.22, 2.5)	(4.30, 2.2) (4.41, 2.5)	(8.83, 2.5) (7.51, 2.5)	(13.3, 2.7) (10.7, 2.5)
4	(1.45, .78) (1.13, .65)	(1.46, .78) (1.14, .65)	(1.49, .79) (1.16, .65)	(1.53, .80) (1.19, .65)	(2.80, 1.1) (4.30, 2.5)	(5.37, 1.4) (7.52, 2.5)	(8.85, 1.7) (10.7, 2.5)
7	(2.53, .78) (2.03, .65)	(2.54, .78) (2.03, .65)	(2.55, .78) (2.05, .65)	(2.58, .79) (2.07, .65)	(3.32, .89) (4.24, 2.5)	(4.91, 1.1) (7.48, 2.5)	(7.24, 1.3) (10.7, 2.5)
10	(3.62, .78) (2.91, .65)	(3.62, .78) (2.92, .65)	(3.63, .78) (2.93, .65)	(3.65, .78) (2.94, .65)	(4.17, .84) (4.18, 2.5)	(5.30, .94) (7.44, 2.5)	(7.01, 1.1) (10.7, 2.5)

Table 5.2 As in Table 5.1 but the second order expansion is valid for the Kim regime.

well in the Kim regime. As in the Lorenz regime, the Kim regime is characterized by an almost constant value of $L_0 \approx 2.5$. Proceeding as before by taking $U-c/\beta_{rk} = 0 = \beta/\beta_T$ in eq. (5.4), we find $L_0 = \sqrt{\sqrt{2}-1} (M^2+1)^{1/2} = 0.64 (M^2+1)^{1/2}$. For the three values of M^2 examined ($M^2 = 100, 15, 1.4$), this gives $L_0 = 6.4, 2.6$ and 1.0 respectively; the exact values are 6, 2.5 and 1.0 respectively.

(iii) Phillips regime

In this regime, we have $\chi = \beta k / U-c \approx \beta_T k / U-c \ll 1$, $\beta_T / \beta \approx 1$, i.e. the wave amplitudes are small so that the zonal shear dominates. We treat β_T / β as a fixed order unity parameter and expand $f(x)$ around $x_0 = 0$. We find $f'(x_0) = 0$, i.e. x_0 is a critical point. However, the algebra proved too complex to obtain the second order correction $f''(x_0)$ analytically. The lowest order approximation is thus

$$f(x_0) = \frac{1}{2} \left\{ (a_1^2 + 2b_1 f_1 + e_1^2) \pm (a_1 + e_1) \sqrt{(a_1 - e_1)^2 + 4b_1 f_1} \right\} \quad (5.6)$$

Note that unstable modes can be propagating as f can be complex. Differentiating eq. (5.6) with respect to L^2 and setting the derivative equal to zero, we obtain an equation of the fourth degree. An asymptotic solution can be obtained in the limit $\gamma \equiv \beta / 2\mu^2 U_T \ll 1$;

2γ is the minimum critical shear of the 2-level model divided by the zonal shear. The value of L_0 valid in this limit is

$$1 + L_0^2 = \frac{1}{3\sqrt{4}} \gamma^{2/3} M^2 \quad (5.7)$$

For $M^2 = 15$, eq. (5.7) gives $L_0 = 1.2, 1.2, 1.7$ and 1.8 for $(B_r k / U - c, B k / U - c) = (0.1, 0.1), (0.4, 0.4), (0.1, 0.4)$ and $(0.4, 0.1)$ respectively in the Phillips regime. The exact values are

$L_0 = 1.5, 1.5, 2.0, 2.0$ respectively. Equation (5.7) is not valid in as large a region in parameter space as eqs. (5.3) and (5.5), as the latter contain higher order corrections. However, for small wave amplitudes, eq. (5.7) does give satisfactory results.

(iv) Mixed wave regime

In this regime, the barotropic and baroclinic basic wave amplitudes are larger and of comparable magnitude, i.e. $\chi = \frac{U-c}{Bk} \approx \frac{U-c}{B_r k} \ll 1$, $\frac{B_r}{B} \approx 1$. Proceeding as before, we expand $f(\chi)$ around $\chi_0 = 0$, with B_r/B a fixed parameter of order unity. As before, χ_0 is a critical point, but the algebra is again too cumbersome to progress beyond the lowest order. The lowest order approximation is

$$f(\chi_0) = (s_0 t_{-1} + c_0 c_{-1} + g_0 g_{-1} + t_0 s_{-1}) \pm \left\{ (s_0 t_{-1} + c_0 c_{-1} - g_0 g_{-1} - t_0 s_{-1})^2 + 4 (c_0 g_0 s_{-1} t_{-1} + c_{-1} g_{-1} s_0 t_0) \right\}^{1/2} \quad (5.8)$$

Even for the lowest order solution, it was not possible to find L_0 analytically due to the rather involved algebra. However, an estimate

of L_0 may be obtained as follows. Numerical calculations show that the most unstable modes are propagating and the corresponding meridional wavenumber does not vary very much in this regime. It can be shown from eq. (5.8) that a necessary condition for a propagating unstable mode with $B_1/B = 1$ is

$$(L^2 - 1)(L^4 - L^2 - M^4) < 0$$

We obtain an estimate of L_0 by simply minimizing the left hand side of the above. This gives

$$L_0^2 = \frac{1}{3} (2 + \sqrt{1 + 3M^4}) \tag{5.9}$$

Eq. (5.9) gives $L_0 = 7.6, 3.0, 1.2$ for the three cases

$M = 10, 3.9$ and 1.2 respectively; the numerical calculations show that L_0 for this regime are $6, 2.5, 0.7$ respectively.

V.5 Parametric dependence of meridional scale

In the previous section, we have obtained analytical expressions for the meridional wavenumber of the most unstable perturbation in the Lorenz, Kim, Phillips and mixed wave regimes. The expressions are obtained by expanding in appropriate parameters which are small compared to unity. For the Lorenz and Kim regimes, second order corrections are included in the approximations. In the Phillips and mixed-wave regimes, only the lowest order solutions are obtained. By comparing with numerical results, the approximations have been found

to be valid locally in each regime. We present in this section the parametric dependence of the meridional scale of the most unstable mode for each regime. The simplest approximations will be used. We let $L_x = 1/k$ be the zonal scale of the basic wave; $L_y = 1/l$, $L_n = 1/r$ be the meridional scale of the most unstable mode and the radius of the deformation respectively. We also let $L_{xy} = 1/\sqrt{k^2+l^2} = L_y/\sqrt{1+\frac{k^2}{l^2}}$, this scale is approximately equal to the meridional scale if $k^2 \ll l^2$.

(i) Lorenz regime: $L_o = \sqrt{\sqrt{2}-1} = 0.64 \Rightarrow L_y = 1.55 L_x$

(ii) Kim regime: $L_o = \sqrt{\sqrt{2}-1} (M^2+1)^{1/2} \Rightarrow L_y = 1.55 \frac{L_n L_x}{\sqrt{L_n^2 + L_x^2}}$

$$\begin{cases} M^2 \gg 1 \Rightarrow L_y = 1.55 L_n \\ M^2 \ll 1 \Rightarrow L_y = 1.55 L_x \end{cases}$$

(iii) Phillips regime: $1 + L_o^2 = \frac{1}{3\sqrt{4}} \gamma^{2/3} M^2 \Rightarrow L_{xy} = 1.26 \left(\frac{U_T}{r\beta}\right)^{1/3}$

(iv) Mixed-wave regime: $L_o^2 = \frac{1}{3} (2 + \sqrt{1+3M^4})$

$$\begin{cases} M^2 \gg 1 \Rightarrow L_y = 1.32 L_n \\ M^2 \ll 1 \Rightarrow L_y = L_x \end{cases}$$

In the Lorenz regime, vertical stratification is not important and the meridional scale is of the order of the zonal scale. In the Kim regime, the meridional scale involves both the zonal scale and the radius of deformation. For weak stratification, it is of the order of the radius of deformation while for strong stratification, it is close to

the zonal scale. In the Phillips regime, the horizontal scale depends on the radius of deformation, vertical shear and β . In the mixed wave regime, weak stratification gives the radius of deformation as the meridional scale while for strong stratification, it is of the order of the zonal scale.

Pedlosky (1975a) analyzed the stability of a baroclinic Rossby wave in a neutral zonal shear flow. He found that in the limit of small wave amplitude, the instability took the form of a resonant triad consisting of the basic wave and two perturbation waves. The most unstable mode had a meridional scale of the order of the radius of deformation. His analysis lies in the Phillips regime of parameter space, with the basic wave scale close to the radius of deformation so that the zonal flow is neutral ($k^2 u_1 / \beta = 1$). Our approximation in the Phillips regime requires the zonal flow by itself to be unstable ($k^2 u_1 / \beta > 1$) to small perturbations, thus we do not recover Pedlosky's results. For a basic wave scale larger than the radius of deformation, the corresponding zonal flow is generally unstable and our analysis of the Phillips regime applies.

In this chapter, we have examined the stability of a basic flow consisting of a Rossby wave in a zonal shear flow. The Rossby wave is taken to be of synoptic, planetary and very long scale. Unstable perturbations are examined for different values of basic wave amplitudes. In appropriate regions of parameter space, we recover the Phillips, Lorenz and Kim regimes, characterized by weak basic wave amplitudes, large barotropic wave amplitude and large baroclinic wave amplitude respectively. A fourth regime, the mixed wave regime where the baro-

tropic and baroclinic wave amplitudes are comparable and both large, is also identified. Two important length scales are present: the basic wave scale and the radius of deformation. When the former is much larger than the latter, higher harmonics of the basic wave scale are excited. The energy and heat transport spectra, energetics and meridional scale of the most unstable modes have also been examined. We found a spectrum of waves is generated by eddy-eddy interaction between the basic wave and the perturbation. In the next chapter, we will apply our stability analysis to the atmosphere by considering realistic atmospheric values of the various parameters.

VI. APPLICATION TO THE ATMOSPHERE

In the previous two chapters, we have presented a parameter study of the stability of a non-axisymmetric flow, namely, a Rossby wave in a zonal shear flow. In the Introduction, it was suggested that when the basic wave is of planetary scale, the scale selection mechanism due to eddy-eddy interaction may generate realistic kinetic energy and heat transport spectra in the planetary scales. To examine this, we take wavenumbers 1 and 2 as the basic wave and realistic winter values of the other parameters of the stability problem.

Two layer models of baroclinic instability of a zonal flow predict that there is a minimum critical zonal shear separating conditions which are stable from those which are baroclinically unstable. This minimum critical shear may be translated to a critical meridional temperature gradient with the aid of the thermal wind equation. Stone (1978) has shown that the observed mean tropospheric temperature gradients coincide closely with this critical temperature gradient in mid and high latitudes in all seasons. His results suggest the zonal shear should be taken to be close to its critical value: $k^2 U_T / \beta = 1$. For typical winter conditions, this corresponds to $U_T = 5.6 \text{ m/sec}$, and a realistic value of the barotropic component of the zonal flow is $U = 15 \text{ m/sec}$. Non-dimensionally, this gives $k^2 U / \beta = 2.7$. The dispersion relation for the baroclinic Rossby mode then requires wavenumbers 1 and 2 to propagate eastward at 9.5 m/sec . This phase velocity is typical of Green modes. Having specified the basic wave-number and the zonal flow components, there remains an additional

parameter - the amplitude of the basic wave. Wavenumber spectra of travelling planetary scale waves indicate that peak power is at wavenumbers 1 - 2 with period of about 15 - 30 days (Arai, 1973; Deland, 1973). This does indeed give a typical phase velocity of around 10 m sec. The geopotential amplitude at such scales is about 60 m (Arai, 1973). We will take as the basic wave amplitude $B_{TK}/U-c = 0.5$. For wavenumber 1, this corresponds to a geopotential amplitude of 140 m, and 70 m for wavenumber 2. The amplitude for wavenumber 1 is large, but time series of geopotential amplitude do show instances when wavenumber 1 attains an amplitude close to 140 m in winter (Arai, 1970). For comparison, typical geopotential amplitudes for planetary scale stationary waves in winter are about 50 - 150 m in the troposphere (Muench, 1965; van Loon et al, 1973). For basic wavenumbers 1 and 2, the parameter values $\mu^2 U/\beta = 1$, $\mu^2 U/\beta = 2.7$ and $B_{TK}/U-c = 0.5$ are located in the Kim regime of parameter space.

In Fig. 6.1, we show the growth rate $\left| \frac{\sigma_i/k}{U-c} \right|$ of the most unstable mode for basic wavenumber 1 as a function of wave amplitude $B_{TK}/U-c$ and meridional wavenumber l/k , for $N = 10$, when convergence has been obtained. The meridional wavelength of maximum instability corresponds to $l/k \approx 5$, i.e. a meridional scale close to the radius of deformation. Modes with small values of l/k are non-propagating relative to the basic wave, while those with larger values are propagating. Thus waves with small scales, close to the radius of deformation, feel the zonal shear more.

For the wave amplitude $B_{TK}/U-c = 0.5$, the structures and energetics of all the unstable modes with $l/k = 5$, the meridional

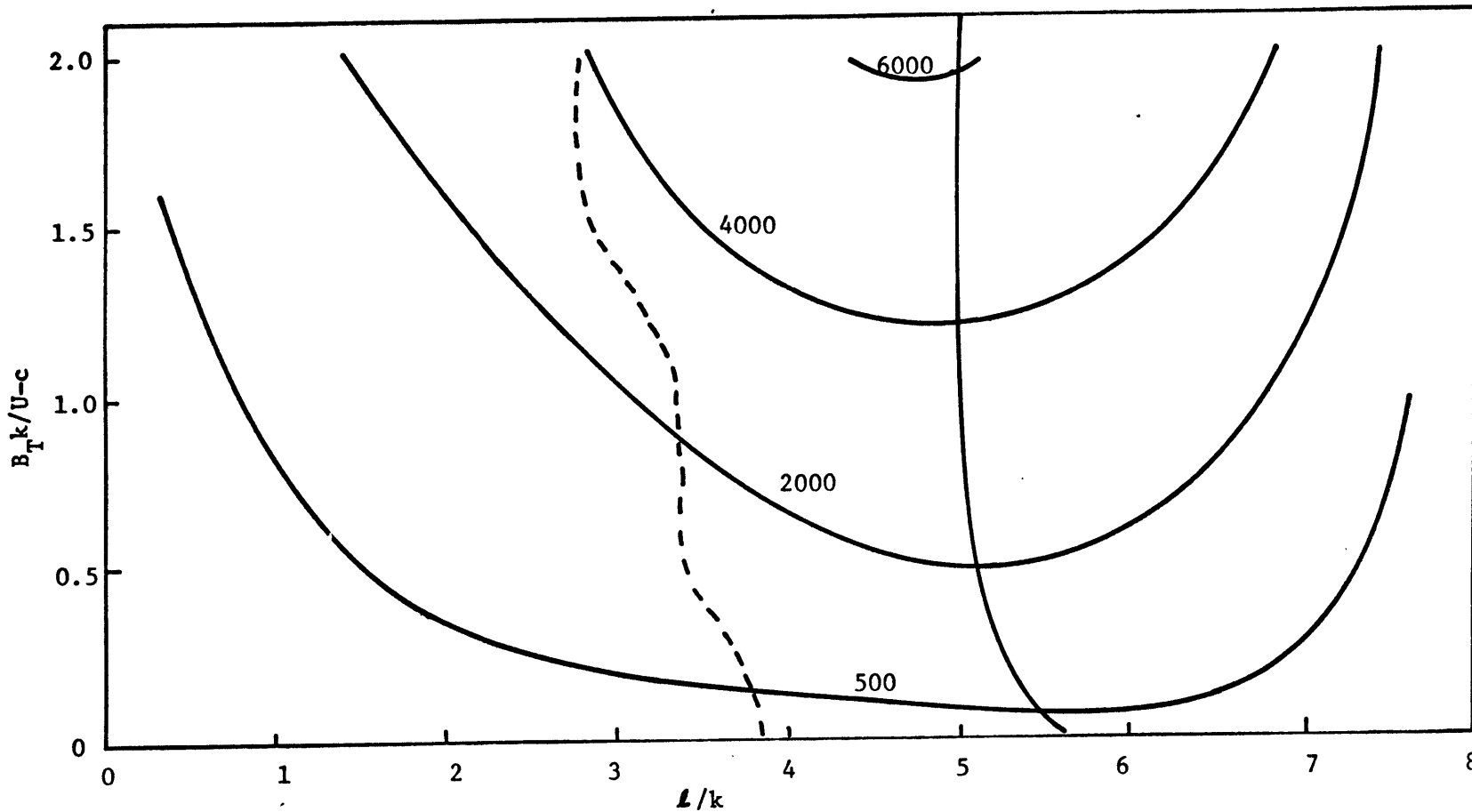


Fig. 6.1 Growth rate $\left| \frac{\sigma_i/k}{U-c} \right| \times 10^3$ of the most unstable mode as a function of wave amplitude ($B_T k / U - c$) and meridional wavenumber (l / k) for $N=10$. Propagating modes (relative to basic wave) exist to the right of dashed line. $\mu^2 U / \rho = 1$, $k / \mu = 0.13$.

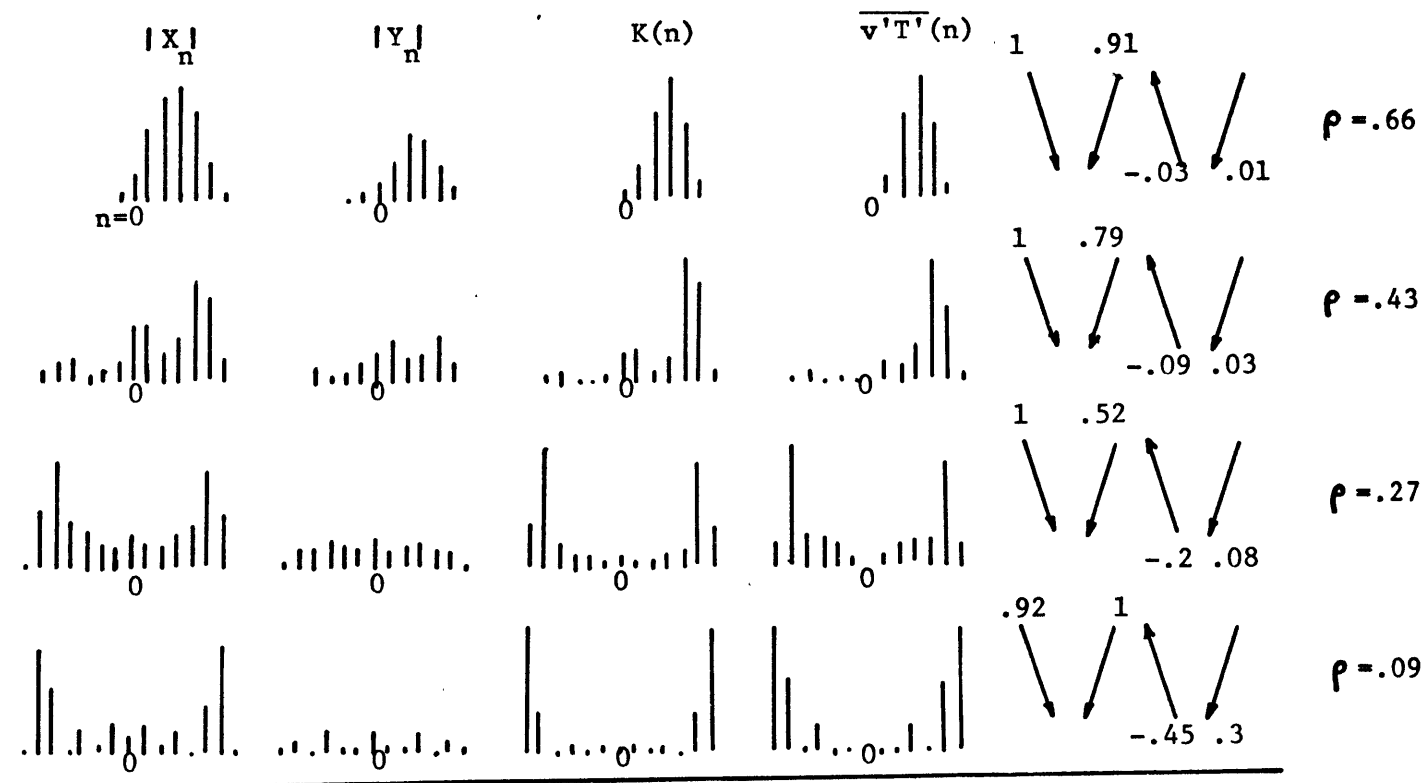


Fig. 6.2 Spectra of $|X_n|$, $|Y_n|$, $K(n)$ and $\overline{v'T'}(n)$ of all unstable modes of $l/k=5$. Also shown are the energetics and correlation coefficient for meridional heat transport (ρ). The non-dimensional frequencies, from top, are $\lambda = \pm .4186 \pm 1.9328i$, $\pm .0658 \pm 1.3135i$, $\pm .0319 \pm .6511i$, and $\pm .2076i$. $N=10$, $\frac{B_T k}{U-c} = 0.5$, $\frac{E^2 U}{\beta} = 1$, $\frac{k}{r} = 0.13$.

wavenumber of maximum instability, are shown in Fig. 6.2. The fastest growing mode is of planetary scale, with kinetic energy maximum at $n_0=3$. It propagates relative to the basic wave as the spectra are not symmetric about $n=0$. The dimensional phase speed of the perturbation relative to the earth, $c_{ph}(n)$ is

$$c_{ph}(n) = c - \frac{\sigma_r}{nk} \quad (6.1)$$

In equation (6.1), c is the phase speed of the basic wave while

σ_r is the real part of the dimensional eigenvalue (see eq. 4.3).

Thus $-\sigma_r/nk$ is the dimensional phase speed of component n of the perturbation, relative to the basic wave. For the unstable modes shown in Fig. 6.2, σ_r can be positive or negative, corresponding to westward and eastward propagation relative to the basic wave

respectively, for positive n . For the dominant unstable component $n=n_0$ for the four perturbations of Fig. 6.2, we find

$$\left| \frac{\sigma_r}{n_0 k} \right| / c = 0.22, 0.0026, 0.010, 0 \text{ respectively.}$$

Thus the dominant unstable component has a phase speed close to that of the basic wave for each case. Relative to the basic wave, the unstable modes have decreasing phase speeds with decreasing growth rates; the dominant zonal scale shifts toward the radius of deformation as the growth rate decreases.

For the least unstable mode, there is little amplitude in the spectra outside of $|n|=6$. The efficiency of heat transport as measured by the correlation coefficient decreases with growth rate.

For the most unstable mode, the non-dimensional eigenvalue

$$\lambda = \pm 0.4186 \pm 1.9382i \text{ translates into an } e \text{ -folding time}$$

of 4.8 days and as remarked earlier, a phase velocity of the dominant component close to that of the basic wave. This represents a disturbance which grows at the baroclinic time scale and propagates eastward at around 10 m sec. Fig. 6.3 shows the wavenumber spectra of meridional sensible heat flux for stationary and transient eddies, at 850 mb, 60°N in winter. The data are taken from Kao and Sagendorf (1970). Planetary scales dominate both spectra, with peaks at wavenumber 3 for both cases. We see that the agreement between the observed heat transport spectra and the spectra of the most unstable mode we obtained is fairly good, given the 2-level approximation of the model. The energetics of the most unstable mode shows that baroclinic eddy-eddy interaction is comparable to baroclinic eddy-mean flow interaction, while the barotropic interactions are small.

When the basic wave is wavenumber 2, the perturbation consisting of harmonics of the basic wave is made up of wavenumbers 0,2,4,6,..... It can be shown that if the perturbation is taken to consist of all wavenumbers, i.e. wavenumbers 0,1,2,3,....., the stability problem decouples into two sub-problems, which correspond to perturbations of even and odd wavenumbers. These perturbations will be referred to as even and odd perturbations respectively. Note this does not happen for wavenumber 1 basic wave as taking harmonics of the basic wavenumber results in all possible wavenumbers. For wavenumber 2 basic wave, the eigenvalues corresponding to the even and odd perturbations are not equal in general, thus odd wavenumbers will not grow at the same rate as even wavenumbers. To avoid ambiguity, subsequent results will be scaled using wavenumber 2 as length scale ($k = 2/a \cos \varphi_0$). For wave

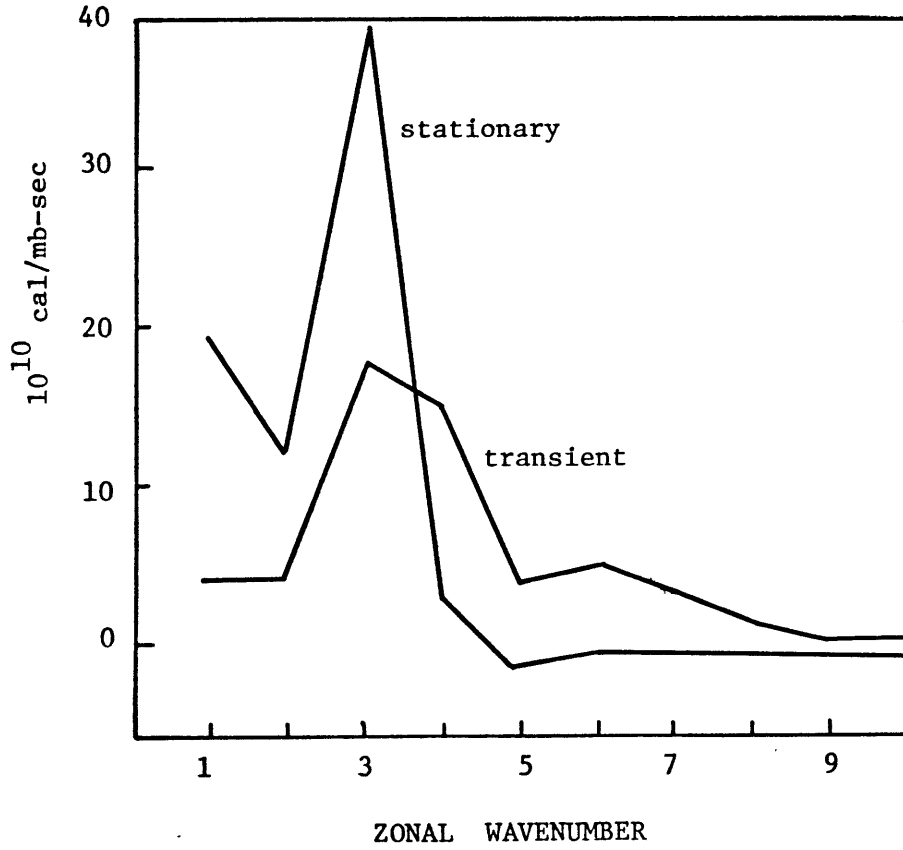
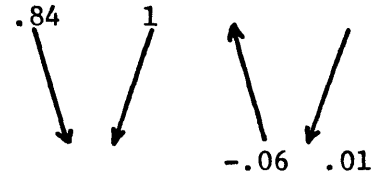
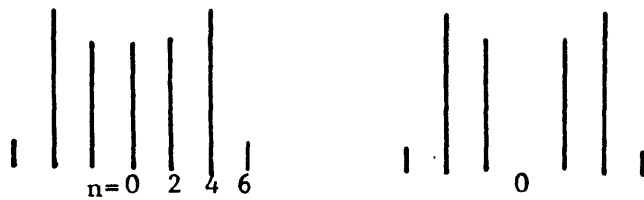


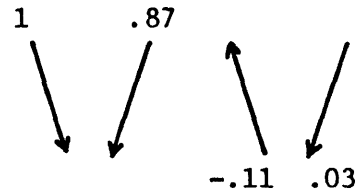
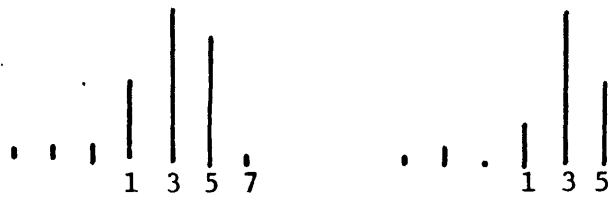
Fig. 6.3 Wavenumber spectra of meridional sensible heat flux for stationary and transient eddies, at 850 mb, 60° N in winter. (from Kao and Sagendorf, 1970)

$$\frac{\ell}{k} = 2.6 \quad \lambda = \pm .85281$$



$$\rho = .53$$

$$\frac{\ell}{k} = 2.5 \quad \lambda = \pm .0937 \pm .79341$$



$$\rho = .52$$

$K(n)$

$\overline{v'T'(n)}$

Fig. 6.4 Kinetic energy ($K(n)$) and heat transport ($\overline{v'T'(n)}$) spectra and correlation coefficient for heat transport (ρ) for most unstable even (top) and odd (bottom) perturbations. λ is the non-dimensional frequency. $N=10$, $\frac{B_T k}{U-c} = .5$, $\frac{k}{\ell} = .26$. Also shown are the energetics.

amplitude $B_1 k / U - c = 0.5$, the most unstable mode is an even perturbation. The growth rate of the corresponding odd perturbation is smaller. Fig. 6.4 shows the kinetic energy and heat transport spectra, the energetics and correlation coefficient for heat transport, for the most unstable even and odd perturbations. Ten wavenumbers are retained in each case. The growth rates for the even and odd perturbations are 5.5 and 5.9 days respectively, at almost the same meridional wavenumber. Their meridional scales are close to the radius of deformation. Relative to the basic wave, the even perturbation is stationary. The odd perturbation propagates at close to the basic wave speed relative to the earth. The kinetic energy and heat transport spectra peak at wavenumbers 4 and 3 for the even and odd perturbations respectively. Most of the amplitude is in the planetary scales in both cases. The energetics show that baroclinic interactions dominate, with eddy-eddy interaction comparable to eddy-mean flow interaction. The correlation coefficients for meridional heat transport are relatively large for both cases. As in the case when the basic wave is wavenumber 2, the kinetic energy and heat transport spectra obtained are fairly realistic compared to observed spectra for planetary scale waves.

VII. CONCLUSIONS

In this thesis, we have taken the first steps in the investigation of the hypothesis presented in the Introduction: efficient heat transporting winter eddies are generated by instability of a baroclinic flow with external forcing. This hypothesis was formulated based on physical considerations and observational evidence of the planetary scale waves of the atmosphere. We showed with a simple model of forced stationary waves that the efficient heat transport of winter SE's is not well reproduced. We then presented a parameter study of the stability of the baroclinic Rossby wave in a zonal shear flow. Linearized theory was used in the stability study; the perturbations consist of truncated zonal Fourier harmonics. This study is relevant to our hypothesis because it provides a scale selection mechanism via eddy-eddy interactions.

There are two important zonal scales in the stability problem: the basic wave scale and the radius of deformation. The former occurs as an explicit scale while the latter is the natural response scale of a perturbed baroclinic zonal flow. The properties of unstable modes thus depend on the ratio of these two scales. Three values of this ratio were considered: $H/k = 10, 3.9$ and 1.4 . They correspond to a very large scale, planetary scale and synoptic scale basic wave respectively. The possible energy sources for instability are the APE associated with the vertical shear of the zonal flow, and the KE and APE associated with the horizontal and vertical shears of the basic wave respectively. We partitioned parameter space according to the dominant

energy source of instability: the Lorenz and Kim regimes are characterized by significant horizontal and vertical shears of the basic wave respectively, while the Phillips regime is characterized by a strong zonal shear flow. A fourth regime, the mixed wave regime, where the horizontal and vertical shears of the basic wave are comparable and both large, is also identified. Growth rates, vertical structure, kinetic energy and heat transport spectra and energetics were examined for the most unstable mode in each regime.

The unstable modes consist of harmonics of the basic wavenumber and thus do not have a unique zonal scale. A measure of its zonal scale is the perturbation component which has the maximum kinetic energy. Non-dimensionally, this scale is $|n_{max}| k/\mu$, where the kinetic energy spectrum $K(n)$ peaks at $n = n_{max}$. The following table shows this scale in parameter space, for the three values of $H/k = 10, 3.9$ and 1.4 .

	$\frac{B_T k}{U-c} = 0.1$			1			10		
$\frac{B k}{U-c} = 0.1$	0.6	.77	.85	0.6	.52	0	0.1	0	0
1	0.5	.26	.85	0.6	.77	.85	0.3	0	0
10	0	0	0	0	0	0	0.1	.26	0

In the Phillips regime, where $(B_T k/U-c, B k/U-c) \leq (1,1)$, $|n_{max}| k/\mu$ is order unity, which means the most unstable mode has a zonal scale close to the radius of deformation. This is expected as the theory of baroclinic instability of a zonal flow with vertical shear predicts the

fastest growing mode to have the radius of deformation as zonal scale. In the Lorenz and Kim regimes, where $B_T k / U - c \ll 1$, $B_k / U - c > 1$ and $B_k / U - c \ll 1$, $B_T k / U - c > 1$ respectively, $\ln_{\max} k / \mu$ is close to zero. Thus the perturbation zonal component contains most of the amplitude. Kim (1978) has shown that this modal structure is related to the fact that meridional currents are unstable irrespective of their strength. Our basic Rossby wave has only x-structure in the streamfunction and thus represents a meridional current. Stability analysis of zonal currents have shown that a strong β -effect stabilizes the current (Kuo, 1949; Charney and Stern, 1962; Pedlosky, 1964). Thus in the Lorenz and Kim regimes, when the β -effect is strong, this perturbation modal structure minimizes the meridional component of perturbation velocity, which is always subject to the β -effect. Thus perturbations can overcome the stabilizing β -effect by orienting themselves in the zonal direction. In the mixed wave regime where $(B_T k / U - c, B_k / U - c) \gg (1, 1)$, there is a tendency toward this perturbation modal structure also.

In addition to selecting zonal scales, eddy-eddy interaction also selects a finite meridional scale in the Lorenz, Kim and mixed wave regimes. To examine the nature of this selection mechanism, we consider more closely the instability mechanisms. As we discussed earlier, unstable modes result because of baroclinic instability of the zonal shear flow, baroclinic or barotropic instability of the wave field. Baroclinic instability describes the release of APE of horizontal temperature gradients associated with the vertical shear of horizontal

currents. The energy release is accomplished by motion in the direction parallel to the horizontal temperature gradient. In the case of a zonal flow with vertical shear, the associated meridional temperature gradient means that APE of the zonal flow is released by motion in the meridional direction. For a meridional current with vertical shear, the associated temperature gradient is in the zonal direction, and release of APE of the meridional current is accomplished by motion in the zonal direction. Thus in both cases, conversion of zonal APE to eddy APE is accompanied by a transport of heat down the temperature gradient. Phillips'(1954) and Kim's (1975) analyses are examples of these two cases respectively. In Phillips' case, the most unstable mode has the radius of deformation (L_R) as the zonal scale and has infinite meridional extent. Barotropic instability is also present in Kim's analysis, but if we consider a planetary scale basic wave, barotropic interactions are unimportant. In this case, the most unstable mode has a meridional scale close to L_R and in the zonal direction, the perturbation zonal component has the largest amplitude. Thus in both cases, the horizontal wavevector of the most unstable mode aligns itself with the basic current. This is summarized in the table below:

regime	\underline{U}	$\underline{\nabla T}$	energy release mechanism	$\underline{k} = (k, l)$
Phillips	$(u(z) , 0)$	$(0 , T_y)$	$\overline{v'T'}$	$(L_R^{-1} , 0)$
Kim	$(0 , v(x,z))$	$(T_x , 0)$	$\overline{u'T'} \quad (\overline{u'v'})$	$(\sim 0 , L_R^{-1})$
Lorenz	$(0 , v(x))$	$(0 , 0)$	$\overline{u'v'}$	$(\sim 0 , L_x^{-1})$

In the above, \underline{U} and $\underline{\nabla T}$ denote the two-dimensional basic current and its associated temperature gradient respectively; u', v', T' denote perturbation zonal velocity, meridional velocity and temperature respectively; an overbar denotes zonal average; $\underline{k} = (k, l)$ is the wavevector of the most unstable mode; $L_x = 1/k$ is the zonal scale of the basic wave. The motion is barotropic in the Lorenz regime and energy release is accomplished by transport of momentum down the velocity gradient; and \underline{k} aligns itself parallel to the basic current. In both the Kim and Lorenz regimes, the most unstable perturbation does not have a unique zonal scale but the component with the largest amplitude is the zonal component.

In the case of interest to the atmosphere, the basic wave is a planetary scale baroclinic Rossby wave with the zonal flow near minimum critical shear. Thus instability mechanisms of the Phillips and Kim regimes are both present while barotropic interactions are small. We found realistic kinetic energy and heat transport spectra which peak at wavenumber 3 for the most unstable mode; the response is thus maximum at a zonal scale intermediate between those of the Phillips and Kim regimes. The meridional scale remains at L_λ . The perturbation wavevector is no longer along the x or y directions, but is now oriented at approximately 60° to the horizontal for the dominant perturbation component. This is because the basic flow now consists of zonal and meridional currents of comparable magnitudes. This orientation of the perturbation wavevector optimizes release of APE of the basic flow. Our result that the most unstable mode has a zonal and meri-

dional scale both close to the radius of deformation is important for closure assumptions used in parameterizations of heat transport by large scale eddies (Green, 1970; Stone, 1972; Held, 1978). Green (1970) assumed a parametric dependence for the ratio of meridional to zonal scale to be the planetary scale divided by the radius of deformation. Stone (1972) and Held (1978) implicitly assumed this ratio to be order unity. If the scale selection mechanism in our study is appropriate, our results suggest that Stone and Held's assumption is more valid.

The good agreement obtained between the observed and calculated heat transport spectra in the planetary scales for the most unstable mode lends support to our hypothesis about the generation of efficient heat transporting winter SE's, formulated in the Introduction. We discussed earlier that our basic wave is a propagating Rossby wave and cannot be identified with a true forced stationary wave. However, the vertical structure of stationary wavenumber 1 has considerable tilt with height: the results of Muench (1965) and van Loon et al (1973) show that stationary wavenumber 1 has a phase shift of almost 180° in the troposphere. Thus its vertical structure is similar to that of the baroclinic Rossby wave. We anticipate destabilizing and scale selection mechanisms similar to those present in our study will operate, when the basic wave is a forced wave. Our results thus motivate further study of the stability of forced winter stationary waves.

In addition to the insight it may give to the problem of the stability of forced stationary waves, our results are of interest to planetary scale TE's. These eddies are one of the four major types of atmospheric eddies classified in Chapter 1. They account for a substan-

tial portion of the total eddy KE and heat transport (Table 1.1). Our study may shed some light on the source of these eddies. We discussed in Chapter II that the baroclinic Rossby wave may be identified with a Green mode. These longwave modes, being slowly growing, are inefficient at transporting heat; in our model, the baroclinic Rossby wave transports no heat at all. These Green modes can grow to finite amplitude because of the weak stabilizing nonlinear wave-mean flow interaction. If they reach finite amplitude, these modes will affect the baroclinic stability problem. Our study shows that the resulting most unstable mode has KE and heat transport spectra in the planetary scales, and is also efficient at transporting heat. This is a plausible source for the planetary scale TE's that transport heat.

REFERENCES

- Arai, Y., 1970: A statistical study of ultra-long waves. J. Meteor. Soc. Japan, 48, 469-478.
- _____, 1973: On the movement of planetary waves in wavenumber-period space. J. Meteor. Soc. Japan, 51, 230-243.
- Berkofsky, L. and E. Bertoni, 1955: Mean topographic charts for the entire earth. Bull. Am. Meteorol. Soc., 36, 350-354.
- Brown, J. Jr., 1964: A diagnostic study of the tropospheric diabatic heating and the generation of available potential energy. Tellus, 16, 371-388.
- Charney, J.G., 1947: The dynamics of long waves in a baroclinic westerly current. J. Meteor., 4, 135-163.
- _____, and P.G. Drazin, 1961: Propagation of planetary scale disturbances from the lower into the upper atmosphere. J. Geophys. Res., 66, 83-109.
- _____, and A. Eliassen, 1949: A numerical method for predicting the perturbations of the middle latitude westerlies. Tellus, 1, 38-54.
- _____, and M.E. Stern, 1962: On the stability of internal baroclinic jets in a rotating atmosphere. J. Atmos. Sci., 19, 159-173.
- Deland, R.J., 1973: Spectral analysis of traveling planetary scale waves: vertical structure in middle latitudes of Northern Hemisphere. Tellus, 25, 355-373.
- Derome, J. and A. Wiin-Nielsen, 1971: The response of a middle-latitude model atmosphere to forcing to topography and stationary heat sources. Mon. Wea. Rev., 99, 564-576.
- Eady, E.J., 1949: Long waves and cyclone waves. Tellus, 1, 33-52.
- Fjortoft, R., 1953: On the changes in the spectral distribution of kinetic energy for two-dimensional, nondivergent flow. Tellus, 5, 225-237.
- Fullmer, J.W.A., 1979: The baroclinic instability of simple and highly structured one-dimensional basic states. Ph.D. thesis, Dept. of Meteorology, Massachusetts Institute of Technology, 235 pp.
- Gall, R., 1976: Structural changes of growing baroclinic waves. J. Atmos. Sci., 33, 374-390.

- Gill, A.E., 1974: The stability of planetary waves on an infinite beta-plane. *Geophys. Fluid Dyn.*, 6, 29-47.
- Green, J.S.A., 1960: A problem in baroclinic instability. *Quart. J. Roy. Meteor. Soc.*, 86, 237-251.
- _____, 1970: Transfer properties of large-scale eddies and the general circulation of the atmosphere. *Quart. J. Roy. Meteor. Soc.*, 96, 157-185.
- Haines, D.A. and J.S. Winston, 1963: Monthly mean values and spatial distribution of meridional transport of sensible heat. *Mon. Wea. Rev.*, 91, 319-328.
- Held, I.M., 1978: The vertical scale of an unstable baroclinic wave and its importance for eddy heat flux parameterizations. *J. Atmos. Sci.*, 35, 572-576.
- Holopainen, E.O., 1970: An observational study of the energy balance of the stationary disturbances in the atmosphere. *Quart. J. Roy. Meteor. Soc.*, 96, 626-644.
- Julian, P.R. et al, 1970: On the spectral distribution of large-scale atmospheric kinetic energy. *J. Atmos. Sci.*, 27, 376-387.
- Kao, S.K. and J.F. Sagendorf, 1970: The large-scale meridional transport of sensible heat in wavenumber-frequency space. *Tellus*, 22, 172-185.
- Kim, K., 1975: Instability and energetics in a baroclinic ocean. Ph.D. Thesis, Joint Program in Oceanography, Massachusetts Institute of Technology - Woods Hole Oceanographic Institution, 175 pp.
- _____, 1978: Instability of baroclinic Rossby waves; energetics in a two-layer ocean. *Deep-Sea Research*, 25, 795-814.
- Kirkwood, E. and J.F. Derome, 1977: Some effects of the upper boundary condition and vertical resolution on modelling forced, stationary, planetary waves. *Mon. Wea. Rev.*, 105, 1239-1312.
- Kuo, H.L., 1949: Dynamic instability of two-dimensional non-divergent flow in a barotropic atmosphere. *J. Meteor.*, 6, 105-122.
- Lindzen, R.S. et al, 1968: Oscillations in atmospheres with tops. *Mon. Wea. Rev.*, 96, 133-140.
- Lorenz, E.N., 1972: Barotropic instability of Rossby wave motion. *J. Atmos. Sci.*, 29, 258-264.
- Merkine, L. and M. Israeli, 1978: The stability of a stationary Rossby wave in a baroclinic zonal flow. *J. Atmos. Sci.*, 35, 1388-1398.

- Moura, A.D. and P.H. Stone, 1976: The effects of spherical geometry on baroclinic instability. *J. Atmos. Sci.*, 33, 602-616.
- Muench, H.S., 1965: On the dynamics of the wintertime stratosphere circulation. *J. Atmos. Sci.*, 22, 349-360.
- Oort, A.H., and E.M. Rasmusson, 1971: Atmospheric Circulation Statistics. NOAA Professional Paper 5, 323 pp.
- _____, and J.P. Peixoto, 1974: The annual cycle of the energetics of the atmosphere on a planetary scale. *J. Geophys. Res.*, 79, 2705-2719.
- Pedlosky, J., 1964: The stability of currents in the atmosphere and the ocean, I. *J. Atmos. Sci.*, 21, 201-219.
- _____, 1970: Finite-amplitude baroclinic waves. *J. Atmos. Sci.*, 27, 15-30.
- _____, 1971: Finite-amplitude baroclinic waves with small dissipation. *J. Atmos. Sci.*, 28, 587-597.
- _____, 1975a: On secondary baroclinic instability and the meridional scale of motion in the ocean. *J. Phys. Oceanogr.*, 5, 603-607.
- _____, 1975b: A note on the amplitude of baroclinic waves in the mid-ocean. *Deep-Sea Research*, 22, 575-576.
- Phillips, N.A., 1954: Energy transformations and meridional circulations associated with simple baroclinic waves in a two-level quasi-geostrophic model. *Tellus*, 6, 273-286.
- Smagorinsky, J., 1953: The dynamical influence of large-scale heat sources and sinks on the quasi-stationary mean motions of the atmosphere. *Quart. J. Roy Meteor. Soc.*, 97, 342-366.
- Stone, P.H., 1972: A simplified radiative-dynamical model for the static stability of rotating atmospheres. *J. Atmos. Sci.*, 29, 405-418.
- _____, et al, 1975: Seasonal changes in the atmospheric heat balance simulated by the GISS general circulation model. *Proc. WMO/IAMAP Symp. on Long-term Climatic Fluctuations*, Geneva, WMO Publ. No. 421, 383-389.
- _____, 1977: Generation of atmospheric eddies in theory and modelling of ocean eddies: Contribution of the U.S. Delegation to the Yalta Polymode Theoretical Institute. P. Rhines, ed., U.S. Polymode Organizing Committee, Cambridge, 22 pp. (Available from the U.S. PMOC).
- _____, 1978: Baroclinic adjustment. *J. Atmos. Sci.*, 35, 561-571.

- Tenenbaum, J., 1976: Spectral and spatial energetics of the GISS model atmosphere. Mon. Wea. Rev., 104, 15-30.
- van Loon, H., et al, 1973: Zonal harmonic standing waves. J. Geophys. Res., 78, 4463-4471.
- van Loon, H. and J. Williams, 1976: The connection between trends of mean temperature and circulation at the surface: Part 1. Winter. Mon. Wea. Rev., 104, 365-380.
- Wilkinson, J.H. et al, 1971: Handbook for Automatic Computation: volume II. Springer-Verlag, 439 pp.
- Yamagata, T., 1976: Stability of planetary waves in a two-layer system. J. Oceanogr. Soc. Japan, 32, 116-127.
- _____, 1977: Stability of planetary waves in a two-layer system (small M limit). J. Meteor. Soc. Japan, 55, 240-247.
- Yao, M.S., 1979: Maintenance of quasi-stationary waves in a 2-level quasi-geostrophic spectral model with topography. Preprint.

BIOGRAPHICAL NOTE

The author was born on August 28, 1953 in Hong Kong. In 1968, he immigrated with his family to Canada. He received a B.S. degree in physics and mathematics with First Class Honours from the University of British Columbia in May, 1974. He enrolled as a graduate student at the Massachusetts Institute of Technology in September, 1974.